University of Utah

Department of Chemical Engineering
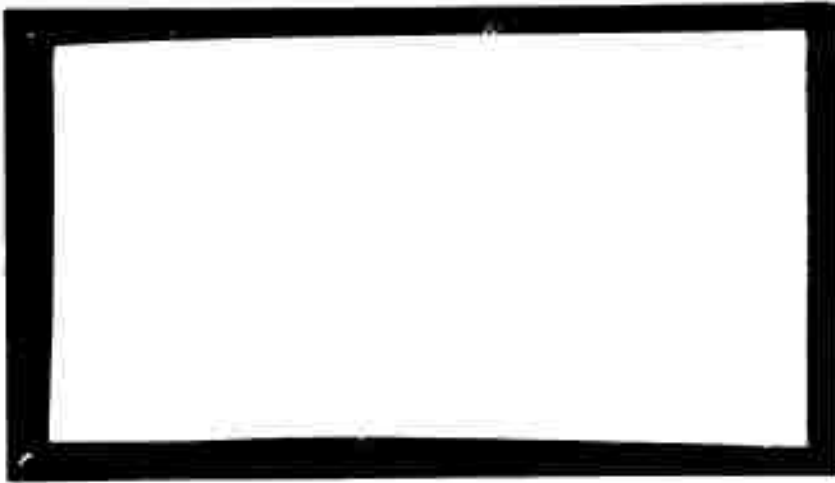
1. Distribution of this document is unlimited.

Salt Lake City, Utah

AFOSR 66-1769

TECHNICAL REPORT

NON-ACOUSTIC COMBUSTION INSTABILITY

OF SOLID PROPELLANTS

UNDER GRANT AF AFOSR 446-63

August 1, 1966

Report prepared by: M. W. Beckstead

Report approved by: *Norman W. Ryan*
Norman W. Ryan
Principal Investigator

PREFACE

This report is taken from the thesis of M. W. Beckstead
(Ph.D., University of Utah, 1965). The work was performed
under sponsorship of the Air Force Office of Scientific Re-
search, Grant AF-AFOSR 446-63. It was presented at the AIAA
Third Aerospace Sciences Meeting in New York City, January,
1965.

ABSTRACT

Non-acoustic combustion instability has been examined in an uncatalyzed, a catalyzed, and two aluminized composite propellants. These propellants were studied, burning cigarette fashion, in a burner capable of operating at values of L* as small as 5 cm. It was observed that the frequency of the pressure oscillations varied with the value of L*, frequency decreasing with increasing L*. The data were correlated by plotting frequency versus the reciprocal of L*, yield'..g a series of constant pressure curves. This pressure effect was eliminated by using dimensionless variables, allowing all of the data for a given propellant to be correlated along the same line.

A one-dimensional model is proposed that considers sinusoidal perturbations, allowing for growth of the disturbance. The pressure, the burning rate, the distributed temperature in the propellant, and the energy flux from the burning gases are the quantities perturbed. The analysis is developed utilizing an energy balance on the solid phase that accounts for energy accumulation in the solid and a mass balance on the rocket chamber that considers mass accumulation in the gas phase. The assumption is made that the energy flux from the gas phase either oscillates in phase with the pressure or is slightly out of phase.

The analysis, thus developed, reduces to an expression relating the reciprocal of the dimensionless L* to the dimensionless frequency

in terms of the growth factor and propellant parameters. The principal
parameters involved are the activation energy, the mean surface
temperature, and the heat of gasification for the propellant. With
the proper choice of these parameters the theoretical analysis yields
results that agree quantitatively with the observed experimental results.
The theoretical results also appear to be in qualitative agreement
with most of the experimental and theoretical results obtained by
other investigators.

The results of this investigation do not answer all of the many,
unanswered questions in non-acoustic instability but can be considered
significant in three respects. First, an experimental, L^*-frequency
dependency was observed in non-acoustic instability, and was corre-
lated through the use of a dimensionless frequency and L^*. Secondly,
a mathematical expression has been derived that agrees quantitatively
with the observed, experimental results, subject to certain assumptions.
Finally, the results of this investigation can be used to correlate
qualitatively some of the apparently unrelated observations of other
investigators.

TABLE OF CONTENTS

LIST OF FIGURES

LIST OF TABLES

CHAPTER I

INTRODUCTION

Combustion instability in solid propellants has received considerable attention over the years because of the destructive effects it has on a rocket motor. It may cause only a slight vibration or change in the thrust of the rocket; it may result in complete destruction of the rocket motor; or in some cases it may extinguish the burning propellant and thus terminate. None of the manifestations of combustion instability in a rocket motor is desirable.

Combustion instability as applied to solid propellants can roughly be divided into two categories: acoustic and non-acoustic. The wave equation, written for the combustion chamber of a rocket motor, will give the acoustic frequency of the chamber, and pressure oscillations corresponding to this frequency can be considered as acoustic oscillations or acoustic instability. The majority of the published literature concerning combustion instability in solid propellants falls into this category. A theoretical analysis of acoustic instability advanced by Hart and McClure [17] has been quite extensively developed and appears at the present to be the most readily accepted theory in that area.

Oscillations have also been reported [see for example, 1,3,21,26, 33,35,39] which have occurred at frequencies much lower than the acoustic frequency of the chamber in which they have appeared. This type of

instability has been termed non-acoustic or low frequency instability
(typically 0-500 cps), and is that which will be considered in the
present investigation (the designation "non-acoustic instability"
being abbreviated to NAI). This phenomenon will not be referred to
as low frequency instability because the author feels that this termi-
nology can be deceiving and is not as descriptive as that of non-acoustic
instability. The areas of interest in NAI can be classified as chuffing
and non-acoustic oscillatory combustion. Chuffing is the periodic
ignition and extinguishment of propellant (see Figure 1), whereas oscil-
latory instability is characterized by periodic or quasi-periodic
pressure disturbances about a mean pressure (see Figure 1 also).

It has been stated earlier that there is not a great deal of
published literature in the field of non-acoustic instability, and
most of what is available has appeared in very recent years. There
are several reasons why more research is being done on NAI now than
before. One reason is that metal additives have been incorporated into
propellants in an effort to suppress acoustic instability. A degree of
success has been attained, but the presence of metal additives has
apparently aggravated the mechanism that initiates NAI. A second
reason appears to be due to the fact that many of the newer and more
modern rockets operate at relatively low pressures compared with the
pressures employed in earlier rockets, and these lower pressures seem
to encourage the appearance of NAI. Still another reason stems from
the fact that motors have increased in size to the extent that the
characteristic acoustic frequencies have correspondingly been reduced
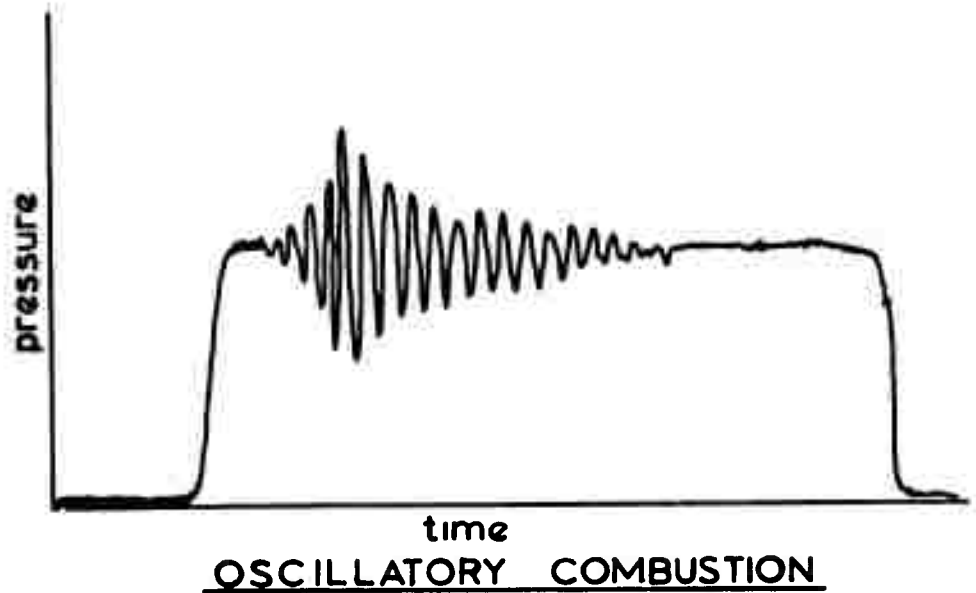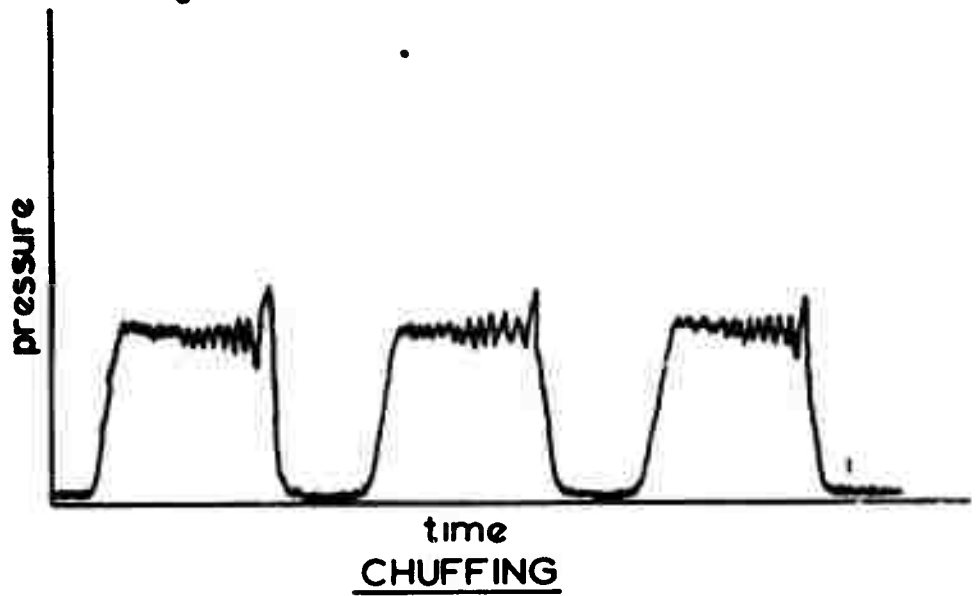
Figure 1. Non-Acoustic Combustion Instability.

until they now are of the same order of magnitude as non-acoustic oscillations in smaller motors. The problem thus arises of possible coupling between acoustic and non-acoustic instability.

Some of the earliest reported work wherein the investigator recognized the possibility of a different mechanism than that which exists in acoustic instability, was that of Huffington in 1954 [21] and 1956 [10]. He observed and reported on the phenomenon of chuffing using cordite as propellant. Experimental results indicated that the frequency of oscillations increased with pressure. He also observed that the distance the surface regressed during a chuff was constant for a given pressure. The Frank-Kamenetskii thermal explosion theory [13] was used to explain the experimental results. This theory is based on the assumption that exothermic reactions are occurring throughout a homogeneous medium, causing self-heating. For a critical thickness of material, the reactions will reach a run-away condition and an explosion will occur. In Huffington's work the distance the propellant regressed during a chuff was proposed as being the critical thickness and data were correlated on this basis. While some double-base propellants apparently do have exothermic reactions occurring throughout the solid phase, many propellants for which the existence of such reactions is questionable have exhibited chuffing and non-acoustic instability [26]. This fact has discouraged extensive use of the thermal explosion theory.

However, Angelus and Young [3,35] using modified double-base propellants have followed a course indicated by the thermal explosion theory, by correlating the induction time between chuffs with the average pressure during a chuff. Angelus was one of the first

investigators in this country to actually carry out research in the area of non-acoustic instability [3]. He observed it in propellants to which fine metal particles had been added in order to reduce acoustic instability. In addition to seeing the same qualitative dependence of oscillating and chuffing frequencies on pressure that Huffington observed, Angelus and Yount have also reported that the amplitude of the oscillations decreases with pressure.

Another laboratory which has done extensive experimental work in the area of interest is the U. S. Naval Ordnance Test Station (NOTS) at China Lake, California [12,19,26,28,30]. Although some of the experimental results have been qualitatively similar to those obtained by Angelus [12], the thermal explosion theory has not been used in analyzing the data obtained. It has been postulated that part of the cause of non-acoustic instability may be the incomplete combustion of oxidizer or metal particles (in metallized propellants) coupled with the mass flow through the nozzle, and experiments have been carried out in which unoxidized metal and oxidizer have been gathered from the exhaust of unstably burning propellant [28]. This effect should become stronger for short residence times in the motor (or small free volume) when unburned products would be swept out the nozzle, and experimental results indicate [1,2,28,35] that low L* (ratio of motor free volume to nozzle throat area) may be a necessary condition for non-acoustic instability.

The data gathered at NOTS have been correlated in terms of a "preferred frequency-pressure" regime [12] which indicates a band of

frequencies within which the non-acoustic oscillations lie at a given pressure and for a specific propellant. Data taken with a large experimental burner having acoustic modes which lie in the non-acoustic frequency range indicate that low frequency acoustic oscillations fall approximately within the preferred band of frequencies defined by non-acoustic oscillations. This means that the coupling between acoustic and non-acoustic instability which was mentioned earlier can actually take place and could be a very serious problem with large solid propellant boosters.

A theoretical model for low frequency instability in solid propellant rocket motors has been proposed by Akiba and Tanno [1]. They assumed steady-state conditions and then through use of standard perturbation techniques examined the limits of combustion stability. The equations which they used were the unsteady heat conduction equation

$$\frac{\partial T}{\partial t} = \alpha \frac{\partial^2 T}{\partial x^2} + r \frac{\partial T}{\partial x} \tag{1.1}$$

(for a definition of all symbols, see the Table of Nomenclature in Appendix A), a surface energy balance

$$k_g H_{s^+} = k_s H_s - \rho r Q \tag{1.2}$$

(where H_s is the temperature gradient at the surface, and Q is the heat evolved by surface reaction) and an equation relating the dependence of the temperature gradient at the surface (on the gas phase side) to the pressure

$$\frac{k_g}{k_s} H_{s+} = (T_f - \bar{T}_s) K_g \frac{\bar{P}^n}{\bar{r}} \qquad (1.3)$$

where K_g is a chamber time constant ($K_g = \frac{ML^*}{C_D RT_f}$).

By substituting a perturbed temperature, pressure, burning rate, and temperature gradient at the surface, assuming that the gaseous phase responds much faster than the perturbations under consideration (low frequency oscillations), and eliminating the steady-state terms in the customary manner, they obtained a chamber transfer function and a combustion transfer function. The Nyquist stability criterion was then applied to these transfer functions in order to determine stability limits for the burning propellant. The theoretical results indicated that the reciprocal of the motor free volume ($1/L^*$) was proportional to pressure raised to twice the burning rate exponent (n). The experimental results which were presented for a double-base propellant appeared to agree quite well with the theoretical predictions. However, it is difficult to determine the precise meaning of their results because no explanation was made of experimental apparatus or the criteria used to determine the recorded data points. One drawback to the theoretical results of this method of determining a stability limit is that it predicts a critical frequency at the stability boundary only and does not give any relationship for the dependency of the frequency of the oscillations for other conditions, nor was any reference in the paper made as to the agreement between this predicated, critical frequency and the actual, experimental frequencies.

Sehgal and Strand [35] have modified the model proposed by Akiba and Tanno by using a mass balance on the rocket in place of Equation (1.3) in order to obtain a chamber transfer function. The mass balance which was used was

$$\frac{d}{dt} (\rho_g V_{ch}) = \rho_s r A_b - C_D P_{ch} A_t \qquad (1.4)$$

where C_D is a nozzle discharge coefficient. The rest of the analysis followed the same outline as that of Akiba and Tanno with the exception that the paper in general was more complete. The experimental data were obtained from regressive burning grains which burned until the low pressure extinction limit was reached for the existing conditions. The remaining amount of propellant was measured and the value of L* for the chamber at this point was then calculated. The data determined in this manner are not strictly compatible with the theoretical assumptions because the analysis concerned itself with instability triggered by small perturbations, whereas the data presented [see also 2] corresponded to flame extinction after a period of finite pressure oscillations. Anderson, Strehlow and Strand [2] have reported additional data of this type for various polyurethane-based propellant compositions. They observed that as the percentage of aluminum in the propellant increased, so did the slope of the data although the burning rate exponent remained approximately the same. Thus for increasing aluminum content there appears to be an increasing discrepancy in the analysis. Studies were also carried out which indicated that incomplete combustion was not a serious problem for the range in which data were taken.

From the above discussion of the research which has been carried out in the area of NAI, it can be seen that different reports are sometimes contradictory and that none are conclusive. Although a considerable effort has been made in very recent years and is continuing at the present, neither a precise mechanism nor a completely satisfactory mathematical model has been prepared to explain the occurrence of non-acoustic instability. The present investigation does not purport to answer the questions but the intent is that it will add to the available knowledge and understanding of the subject in a positive way.

At the time when the present study was begun (1962), very little information concerning NAI was available in the literature. Most of the above work had just been started or was in progress but had not yet been reported. Therefore, the initial goal that was established was to learn more about the general nature of the problem. As experimental procedures were developed and results began to be positive in nature, this goal was more precisely defined as determining the stability limits for a particular group of propellants. An uncatalyzed, a catalyzed, and an aluminized composite propellant were chosen in an attempt to obtain fairly representative data without studying a wide variety of propellants. These propellants have been designated as Utah G, F, and TF propellants respectively, and their exact compositions and physical properties are given in Appendix B. Experiments were carried out with the hope that from the observations, a mathematical approach considering the propellant properties and the chamber conditions might be established which would allow the prediction

of a stability boundary for the onset of instability. In an attempt
to fulfill this goal a mathematical model is proposed and developed
in Chapter II.

Negative initial experimental results from shaped grains led to
the decision to employ a burner capable of operating at very small
free volume (low L*). Subsequently an end burner similar to one used
at the Naval Ordnance Test Section [12] was designed and constructed.
The data presented in the following chapters were all obtained using
this burner in its various configurations.

CHAPTER II

THEORETICAL ANALYSIS

This chapter proposes a model of non-acoustic instability, states the attendant assumptions, and presents the derivations of the resultant equations, but before proceeding it seems appropriate to comment briefly on the general nature of the system involved.

A composite solid propellant consists of a crystalline oxidizer and a polymeric binder which acts as a fuel. The oxidizer is often added as a bimodal mixture in order to improve the mixing qualities of the propellant while it is being compounded. The resultant material is a heterogeneous aggregate of intimately mixed crystals of odd shapes and sizes and the fuel binder. This heterogeneous nature of solid propellants makes it difficult if not impossible to describe the problem of combustion instability mathematically without making many, rather drastic assumptions.

A. A Model of Non-Acoustic Combustion Instability

Several assumptions relating to the propellant and the rocket chamber have been made by others considering similar problems concerned with propellant combustion. These assumptions will, therefore, be considered as "usual simplifying assumptions" and will not be discussed in detail here. These include assuming that: the solid is mathematically semi-infinite, the physical properties of the propellant and the burned

gas do not change with temperature over the range of interest, the
solid is homogeneous and isotropic, the gas obeys the ideal gas law,
isentropic flow exists through a sonic nozzle, and burning occurs
uniformly on the assumed flat surface of the propellant. The assump-
tion of homogeneity is probably the most questionable of the assumptions
and will be considered more in detail at a later time. Other assump-
tions peculiar to the problem at hand will be pointed out as they are
made.

Other investigators [18,25] have made order of magnitude cal-
culations which indicate that the mechanism of energy transport in
the solid phase must be considered in an analysis of low frequency
combustion instability (which is directly applicable to the problem
being considered). The following paragraphs include a brief discussion
of the physical considerations involved in analyzing the energy distri-
bution in the propellant and its response to low frequency perturbations.

An examination of the steady-state temperature distribution in a
burning solid propellant appears to be a good starting point for the
following discussion. A schematic sketch of this postulated, idealized
temperature profile has been included as Figure 2. Temperature is
taken as the ordinate, and the the distance into the propellant is
measured in the positive x-direction. The origin is considered as
being stationary and at the burning surface with the propellant moving
toward it at a velocity equal to the linear burning rate. The area
beneath the profile is proportional to the sensible energy of the pro-
pellant. It is this energy and its response to external (gas-phase)
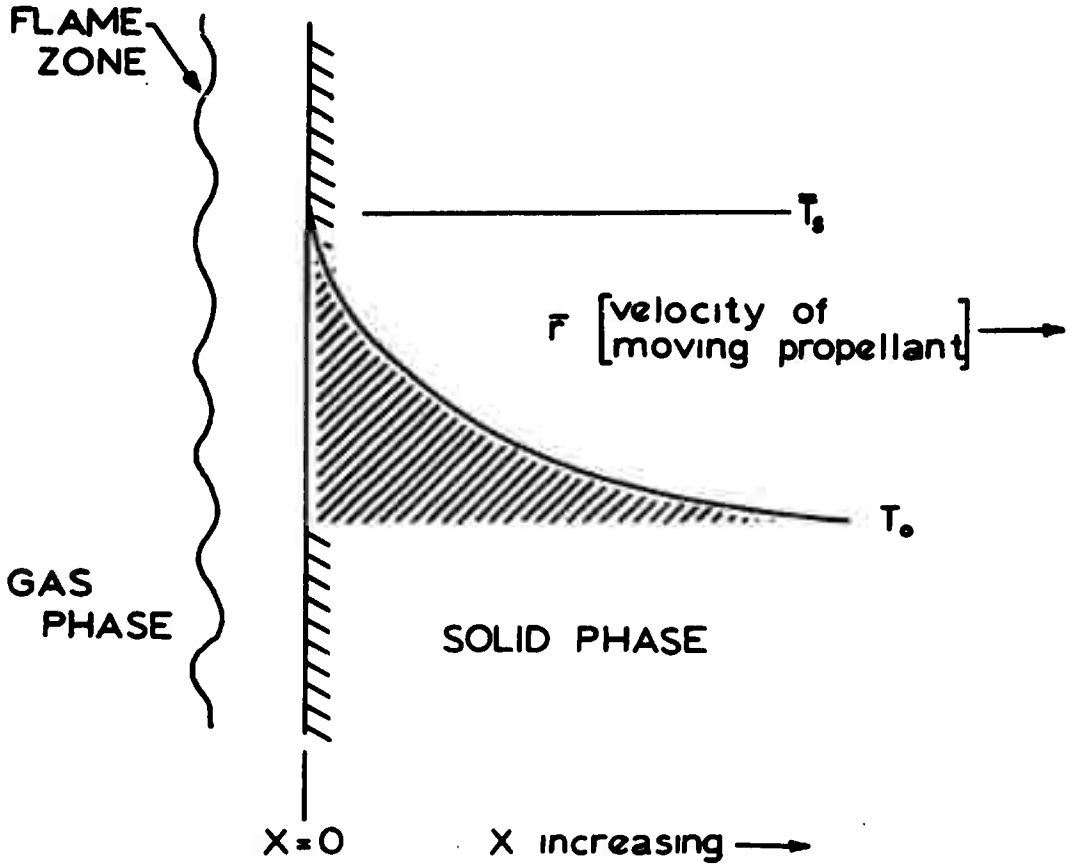
Figure 2. Idealized steady-state temperature profile in a burning solid propellant.

perturbations which will be considered in the following analysis.
Consider the steady-state heat conduction equation

$$\alpha \frac{d^2\bar{T}}{dx^2} + \bar{r} \frac{d\bar{T}}{dx} = 0 \tag{2.1}$$

Applying the boundary conditions

$$\text{at } x = 0, \quad \bar{T} = \bar{T}_s$$

$$\text{at } x = \infty, \quad \bar{T} = \bar{T}_0$$

gives the solution to (2.1) as [for example, see 38, p. 79, or 35]

$$T = T_0 + (T_s - T_0) e^{-\frac{r}{\alpha} x} \tag{2.2}$$

Therefore, the steady-state temperature profile is dependent upon the average surface temperature, the thermal diffusivity, the burning rate, and the initial uniform temperature, T_0. It is generally accepted that the surface temperature varies with pressure (increasing as pressure increases), though the explanation is disputed [see 22,4,23]. However, the burning rate dependence upon pressure is much greater than that of the surface temperature, though related to it, so that the burning rate is the more important parameter in determining the shape of the profile, and, therefore, the amount of energy stored in the solid.

At steady-state conditions the burning rate of the propellant is regulated by the rate of energy feedback from the burning gas. In the following analysis this energy will be considered as an external

flux and will be equated to the rate of energy consumption by the propellant due to heating and reactions at the surface.

The manner in which this energy transport is accomplished will be considered as being mainly due to thermal conduction with radiation effects being of a secondary importance [6,37]. It has been pointed out [6,7] that the effects of radiation should become greater at very low pressures and low burning rates and therefore, these conditions will be considered further at a later time and are discussed in some detail in Appendix G.

If the system thus described is subjected to a small perturbation, then the equilibrium between these energy fluxes will be disturbed as will the burning rate, the mass of gas generated, the mass flux through the nozzle, and the chamber pressure. In responding to a perturbation of this nature the solid is able to act as a thermal capacitance in the sense that a surplus of energy can be stored momentarily and released later, causing the rate of energy consumption to be out of phase with the rate of energy supply. If the energy fluxes and the above-mentioned mass fluxes react to each other in such a manner that the perturbation grows, then the system is unstable for the given conditions.

The thermal capacitive effect mentioned above can be readily associated with the time-dependent difference between the energy supply and consumption in the solid. This idea is developed rigorously in the following analysis. The relationship between this thermal capacitance and the other variables of the system that could describe instability is not readily obvious. However, a time-dependent mass balance describing

the mass flow through the rocket chamber will be utilized to provide a relationship of this nature.

It is hoped that this brief discussion of the phenomenological occurrences taking place in a rocket motor during unstable combustion will enable the reader to better understand the mathematical developments of the following sections. In the analysis that follows, a standard perturbation technique will be applied wherein the derived equations will be subjected to small perturbations. The first-order perturbation terms will be kept after steady-state terms are subtracted out, and second-order terms will be neglected altogether.

B. A Perturbed Energy Balance

Other investigators [1,15,35,36] considering the problem of combustion instability in solid propellants have utilized a surface energy balance in their analyses. These developments have considered the temperature gradient at the surface as being indicative of the energy flux to the surface, and have applied Fourier's law of heat conduction to the burning surface of the propellant (for example, see Equation (1.2)). In the present analysis a slightly more general approach will be taken wherein all of the thermal energy stored in the solid will be considered, and the feed-back flux from the gas phase will not be tied strictly to the surface temperature gradient.

The over-all energy balance for the propellant from the surface to a station deep in the propellant is

$$(f + \rho_p \, r \, C_p \, T_0) \quad - \rho_p \, r \, (q + c_p \, T_s) = \frac{d}{dt} \int_0^\infty \rho_p \, c_p \, T dx \quad (2.3)$$

or, by simplifying

$$f = \rho_p \, r \, [q + c_p \, (T_s - T_0)] + c_p \rho_p \int_0^\infty \frac{\partial T}{\partial t} \, dx \qquad (2.3a)$$

where f is the energy flux to the surface of the propellant, and q is the net energy absorbed, per unit mass, by the gasification process and could possibly be either positive or negative.

It is assumed that the deviations from the steady state are of a sinusoidal nature. Figure 3 shows the growth of pressure oscillations on a chuff, and it can be seen that they are periodic and approximately sinusoidal. It will therefore be assumed that the perturbations of all of the quantities are sinusoidal. The temperature, burning rate, flux, and pressure can now be written as the sum of their steady-state value plus a small perturbation that has a sinusoidal time dependence. The equations are

$$T(x) = \bar{T}(x) + \bar{T}_s \, \theta(x) \, e^{(1+\eta)\omega t} \qquad (2.4a)$$

$$r = \bar{r} \, [1 + \beta \, e^{(1+\eta)\omega t}] \qquad (2.4b)$$

$$f = \bar{f} \, [1 + \phi \, e^{(1+\eta)\omega t}] \qquad (2.4c)$$

$$P = \bar{P} \, [1 + \pi \, e^{(1+\eta)\omega t}] \qquad (2.4d)$$

The exponent from the time-dependent portion of (2.4) can also be expressed in the following manner.

$$(1 + \eta) \, \omega t = (\alpha_g + i\omega) \, t \qquad (2.5)$$

where the term on the right-hand side of the equation can be considered as a complex frequency or preferably as the frequency plus the growth factor (αg).
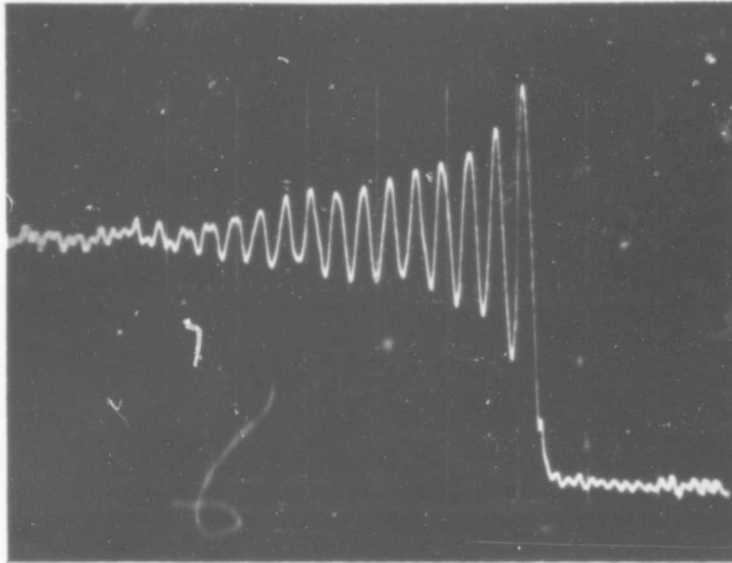
Run No. 42-063

L* ≐ 23 cm.

Ordinate scale = 10 psi/major division

Abscissa scale = 0.025 sec/major divison

Figure 3. Periodic nature of non-acoustic oscillations superimposed on a chuff.

It should be noted here that the pressure, the flux, and the temperature are not necessarily in phase with the burning rate. Consequently, three of the four quantities β, θ, ϕ, and π are in general complex. In this analysis, β is taken as real and the others are complex.

Substitution of Equations (2.4) into Equation (2.3a), subtracting out the steady-state terms, and discarding the second-order perturbation terms yields

$$\frac{\phi}{\beta} = 1 + \frac{c_p \bar{T}_s}{H} \; \frac{\theta_o}{\beta} + \frac{c_p \omega \bar{T}_s}{\bar{r}H} (\eta + 1) \int_0^\infty \frac{\theta(x)}{\beta} \; dx \qquad (2.6)$$

This equation establishes a relationship between the ratio of the flux perturbation to the burning rate perturbation as modified by energy accumulation in the solid. In order to evaluate the integral in (2.6) an equation relating the temperature to the burning rate as a function of distance is needed. The unsteady heat conduction equation will be employed to derive such a relationship.

C. The Perturbed, Unsteady Heat Conduction Equation

Energy transport in the solid phase will now be considered. Heat conduction will be regarded as one dimensional, bulk phase reactions will be neglected, and the frame of reference will be the same as in Figure 2. The unsteady heat conduction equation is

$$\frac{\partial \bar{T}}{\partial t} = \alpha \frac{\partial^2 \bar{T}}{\partial x^2} + \bar{r} \frac{\partial \bar{T}}{\partial x} \qquad (2.7)$$

Substituting Equations (2.4a) and (2.4b) into (2.7) and regrouping results in

$$0 = \left[\alpha \frac{d^2\bar{T}}{dx^2} + \bar{r} \frac{d\bar{T}}{dx} \right] + e^{(1+\eta)\omega t} \left[\alpha \bar{T}_s \frac{d^2\theta}{dx^2} + \bar{r}\bar{T}_s \frac{d\theta}{dx} + \bar{r}\beta \frac{d\bar{T}}{dx} - \bar{T}_s \omega\theta(1+\eta) \right]$$

$$(2.8)$$

The first group of terms in (2.8) is nothing more than the steady-state heat conduction equation and is equal to zero (see Equation 2.1). Simplifying leaves

$$\frac{d^2\theta}{dx^2} + \frac{\bar{r}}{\alpha}\frac{d\theta}{dx} - \frac{\omega(i+\eta)}{\alpha}\theta = - \frac{\beta\bar{r}}{\alpha\bar{T}_s}\frac{d\bar{T}}{dx} \qquad (2.9)$$

The steady-state temperature gradient, which is needed to solve Equation (2.9), can be obtained readily by differentiating Equation (2.2). Substituting this result into (2.9) produces the following second-order, nonhomogeneous equation

$$\frac{d^2\theta}{dx^2} + 2\lambda\frac{d\theta}{dx} - \frac{\omega(1+\eta)}{\alpha}\theta = \frac{4\beta\lambda^2}{\alpha\bar{T}_s}(\bar{T}_s - T_0)\,e^{-2\lambda x} \qquad (2.10)$$

The boundary conditions for the system are

$$\text{at } x = 0, \quad \theta(0) = 0.$$

$$\text{at } x = \infty, \quad \theta(\infty) = 0$$

where θ_0 is the amplitude of surface temperature perturbation. The solution to Equation (2.10) can be obtained by applying the standard techniques for solving differential equations [for example, see reference 37, p. 79]. The solution is

$$\frac{\theta(x)}{\beta} = \left[\frac{\theta_0}{\beta} + \frac{4(\bar{T}_s - T_0)}{\gamma(1+\eta)\bar{T}_s}\right] e^{-\lambda(1+\sigma+i\tau)x} - \frac{4(\bar{T}_s - T_0)}{\gamma(1+\eta)\bar{T}_s}\,e^{-2\lambda x} \qquad (2.11)$$

where λ, α, σ, and τ are defined as follows

$$\lambda \equiv \frac{\bar{r}}{2\alpha} \qquad (2.11a)$$

$$\gamma \equiv \frac{4\alpha\omega}{\bar{r}^2} \qquad\qquad (2.11b)$$

$$\sigma \equiv \left\{ (\tfrac{1+\gamma}{2}) \left[1 + \left(1 + \frac{\gamma^2}{(1+\eta)^2} \right)^{1/2} \right] \right\}^{1/2} \qquad (2.11c)$$

$$\tau \equiv \left\{ (\tfrac{1+\gamma}{2}) \left[-1 + \left(1 + \frac{\gamma^2}{(1+\eta)^2} \right)^{1/2} \right] \right\}^{1/2} \qquad (2.11d)$$

Both σ and τ are introduced to aid in simplifying the form of the equation. The dimensionless frequency, γ, is similar to the frequencies and time constants used by Green [15], Hart and McClure [18], and others [1,35].

The motive for perturbing the unsteady heat conduction equation was to provide a relationship between the perturbed temperature and burning rate as a function of distance. Equation (2.11) provides that relationship, and can now be combined with Equation (2.6) to evaluate ϕ/β. The actual integration of the integral in Equation (2.6) is carried out in Appendix C along with further algebraic manipulations. The results are (see Equation (C-7))

$$\frac{\phi}{\beta} = 1 + G + G_1 \left[(\eta(\sigma+1) + \tau \right] + Y(\sigma+1 - \tfrac{S}{2}) + i \left[G_1(\sigma+1-\eta\tau) - Y\tau \right] \qquad (2.12)$$

where $G \equiv \dfrac{c_p \bar{T}_s}{H} \dfrac{\theta_0}{\beta}$

$$G_1 \equiv \frac{\gamma c_p \bar{T}_s}{2HS} \frac{\theta_0}{\beta} = \frac{\gamma}{2S} G$$

$$Y \equiv \frac{2c_p(\bar{T}_s - \bar{T}_0)}{HS}$$

and $S \equiv \tau^2 + (\sigma+1)^2$

Equation (2.12) describes the coupling between the energy flux and the burning rate perturbations, with the capactive effect of energy storage in the propellant built in. It is now necessary to obtain a relationship involving the motor parameters; a mass balance will be utilized to accomplish this.

D. A Perturbed Mass Balance

Many investigators [for example, see 1,2,26,28,33,35] have observed that the mean pressure and the L* of a rocket chamber have an effect on NAI. This section will be devoted to deriving a relationship involving these variables.

Sehgal and Strand [35] used a mass balance for the rocket chamber to relate these variables, and the same mass balance (see Equation (1.4)) will be used here but will be developed in a slightly different manner. The mass balance for a rocket motor containing burning propellant and exhausting through a sonic nozzle is [see 5].

$$\frac{d}{dt} (\rho_g V_{ch}) = \rho_p\, r\, A_b - \frac{P_{ch} A_t}{C^*} \qquad (2.13)$$

where C* is the "characteristic velocity" for the products of combustion as described in texts on internal ballistics [5]. Differentiating the accumulation term of (2.13), assuming that ideal gas conditions exist in the chamber, and recognizing that the time rate of change of the volume is equal to the area of the burning surface multiplied by the burning rate gives

$$\frac{V_{ch}}{RT_f} \frac{dp}{dt} = r\, A_b\, (\rho_p - \rho_g) - \frac{P\, A_t}{C^*} \qquad (2.14)$$

Recognizing that the density of the gas is negligible compared to that of the solid, dividing (2.14) by A_t, and regrouping yields

$$\frac{L^*}{RT_f} \frac{dP}{dt} = K_N \, r \, \rho_p - \frac{P}{C^*} \qquad (2.15)$$

Substituting the perturbed pressure and burning rate (Equations 2.4b and 2.4d) into (2.15), and eliminating the steady-state terms in the usual manner leaves the following

$$\frac{L^*}{RT_f} \, \omega \, (1+\eta) \, \bar{P}\pi = \rho_p \, K_N \, \bar{r} \, \beta - \frac{\bar{P}}{C^*}\pi \qquad (2.16)$$

Recognizing from steady-state considerations that

$$\rho_p \, K_N \, \bar{r} = \frac{\bar{P}}{C^*}$$

and simplifying, results in

$$\frac{\beta}{\pi} = 1 + \eta\gamma\xi + i\gamma\xi \qquad (2.17)$$

where

$$\xi = \frac{C^* \, \bar{r}^2}{4\alpha RT_f} \, L^*$$

The expression β/π (the ratio of the burning rate perturbation to pressure perturbation) is called the response function. The importance of the response function is quickly realized when one considers the overall goal of an investigation such as the present. If the delicate balance between the pressure and the burning rate is disturbed, the question as to whether conditions will return to an equilibrium state, or run away, is paramount. The response function appears to be intimately involved in the answer to this question.

E. The Response Function

From the definitions of the perturbed quantities (Equations (2.4))
it can be seen that for a positive, negative, or zero growth factor, η,
the following conditions are realized. For $\eta > 0$, there exist growing
perturbations and unstable conditions; for $\eta = 0$, there is neutral
equilibrium representing a stability boundary; and for $\eta < 0$ there
are decreasing perturbations and stable conditions. From Equation
(2.17) it can be seen that for the above conditions the real part of
the response function will be greater than unity, equal to unity, and
less than unity, respectively. It is interesting to note that Hart
and McClure in their analysis of the acoustic instability problem
used the response function as a stability (or amplification) criterion
[17], and at low frequencies the stability limit is defined as the
point where the real part of the response function is equal to unity
[18].

If an independent means of evaluating the growth factor were
available, there would be no need of further considerations in order
to define a stability boundary. However, at the present the only
direct method of approximating the growth factor is from experimental
data, and, therefore, further deliberations are necessary.

F. Derivation of the Frequency-L* Dependency

In Section C an expression for the ratio of the perturbed flux
to burning rate was derived (see Equation (2.12)) and in Section D an
expression for the ratio of perturbed burning rate to pressure was
derived (Equation (2.17)). The present task is to combine these

equations in a meaningful manner which can be used to describe the
physical situation. As both (2.12) and (2.17) contain the burning
rate perturbation, the obvious is to combine them, eliminating the
burning rate effect. This can be done by multiplying (2.12) by (2.17),
the result being

$$\frac{\phi}{\pi} = (1 + \eta\gamma\xi) \text{ Re } (\theta/\beta) - \gamma\xi \text{ Im } (\theta/\beta) + i \left[\gamma\xi \text{ Re } (\theta/\beta) + (1 + \eta\gamma\xi) \text{ Im}(\theta/\beta)\right]$$

$$(2.18)$$

where $\text{Re } (\phi/\beta) = 1 + G + G_1 \left[\eta(\sigma+1) + \tau\right] + \gamma \left(\sigma+1 - \frac{S}{2}\right)$

and $\text{Im } (\phi/\beta) = G_1 (\sigma+1-\eta\tau) - Y\tau$

From (2.18) it can be seen that the problem is now reduced to that of
evaluating the ratio of the flux to pressure perturbations. The following
paragraph considers a relationship of this nature.

It was mentioned in Chapter I that a large experimental burner
having acoustic modes that lie in the non-acoustic range has been
constructed and utilized quite extensively by the Naval Ordnance Test
Station. This burner exhibits a definite "preferred frequency" regime
for given propellants outside of which oscillations are not observed
[12,19,20,28]. It appears reasonable to postulate that the solid
phase is supplying the mechanism necessary to cause oscillations at a
non-acoustic frequency and that the acoustic modes of the burner are
supplying the necessary coupling to allow these oscillations to be
maintained (the acoustic mechanism replacing the low L* or non-acoustic
coupling mechanism). Some work has been done with this burner in

studying the phase relationship between the oscillations of the light
intensity from the burning gases and the pressure oscillations. It
has been observed that the pressure is not always in phase with the
emitted light. This phase shift has been observed in both double-base
propellants [12] and composite propellants [29]. During a typical run
in this burner, oscillations begin to grow as the pressure increases
with the pressure oscillations lagging those of the light intensity.
This phase relationship passes through zero as the amplitude of the
oscillations passes through a maximum. The oscillations die out with
the pressure leading the light. From this it appears that the response
of the solid is a maximum when the pressure and the light intensity
are in phase. If the observed light intensity is associated with the
energy flux, it would appear most profitable to investigate small,
positive or negative phase shifts, or a zero phase shift.

Equation (2.18) can, therefore, be modified to include the phase
angle for the flux-to-pressure perturbation. Doing this and solving
for the dimensionless L* gives

$$\gamma\xi = \frac{F \tan \zeta - 1}{F (1 - \eta\tan \zeta) + (\eta + \tan \zeta)} \qquad (2.19)$$

where $F \equiv \dfrac{\text{Re}(\phi/\beta)}{\text{Im}(\phi/\beta)}$

and $\tan \zeta \equiv \dfrac{\text{Im}(\phi/\pi)}{\text{Re}(\phi/\pi)}$ (ζ being the phase angle)

In Equations (2.18) and (2.19), σ, τ, T_1, G, Y, and S are functions
of γ, η, the propellant parameters, θ_o/β, and $\tan \zeta$. In the following
section two methods of approximating θ_o/β from the propellant properties

will be presented, and i: will be assumed that tan ζ will be small or can be approximated. It can therefore be seen from Equation (2.19) that the frequency is a function of L* and the growth term.

Although the problem appears to have been reduced to a solution for η involving only the two variables γ and ζ, there still exists a problem of a practical nature. Physical properties and burning rate data for propellants can be obtained with a certain amount of accuracy, but numerical values for chemical properties such as the activation energy, heat of gasification for the propellant, heats of reactions for the surface reactions, and the surface temperature are, at best, crude approximations. Realizing this, ranges of values for the above three uncertain parameters were obtained from the literature, where possible(average values were taken from References 22 and 24). A parametric study was then carried out to determine the best agreement of the experimental data with the approximated parameters for various values of tan ζ. A discussion of these results can be found in Chapter V.

G. Evaluation of θ_o/β

Kinetic Limited Case. - A relationship between the surface temperature and the burning rate must be obtained in order to evaluate θ_o/β. The following Arrhenius expression is used

$$r = A e^{-E/RT_s} \tag{2.20}$$

Substituting the perturbed burning rate and surface temperature expressions (Equations (2.4)) into (2.20), assuming that the perturbations

are small compared to unity, and solving for θ_o/β, one finds [see reference 35]

$$\theta_o/\beta = \frac{R\bar{T}_s}{E} \qquad (2.21)$$

Thus, if the value of the surface temperature is determined by kinetic limitations, Equation (2.21) provides an approximation for θ_o/β which can then be used with Equation (2.19) giving the dimensionless L* as a function of the dimensionless frequency and the growth term.

The assumption that the surface temperature determines the burning rate has been popular. It has been utilized in most of the theories of unstable combustion [1,15,17,35] with the numerical value of the activation energy ranging between 16 Kcal/mole and 50 Kcal/mole in the various publications.

Thermodynamic-Limited Case.--Recently it has been proposed that the surface temperature of a composite propellant burning at low pressures is controlled by the equilibrium decomposition of solid ammonium perchlorate [4,23,24]. The chemical equation describing the decomposition is

$$NH_4ClO_4 \rightleftarrows NH_3 + HClO_4 \qquad (2.22)$$
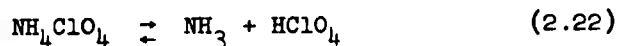
The heat of sublimation for this reaction, calculated from vapor pressure measurements, has been reported as 56 Kcal/mole [22,23]. Experiments carried out by Powling and Smith [24] indicate that the value of the surface temperature is fixed by the pressure up to 60 psia and probably higher. This represents the lower range of working pressures involved in the present study, and therefore warrants further investigation.

Assuming that the surface temperature is determined by the equili-
brium vaporization of Equation (2.22), the Clausius-Clapeyron equation
can then be utilized in the following form

$$\frac{dP}{dT_s} = \frac{P \, \Delta H_s}{R \, T_s^2} \tag{2.23}$$

Substituting the perturbed burning rate and surface temperature
expressions (Equation (2.4)) into 2.23), assuming that the perturbations
are small compared to unity, and solving for θ_0 one finds (see Appendix
D, Equation (D-2))

$$\theta_0 = \frac{R\bar{T}_s}{\Delta H_s} \; \pi \tag{2.24}$$

The fact that (2.24) is a real equation and not complex indicates
that θ_0 is in phase with π which follows logically from the assumption
that the surface temperature is fixed by the pressure. Instead of
attempting to solve for θ_0/β, the expression for θ_0 (Equation (2.24))
will be substituted directly into Equation (2.12), resulting in

$$\frac{\phi}{\beta} = 1 + Y_2 \left(\frac{\pi}{\beta}\right) + Y_1 \left(\frac{\pi}{\beta}\right) [\eta(\sigma+1)+\tau] + Y \left(1+\sigma-\frac{S}{2}\right) + i \left[Y_1 \left(\frac{\pi}{\beta}\right)(1+\sigma-\eta\tau) - Y\tau\right] \tag{2.25}$$

where $Y_1 \equiv \dfrac{\gamma \, c_p \, R \, \bar{T}_s^2}{2HS\Delta H_s}$

and $Y_2 \equiv \dfrac{c_p \, R \, \bar{T}_s^2}{H\Delta H_s}$

Multiplying this equation by the response function in order to eliminate
the burning rate perturbation as was done to obtain Equation (2.18)
gives

$$\frac{\phi}{\pi} = (1+\eta\gamma\xi)\,[1+Y\ (1 + \sigma- \frac{S}{2})]+ Y_2 + Y_1\,[\eta\,(\sigma+1) + ^-] + Y\tau\gamma\xi$$

$$+ i\left[\xi\gamma\,[1 + Y\,(1 + \sigma - \frac{S}{2}\ - \eta\tau)] + Y_1\,(1 + \sigma-\eta\tau) - Y\tau\right] \quad (2.26)$$

Following the same argument that led to Equation (2.19) yields

$$\gamma\xi = \frac{\tan\,\zeta\left\{1 + Y\,(1+\sigma-\frac{S}{2}) + Y_2\,[1 + \frac{\gamma}{2S}\,(\eta(\sigma+1)+\tau)]\right\} + Y\tau - Y_2\,\frac{\gamma}{2S}\,(1+\sigma-\eta\tau)}{1 + Y\,(1+\sigma\ -\frac{S}{2}-\eta\tau) - \tan\,\zeta\,\left[Y\tau + \eta\,[1+Y(1+\sigma-\frac{S}{2})]\right]} \quad (2.27)$$

If the assumption is made that the surface temperature is in phase
with the pressure rather than the burning rate, then Equation (2.27)
applies in place of Equation (2.19).

As to the superiority of the kinetic assumption over the thermo-
dynamic assumption, or vice versa, Nachbar and Williams [22] report
that the evidence of their studies indicates that neither mechanism
can be verified as the only mechanism, nor eliminated as an incorrect
mechanism. Therefore, both assumptions have been considered in the
present analysis and results from using each assumption in connection
with the parametric study will be presented in Chapter V.

H. Summary of Theoretical Considerations

The results of the analysis made in this chapter are essentially
contained in Equations (2.19) and (2.27). Both of these equations
predict that the frequency of the oscillations is related to the L* of
the motor, and furthermore, in dimensionless form this relationship
is independent of the pressure. This result is quite revolutionary

considering that although it is quite generally accepted that low values
of L* are characteristic for non-acoustic instability and various
low frequencies have been observed experimentally, to the author's
knowledge a correlation between L* and frequency has not been reported
in the literature, much less a theoretical prediction of such a
relationship.

The following chapters contain discussions of the experimental
approach and observed results. These results will be interpreted in
terms of the conclusions drawn from Equations (2.19) and (2.27).

CHAPTER III

EXPERIMENTAL PROCEDURES

At the time that the present investigation was begun, very little research had been performed and reported on NAI. A program was therefore initiated and executed with the purpose of producing NAI in certain propellants that were readily available at the University of Utah. The initial experiments made use of shaped grains whose burning area changed (accompanied by a corresponding change in the chamber pressure) as burning progressed. It was hoped that this pressure perturbation would be adequate to trigger instability. Although many variations were employed by using variously shaped grains, neither oscillatory instability nor chuffing was observed in some fifty runs.

It was later discovered that a few of these runs were actually made in what we now know is the unstable regime. The fact that instability was not detected was probably due to the manner in which the pressure transducer was mounted. The transducer was mounted inside a Kistler, WC-14, water-cooled adaptor located in the wall of the burner. The transducer was separated from the gas chamber of the burner by a column of silicone grease approximately 1/8 inch in diameter and 3/4 inch long for the runs in question. When this adaptor was utilized in connection with the low-L* burner (in which NAI is readily observed) oscillations were apparently damped out by the column of grease.

Therefore, the results of the experiments with the shaped grains are considered as inconclusive. However, these results did lead to the decision to design a burner that would operate at very short stay times (i.e., low L*).

A. The Low-L* Burner and Its Instrumentation

The low-L* burner that was designed was modeled after one used at the Naval Ordnance Test Station [26,28]. Figure 4 shows a schematic drawing of the assembled burner. The burner consists of two 10.5-inch flanges with a short section of 1.5-inch i.d., heavy walled pipe between the flanges. In order to be able to vary the length of the burner, several sections of the pipe ranging from one-half inch to 3 inches in length were made.

A cylindrical disc of propellant 1.5 inches in diameter and usually one quarter to three quarters inch thick was placed in the pipe. This section was then positioned between the two flanges so that the propellant was flush against a flange containing a Kistler Model 401 pressure transducer. A carbon nozzle 1 inch in diameter controlled the flow of exhaust gases and was situated in the flange opposite the propellant. Each nozzle was machined so that it would fit flush with the surface of the flange as shown in Figure 4. Figure 5 is a photograph of three of the actual nozzles used in the experiments. The nozzles were made with throat diameters ranging from 0.180 inches to 0.328 inches. This resulted in a range of Kn (the ratio of burning area to nozzle throat area) between 21 and 69 and allowed L* to be varied (for burner lengths of 3 inches or less) from approximately 5 cm. to well over 300 cm.
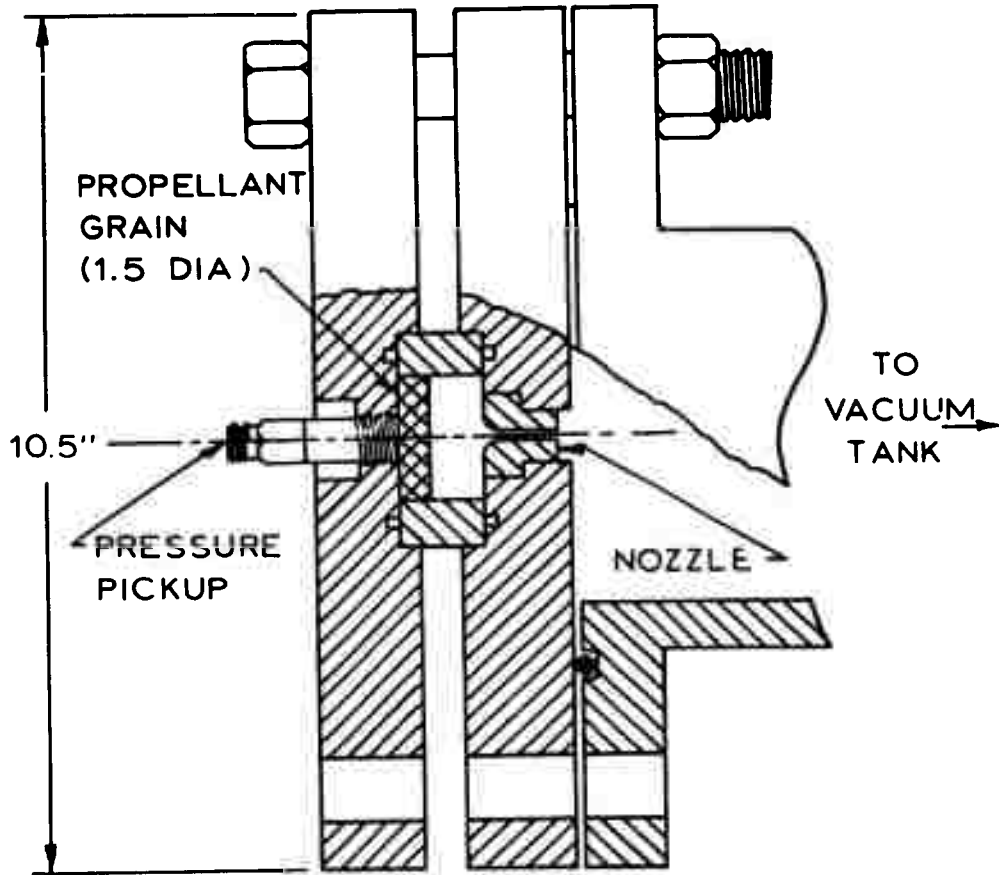
LOW L* MOTOR

Figure 4.   Schematic drawing of low-L* burner.
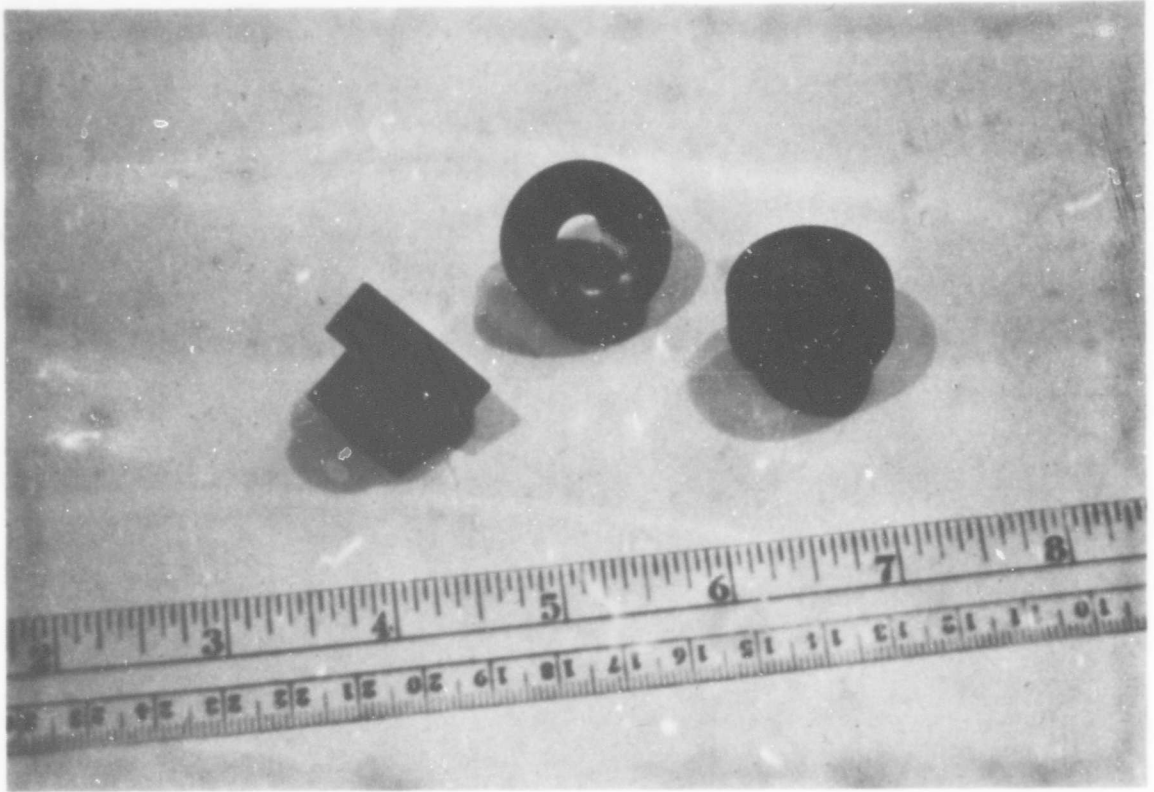
Figure 5. Graphite flow control nozzles used in the low-L*
burner.

The pressure signal from the transducer passed through a Kistler Model 568 charge amplifier, was displayed on a Type 535 Tektronix oscilloscope where it was photographed using Polaroid film, and was recorded on a Model 207, Precision Instrument magnetic tape recorder. For convenience, the signal was also observed visually on a Type 150A Hewlett-Packard oscilloscope. The tape recorder was operated at a tape speed of 15 inches per second and played back at 7 and one-half inches per second giving a two-to-one expansion of the time scale.

B. The Low-L* Burner Adapted for High Speed Motion Pictures

During the course of the experimental studies it was felt that high-speed motion pictures of the unstable combustion process might be informative. In order to facilitate this, plexiglas windows were constructed with flow control nozzles machined at their center. The plexiglas was then attached to the low-L* burner in the manner shown in Figure 6. A Wollensak, Type WF3T, Fastax high speed camera using sometimes black and white and sometimes color film (Eastman Kodak Plus-X and Ektachrome-ER film) was operated at speeds between 500 and 1000 frames per second in making the movies.

The results from these studies were interesting but not quantitative. They showed that the light intensity from the burning propellant oscillated in the same way that the pressure does, but due to the fact that the camera and the oscilloscope were operated independently of each other, a quantitative measurement of this effect could not be made.

PROPELLANT GRAIN (1.5" DIA.)

10.5"

PLEXIGLAS WINDOW—NOZZLE

3.5" 4.0"

VIEWING DIRECTION
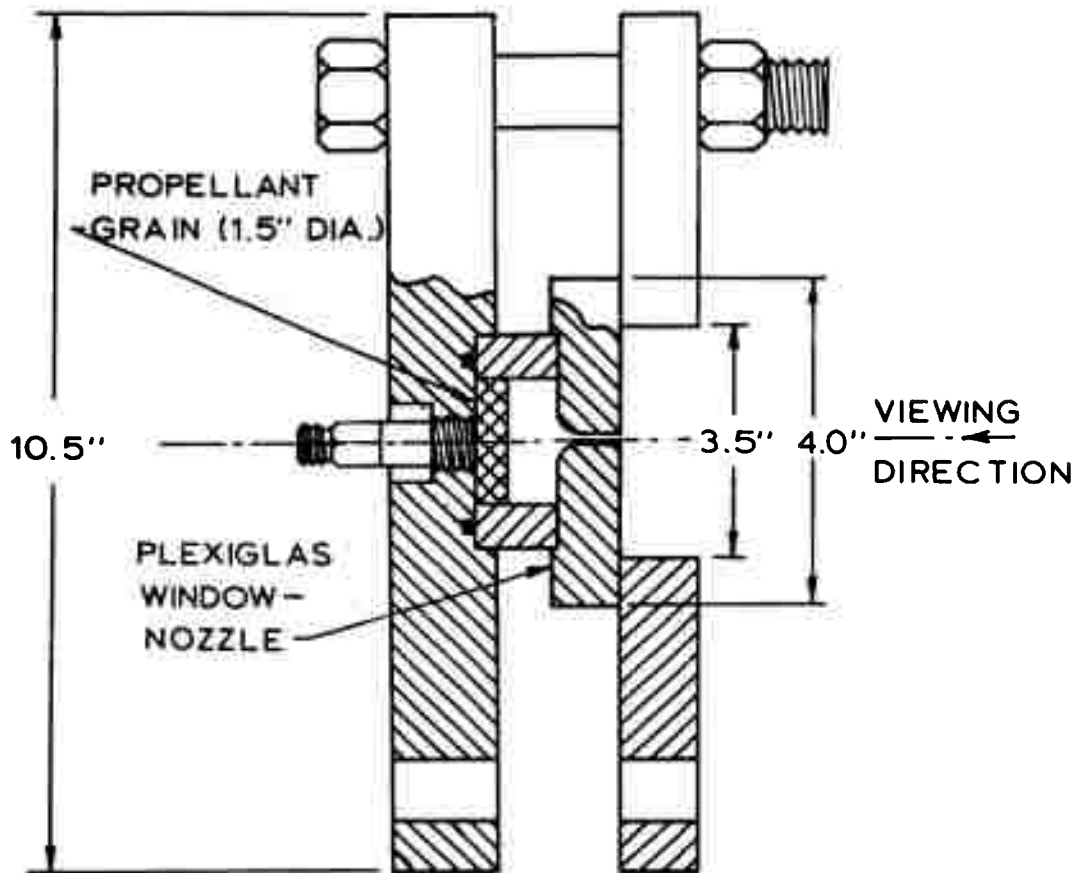
LOW L* MOTOR
(ADAPTED FOR MOVIES)

Figure 6. Low-L* burner adapted for movies.

C. The Vacuum System

After many experimental runs had been made, it was observed that NAI appears to occur more readily at low operating pressures [see also 2,20,28]. A disadvantage of operating at low pressures is that if the ratio of the chamber pressure to the ambient pressure falls below a certain value, critical flow will not be maintained in the nozzle. The exact relationship may be derived as follows: the stagnation temperature for sonic, isentropic flow is

$$T_{ch} = T_t \left(\frac{1 + \Gamma}{2}\right) \tag{3.1}$$

where Γ is the ratio of specific heats. Combining Equation (3.1) with the isentropic relationship between pressure and temperature yields

$$\frac{P_{ch}}{P_t} = \left(\frac{1 + \Gamma}{2}\right)^{\frac{\Gamma}{\Gamma - 1}} \tag{3.2}$$

For the propellants used in this study the ratio of specific heats ranges from 1.20 to 1.24 (see Appendix B). Substituting these values of Γ into (3.2) yields a critical pressure ratio of approximately 1.8. This means that if a ratio of approximately two is not maintained between the chamber pressure and the ambient pressure, then critical flow does not exist in the nozzle.

Many runs were made with sub-critical pressure ratios. The results are therefore in doubt, because their interpretation requires critical nozzle flow. In order to assure critical flow for low pressure firings a vacuum tank was constructed into which the experimental

burner could exhaust at sub-atmospheric pressures. Use of the vacuum
tank for this purpose made possible the investigation of chamber pres-
sures slightly above atmospheric. Although sub-atmospheric pressures
could also have been investigated, it was felt that this would have
been beyond the scope of the present study. The vacuum tank was con-
structed by the Lang Wayne Equipment Company of Salt Lake City, Utah.
It has 45 cubic foot volume and will withstand a vacuum. A Type MD
674, Nash Hytor Vacuum Pump driven by a 5-horsepower motor was utilized
in series with a No. 2-26-6 Nash Air Ejector to draw the necessary
vacuum on the tank. Figure 7 shows a schematic drawing of the vacuum
system.

The tank was constructed so that the experimental burner could be
attached directly to it. A 4-inch i.d. pipe, 12 inches long screwed
into the access opening of the tank, and a 10.5-inch flange was welded
onto the free end of the pipe so that the burner could be bolted directly
to the flange. Two wires were cemented into drilled holes in the wall
of the access pipe to provide pressure-tight ignition leads. Figure 8
is a photograph of the burner attached to the vacuum tank. The ignition
leads can be seen at the top of the photograph, and the charge amplifier
can be seen alongside the burner. The tank itself was placed outside
the building and the access pipe passed through a wall in such a manner
that the flange was indoors.

The effect of exhausting to a pressure lower than atmospheric
can best be demonstrated by the comparison of the pressure traces
of runs made under similar conditions, with and without the vacuum
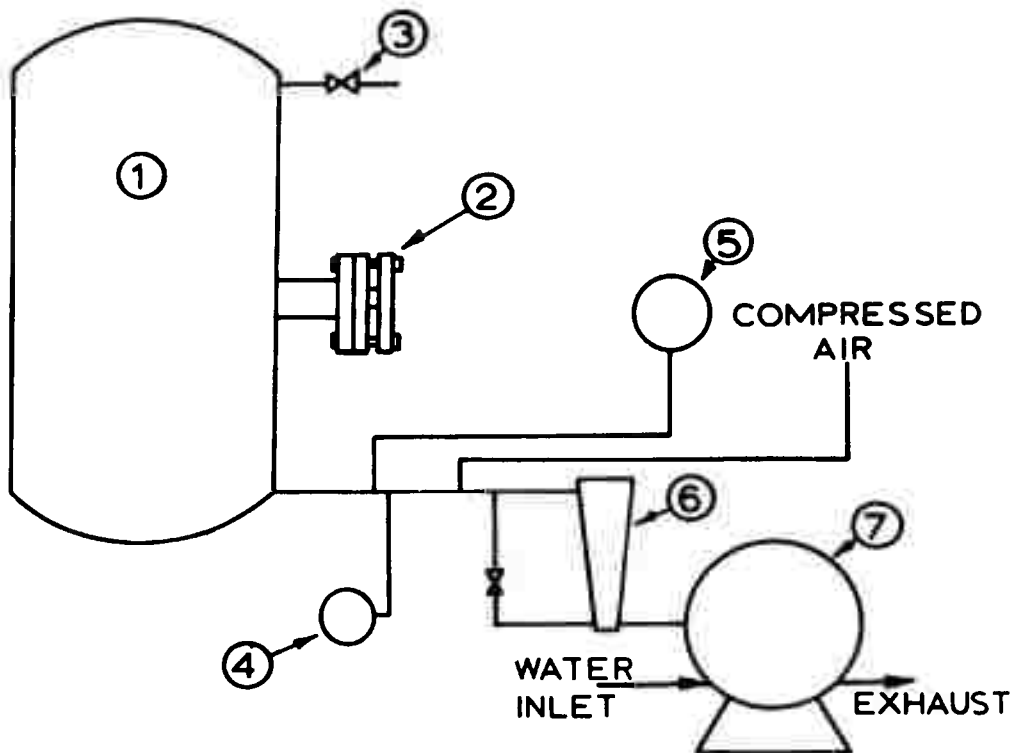
1. VACUUM TANK
2. ASSEMBLED LOW-L° BURNER
3. BLEED VALVE
4. ABSOLUTE PRESSURE GAUGE
5. NH_3 TANK
6. NASH NO. 2-26-6 AIR EJECTOR
7. NASH HYTOR VACUUM PUMP, TYPE MD674

Figure 7. Schematic diagram of the vacuum system.
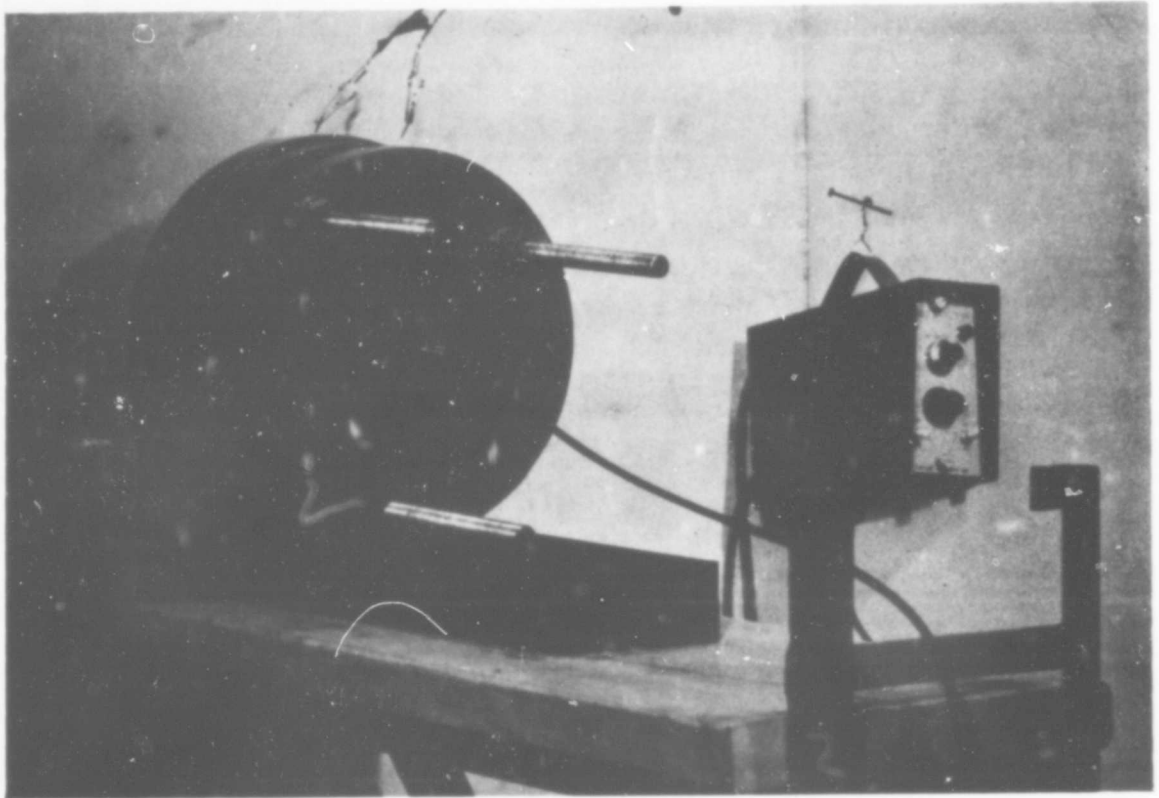
Figure 8. Assembled low-L* burner attached to vacuum
tank. Ignition wires are connected and the charge amplifier
can also be seen.

tank. Figure 9 shows a comparison of two such runs. Although the time scale is the same for the two traces, the bottom picture does not include the total run due to the slow, irregular nature of the chuffing. The general effect of exhausting into a vacuum was, as can be seen: delay times of several seconds often occurring between chuffs with a few oscillations taking place on the chuffs before extinction. However, when exhausting to atmospheric pressure, rapid-fire chuffing occurs with few, if any, oscillations being developed on a chuff. Another effect of utilizing the vacuum tank was that the propellant would often extinguish without reignition when the ambient pressure was less than 5 psia, whereas at atmospheric pressure samples were seldom completely extinguished.

D. Propellants

The initial experiments that were carried out with shaped grains, utilized G and F propellants. The compositions and mixing procedure for these propellants were established at the University of Utah by Ralph Coates [8] and are recorded in Appendix B along with their physical properties. When positive results were not obtained from these initial experiments, it was suggested [27] that a new burner be designed and that a polyurethane propellant be used. As a result, the burner described in Section A of this chapter was designed and constructed. A polyurethane propellant was made and burned in the low-L* burner giving positive results. The formulation which was used was obtained from the Naval Ordnance Test Station and is recorded in Appendix B.
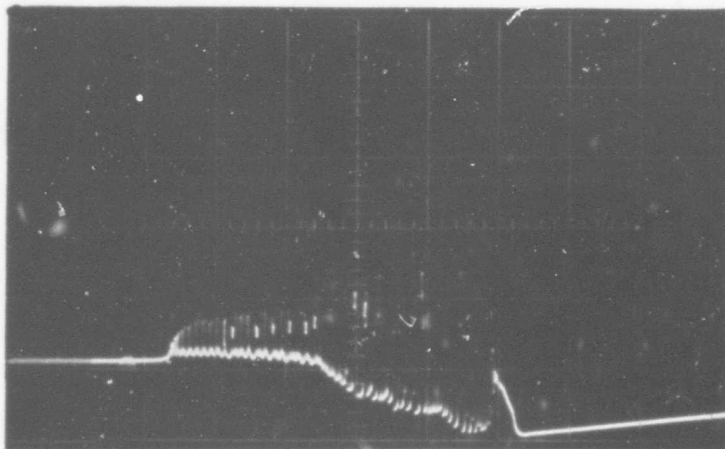
Run No. 310-233, $L_i^* = 30$ cm., $L_f^* = 56$ cm.
Ambient pressure: atmospheric
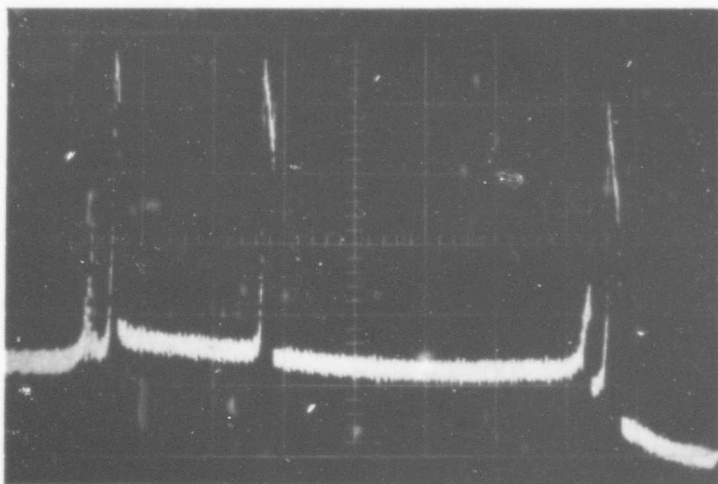
Run No. 49-181. $L_i^* = 38$ cm., $L_f^* = 56$ cm.
Ambient pressure: 5 psia
(This is a play-back from the tape recorder.)

Figure 9. A comparison of pressure-time traces for similar runs made with and without the vacuum tank. Both runs were made with F propellant. The final burn-out is not shown in the bottom trace. The sweep rate is 1 second/major division, and the pressure scale is 10 psi/major division for both traces.

The extremely high viscosity of the propellant in the uncured state discouraged extensive use of this propellant due to the problems encountered in the mixing and casting process. Therefore, after approximately forty runs had been made, it was decided to discontinue use of the propellant even though positive results had been obtained. The raw data from these runs can be found in Appendix E, Table 4. The experience gained from the runs made with the polyurethane propellant provided the experimental understanding necessary to obtain positive results with G propellant by operating at very low pressures and low values of L*. Subsequently, NAI was also observed in F propellant even though other investigators had not been able to observe NAI in comparable propellants.

From the above observations it was decided to use the PBAA propellants (F and G) in the present investigation. A third propellant containing five per cent aluminum (displacing perchlorate from F propellant) was formulated and designated TF propellant. These three propellants formed the basis of the investigation. Exploratory work was initiated with two other propellants designated GB and XF. The GB propellant is an uncatalyzed propellant similar to G excepting that it contains two per cent carbon black. The purpose of the carbon black is to reduce the amount of radiation penetrating the solid (G propellant is slightly translucent). The XF propellant contains ten per cent aluminum and is, therefore, more highly aluminized than any of the other propellants. Appendix B contains the formulations and physical properties of all the propellants with the exception of

the physical properties of the polyurethane propellant. Virtually no conclusions were drawn from the use of this propellant and, therefore, its properties have not been recorded.

E. Experimental Run Procedure

In the initial experiments with shaped grains a great deal of time was spent in preparing the samples for firing. The samples were machined to the proper size, and then several coats of a burning restricter were applied to the sides of the sample to insure even burning. The second experimental apparatus (the low-L* burner) was constructed taking into consideration all of the disadvantages of the first. The design of the burner is very simple, and this has resulted in a minimum amount of effort in preparing a sample for firing. It was hoped that the simplicity of the experimental system might help to compensate for the complexity of the physical process.

The propellant was cast into the same heavy wall tubing that was used in the construction of the walls of the burner. However, the molds were reamed out slightly in order to allow for shrinkage as the propellant cooled. The samples fit snugly in the burner. In order to prepare a sample for a firing, a piece of propellant approximately the desired length was cut from the cast grain with a hacksaw. The grains were usually fifteen to eighteen inches long. The surface of the sample was then scraped smooth with a razor blade until it formed a right angle with the side of the sample and was the desired length. The sample was then forced into the test section that was to be used. In some of the experiments the test section was coated lightly with a

a silicone grease in order to facilitate the entry of the sample into the test section. Later, as an extra precaution against movement of the sample during the firing, or burning down the side, the sample was cemented to the walls of the test section with an epoxy resin. No appreciable difference was noted between runs made using the different procedures.

Samples that did not ignite uniformly would burn irregularly causing an uneven pressure trace, G propellant being the most difficult of the propellants to ignite. It was also the slowest burning propellant and was, therefore, more susceptible to uneven burning. It should be noted that the requirement for the strength of the ignition pulse also varied with the length of the test section. For these reasons the ignition process had to be tailored to fit the needs of almost each separate run, particularly when the sample to be burned was of G propellant.

The primary source of ignition consisted of a length of an exploding, exothermic fuse wire (Lo-R Pyrofuze made by the Pyrofuze Corp.). The wire explodes giving off heat when its temperature increases sufficiently due to the heating from a current passing through the wire. A voltage drop of approximately 60 to 70 volts was necessary to ignite the Pyrofuze. For a typical run involving G propellant a two-inch length of 0.015-inch diameter Pyrofuze wire was used. With the other propellants a length approximately 1.5 inches long of 0.010-inch diameter wire was used. A pyrotechnic paste composed of finely powdered boron, aluminum, and ground crystals of

potassium perchlorate with polyisobutylene as a carrier, was painted
on the surface of the sample as a secondary source of ignition when
test conditions warranted it. The paste was dissolved in methylene
chloride which evaporated when the paste was spread on the sample.

After the propellant sample and the ignitor had been prepared,
the following procedure was carried out: a thin coating of silicone
grease was spread over the transducer to protect it as the propellant
burned out, and the test section was placed between the flanges
with the ignitor lead wires extending from the nozzle. The flanges
were then securely bolted together. For the runs that utilized the
vacuum tank, the necessary vacuum was drawn and the system sealed off
(the vacuum pump was not operated during a firing). The tank was
not completely evacuated for each run because the ignition problems
became more acute as the pressure level became lower. The pressure
was maintained only at a level sufficiently low to ensure critical flow
in the nozzle during the run. The sample was then ignited and the pres-
sure trace recorded. After the completion of a run, a small amount of
ammonia was bled into the vacuum tank in order to neutralize the acidic
combustion gases and their deposits. The tank was then flushed out well
with compressed air. After several runs the tank was washed down with
water and allowed to dry before continued use.

CHAPTER IV

ANALYSIS OF EXPERIMENTAL RESULTS

The results of the experimental firings that were made in con-
nection with the present study have been recorded on magnetic tape
as pressure-time traces. The present chapter discusses the measure-
ments made from these traces and the conditions under which the
firings were made. The tabulation of these results has been divided
into three sets of tables. The first set of tables contain what
can be termed "raw data" (i.e., the pertinent physical measurements).
The second and third sets include data that has been analyzed by two
different methods. The first part of this chapter discusses these
tables, and the remainder of the chapter is devoted to a discussion
of the criteria used in analyzing the data, concluding with a series
of graphs containing the data.

A. A General Discussion of the Reported Data

Tables 4-9 contain the raw data pertinent to each run, including
the nozzle throat diameter, the initial length of the propellant
samples (L_p), the chamber length (L_{ch}), and the ambient pressure.
Observations of the general behavior of the runs are included as the
range of the mean pressure (the mean pressure during a firing was
not always constant particularly during unstable combustion), and a
brief note as to whether the firing was stable or unstable. The
code which was used for the latter entry is quite simple: C stands

for chuffing; O stands for oscillatory burning; S stands for stable
burning; E means that the propellant extinguished; and U means that
the pressure was uneven or that a form of irregular burning was
apparently present. Each separate table contains data for one pro-
pellant only, and the individual runs are grouped according to nozzle
size beginning with the lowest value of L* and increasing.

The second set of tables contains information concerning the
stability limit as a function of L* and pressure. This limit can be
defined mathematically as the set of conditions at which the growth
factor (η) equals zero or in experimental terms, as the point where
the pressure oscillations begin to decay rather than grow. Therefore,
during the course of a firing, if chuffing or oscillatory burning is
followed by stable burning, then the stability limit has been crossed,
and the value of L* at this limit is the critical L*. Tables 10-73
contain the tabulated values that were determined to be the critical
L* for the various propellants tested and the pressure at which the
evaluation was made. Section D of this chapter describes the method
used to determine values of L* from the pressure-time traces. The
data from these tables have been plotted (see Figure 10) as suggested
by the analysis of Akiba and Tanno [1], and Sehgal and Strand [35]
showing the stability limits for the four propellants, TF, XF, F, and
G. In order to eliminate the confusion that would result from plotting
all of the data points of the different propellants, only the lines
representing the data are shown in the figure. The figure indicates
that the aluminized propellants, XF and TF, are more unstable than
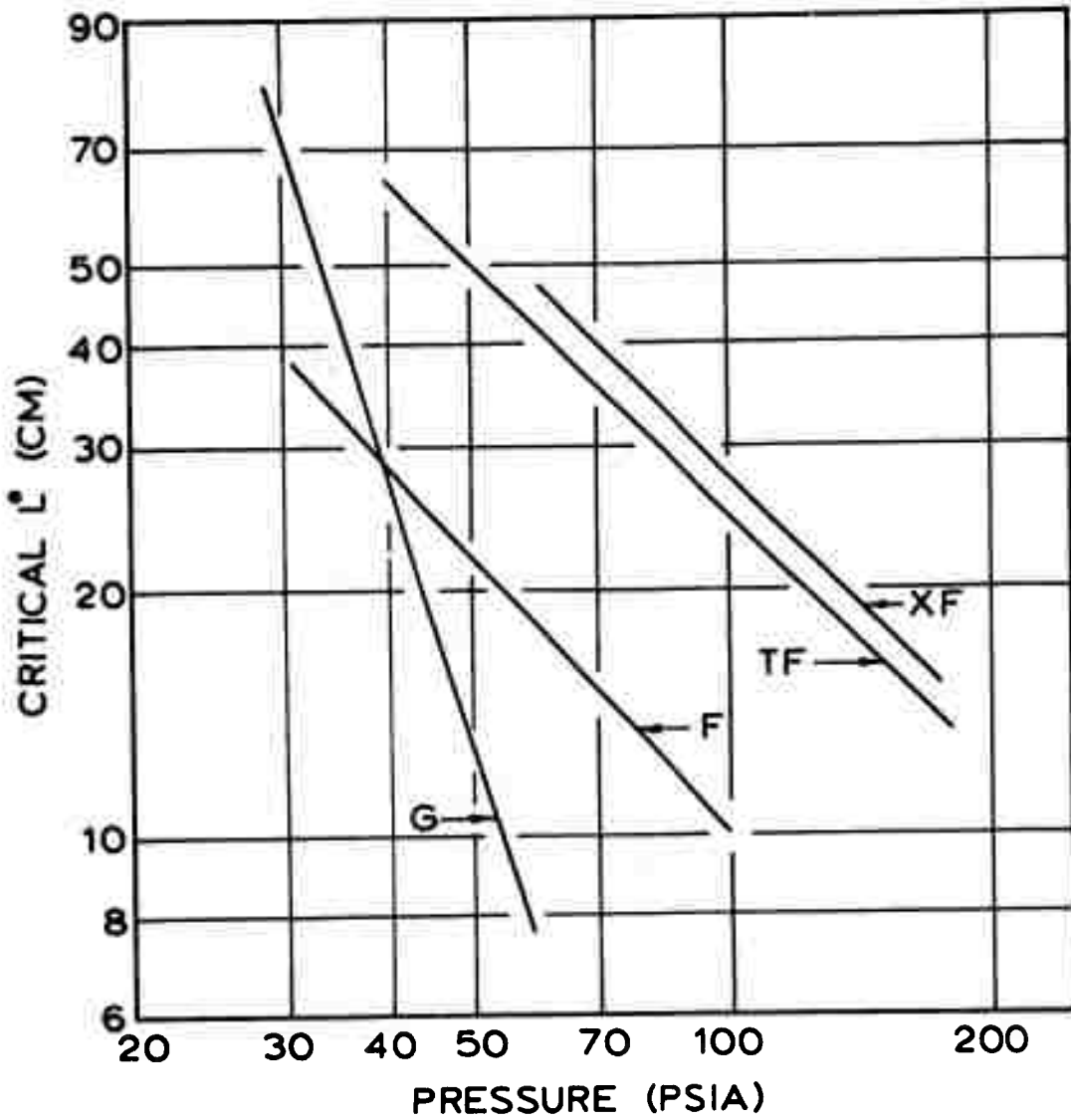
Figure 10. Stability limits of the propellants tested in this
study. Plots represent the best line drawn through the data of
Tables 10-13, Appendix F.

the non-aluminized propellants, and that the slower burning, uncatalyzed G propellant is more stable than the catalyzed propellants.

Tables 14-18 contain the tabulated results of the frequency measurements, the observed pressure, and the L* calculated at the point where the frequency was measured. The dimensionless frequency, γ, and the dimensionless L*, ξ, are also tabulated in these tables. L*-frequency data were not obtained from many firings which exhibited chuffing or oscillatory burning because they were not recorded on the tape recorder, or because the recorder did not function properly. Data from traces that showed evidence of uneven burning or whose pressure varied greatly were not included in these tables even when they were available because of the irregularities involved.

The steady-state burning rate enters into the expressions for both the dimensionless frequency and L*. The value that was used in calculating these dimensionless variables was determined in the following manner: the mean pressure of the oscillations was measured as accurately as possible from the pressure trace, and the linear burning rate was then evaluated for the measured pressure from data that had been obtained previously in strand bomb tests. The burning rate curves for the propellants tested are included in Appendix B with the physical properties.

Table 14 also contains a tabulation of the growth factor, η, that was determined for some of the firings involving TF propellant. The manner of approximating the values of this variable will be explained in Section D of this chapter.

B. **Discussion of Typical Pressure-Time Traces**

The photographs of two pressure-time traces that show the different aspects of non-acoustic instability quite clearly make up Figure 11. The two traces are from firings made with F and TF propellant burning under approximately the same conditions. The first chuff in both traces was of short duration and the second was considerably longer with an oscillating pressure on the crest of the chuff. This indicates that the conditions are in a slightly more stable regime which is in agreement with the observation that stability improves with increasing L* (L* increases as burning progresses). After chuffing twice, both samples reignited and remained burning even though they passed through a period of severe oscillations. From the previous discussion it can be understood that the point at which the amplitude of the oscillating pressure is a maximum defines the stability limit. The oscillations that continued beyond this point were decreasing in amplitude and could, therefore, be considered as occurring in a stable region. This implies that a small perturbation in the pressure would not grow but would be suppressed, and, presumably, that a large disturbance would decay also. Toward the end of the bottom trace such a disturbance occurred causing an immediate increase in the oscillating pressure (i.e., the amplitude did not grow slowly as at the first of the trace). This phenomenon has been interpreted as being due to an air bubble in the propellant or something similar that would cause an almost instantaneous pressure disturbance.

The rapid-fire pressure oscillations at the end of the trace are attributed to uneven residual burning. The reduced burning area
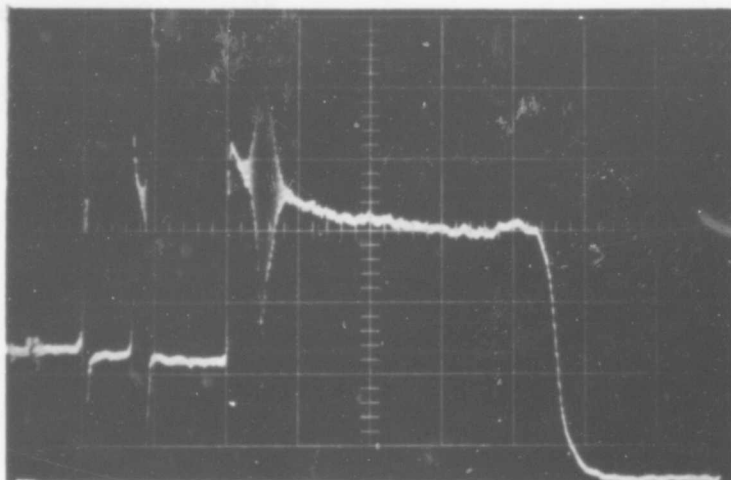
Run No. 410-163   F Propellant
L* range: 8.6 - 46 cm.   P̄ = 70 psia
Ambient pressure: 20 psia
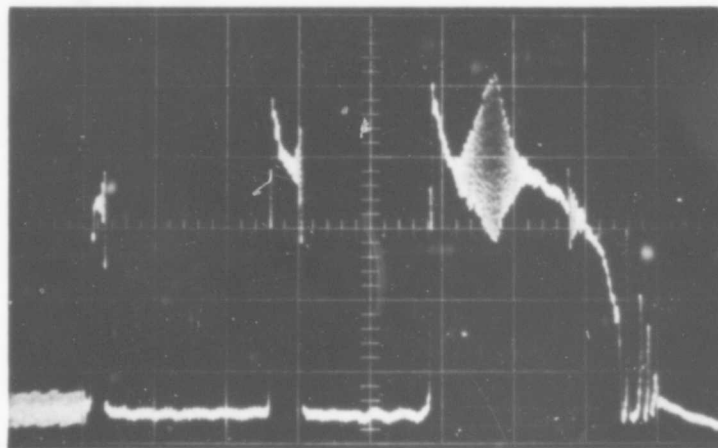
Run No. 48-011   TF Propellant
L* range: 2.0 - 40.6 cm.   P̄ = 78 psia
Ambient pressure: 12.5 psia

Figure 11. Typical pressure-time traces demonstrating NAI.
The ordinate for both photographs is 20 psi/major division and the
time scale is 0.25 sec./major division.

causes the pressure to decrease until it is low enough to enter an unstable regime for the value of L* at those conditions.

It should be pointed out here that the frequency of the oscillations varied throughout the period of instability in both traces. This variation in frequency for changing L* at constant pressure was a general observation for the firings made with F, TF, and XF propellants.

C.   The Anomalous Behavior of G Propellant

The photograph of the trace in Figure 12 corresponds to a firing made with G propellant, and is quite similar in its general nature to those in Figure 11. A difference between this trace and the two previous is that the oscillations attain a "pseudo steady state" where they maintain a constant amplitude, neither growing further nor decaying. This phenomenon is typical of firings made with G propellant. The oscillations would reach a certain amplitude and then continue at that amplitude for a considerable time. Apparently, losses for the slower burning, uncatalyzed propellant were great enough to inhibit further growth in the amplitude of the pressure oscillations. This type of behavior was not observed in firings made with any of the catalyzed propellants.

Another significant difference between this trace and the other two is that the frequency changed very little during the period of constant amplitude oscillations, whereas with the other propellants, the frequency changed continually during a run. This observation was also found to be general for G propellant, whereas no comparable behavior was observed with any of the other propellants. Another
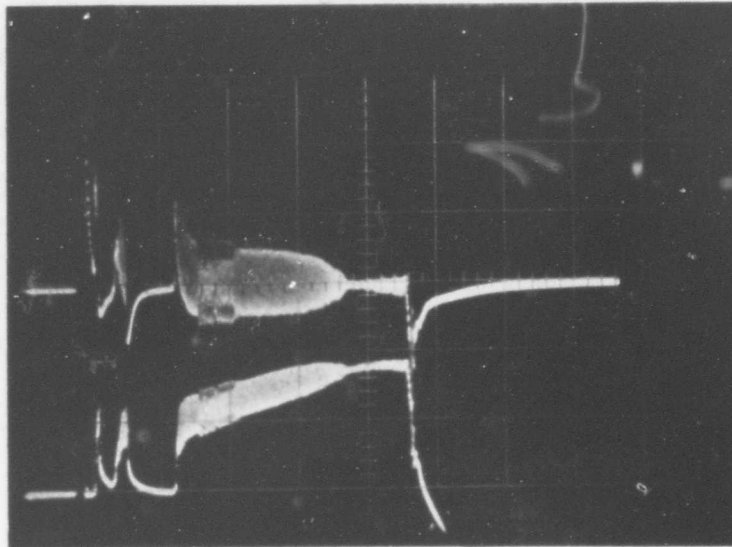
Run Number 39-233   G Propellant
L* range: 13 to 81 cm. $\bar{P}$ = 23 to 30 psia
Top trace: Oscillating component of pressure,
             5 psi/major division.
Bottom trace: Total pressure 10 psi/major division
Sweep rate: 2 seconds/major division

Figure 12. Pressure-time trace for G propellant. Note the constant amplitude oscillations and the slight change in this amplitude near the first part of the firing.

observation that can be made of the trace in Figure 12 concerns the slight change in amplitude that is observed shortly after the initiation of the constant amplitude oscillations. Examination of the expanded trace reveals the presence of what appears to be "beating" or the existence of oscillations of different frequencies. This phenomenon was observed in three or four runs where the physical conditions were essentially identical.

From the above comparison of the firings made with the three propellants (F, TF, and G), it appears reasonable to postulate that the mechanism causing instability is the same for TF and F propellants but is probably different for G propellant. An investigation of the properties of the propellants in an attempt to explain the reason for this difference in behavior shows that the burning rate of G propellant is approximately half that of the other propellants at comparable pressures (see Figure 29, Appendix B). A second difference in the properties of the propellants is involved in their translucence. G propellant is a very light tan color and is slightly translucent to visible light, while TF and F propellants both contain the black-colored copper chromite causing them to be opaque.

In an attempt to determine which of these differences had the greatest effect on the behavior of G propellant, another propellant, designated GB, was compounded having approximately the same burning rate as G but that was opaque to visible light. The opaqueness resulted from adding two per cent carbon black (replacing ammonium perchlorate) to the composition of G propellant. The results of the firings made with this propellant comprise Tables 9 and 18, and show

that it did behave differently from G propellant when fired in similar

conditions. A more complete discussion of the results obtained from

these two propellants will be found later in this chapter.

D. Analysis of Data

The quantitative data that were gleaned from the pressure traces

included the frequency, the L* at locations where the frequency was

measured, the critical L* where applicable, the pressure at those times

when other measurements were made, and for certain runs involving TF

propellant, the growth factor . Although these quantities are not

specifically raw data, they were measured or calculated directly from

the pressure traces and will be referred to as data throughout the remainder

of the text. The frequency was measured from the expanded traces that

were obtained from the play-back of the permanent record made with the

tape recorder. Figure 3 is a typical example of the type of record

that was used for measuring the frequency. Many of the runs contained

chuffs with only four or five cycles of oscillations whose amplitude

was varying widely. For data of this nature, the frequency was measured

over three, four, and five cycles and then averaged.

In order to correlate frequency and L* it was necessary to deter-

mine the value of L* at the same location on the trace where the frequency

was measured. This was done by using a planimeter to integrate the

pressure-time trace. The area beneath the curve of an oscilloscope

trace approximately represents the mass of propellant burned, and the

change in L* is directly proportional to the mass of propellant burned,

assuming that the burning area is constant throughout a firing. This

method of determining values of L* evolves from considering equilibrium mass flow through a sonic nozzle. The resulting equation is

$$m = \frac{A_t}{C^*} \int \bar{P} dt \qquad (4.1)$$

or,

$$\Delta L^* = \frac{1}{\rho_p C^*} \int \bar{P} dt \qquad (4.2)$$

which is to say that the increase in L* over the initial L* is proportional to the area beneath the pressure-time trace. The values of L* at the locations in question were determined by integrating the traces with a planimeter and averaging three such readings.

It has been mentioned previously that the growth factor was approximated for many of the firings involving TF propellant. A standard method of determining coefficients in exponential terms was utilized in calculating the values of η. The double amplitude of the pressure oscillations was plotted verus time on semi-log coordinates. The measured slope of the data plotted in this manner is the growth factor.

A simple, theoretical method of correlating the growth factor with the frequency and L* is not available at the present. Therefore, a trial-and-error method was employed to determine an empirical relationship between these variables. From this study it appeared that the best correlation of the data was obtained by plotting the growth factor versus the reciprocal of the product of the dimensionless frequency and the dimensionless L* to the one-half power. Figure 13 represents data for TF propellant plotted in this manner. Although the
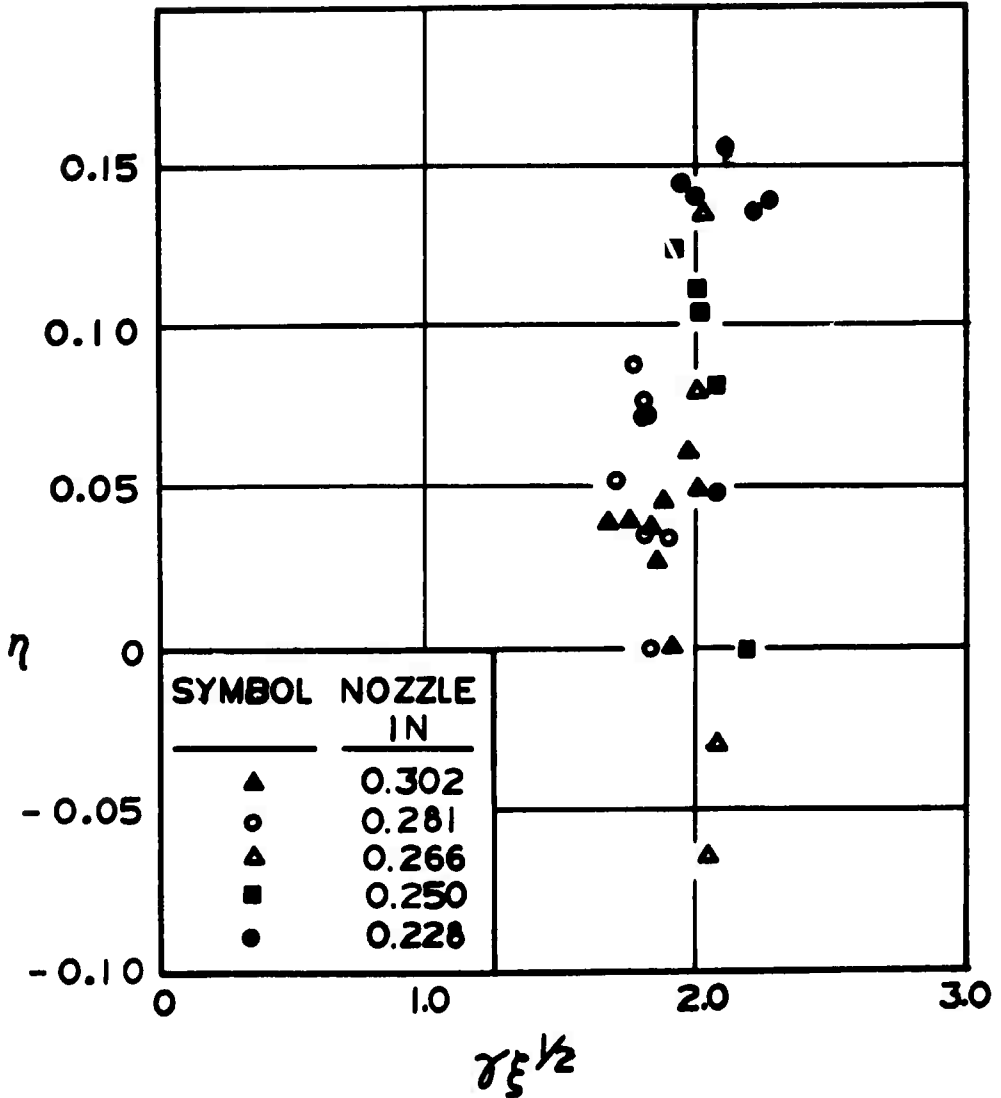
Figure 13. Correlation of the dimensionless growth factor, η, as a function of $1/\gamma\xi^{1/2}$. Data were obtained using TF propellant over a range of pressures.

best line through the data does appear to be curved, for simplicity a straight line through $\gamma\xi^{1/2}$ equal to two could also be considered a reasonable representation of the data. The results obtained from this figure and their application will be discussed more in detail in the next chapter.

The majority of the growth factor values were obtained from series of ten or fewer pressure oscillations with smooth curves drawn through the pressure peaks to define envelopes. (See Figure 3 for an example of the type of expanded pressure traces used.) The precision leaves much to be desired, but is probably better than implied by the heuristic correlation of Fig. 13.

E. Presentation of Experimental Results

There are several methods by which the data obtained in this study can be correlated. Figure 10, containing the data analyzed in terms of a stability boundary, has already been discussed. Data have also been plotted according to the preferred frequency-pressure relationship that was discussed briefly in Chapter I. Figure 14 contains four plots for the five propellants, F, TF, XF, G, and GB. As predicted by the preferred frequency concept, the data fall into fairly narrow band of frequencies for a given pressure. The data obtained with the catalyzed propellants appear to be consistent and not scattered greatly, but the data from the uncatalyzed propellants (particularly G) do not show the same type of trend and are quite scattered. For comparative purposes, data reported by Eisel, et al. [12] for a highly aluminized PBAA propellant have been included with the data for XF propellant. The
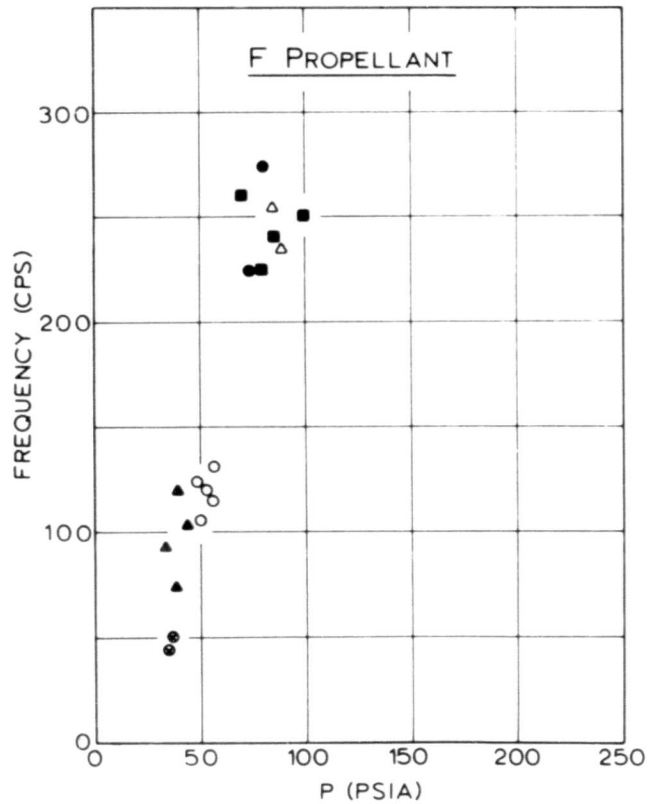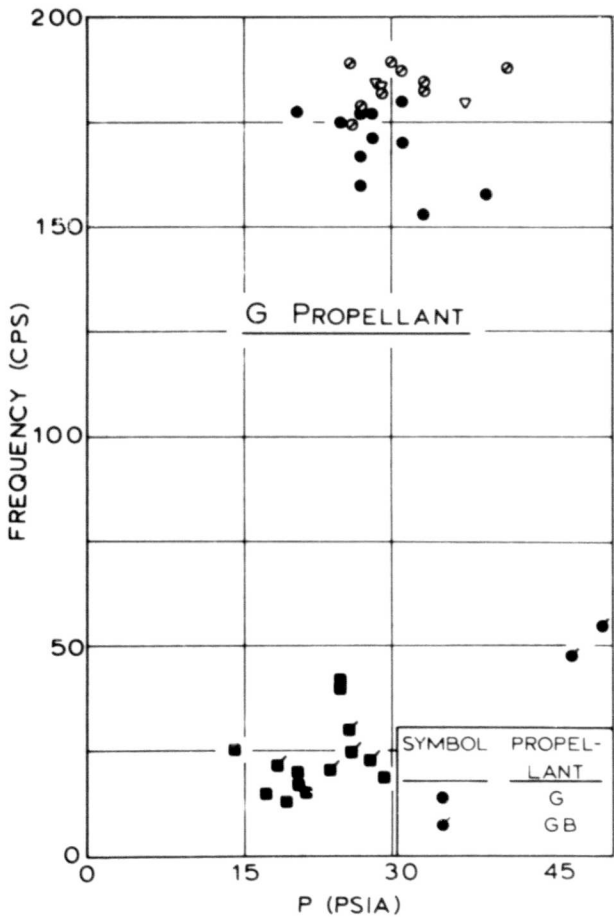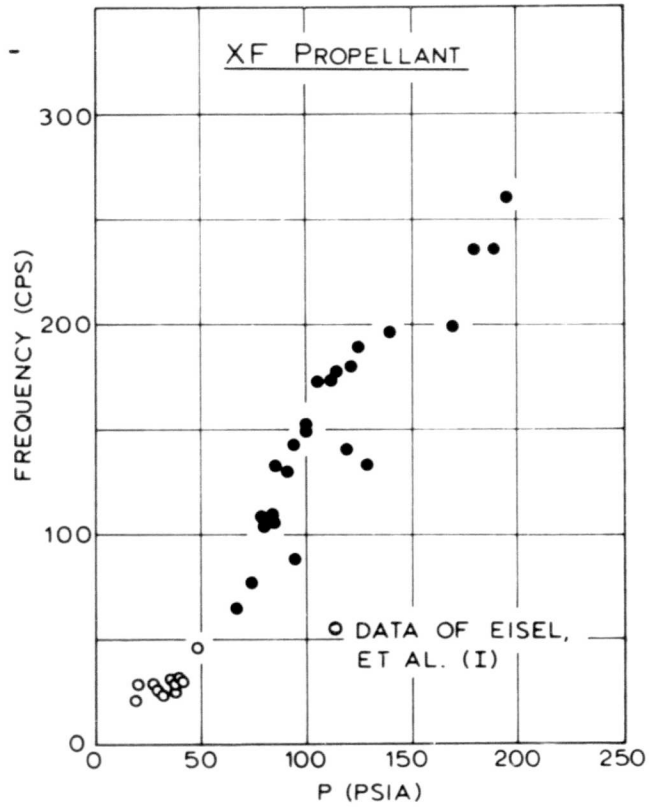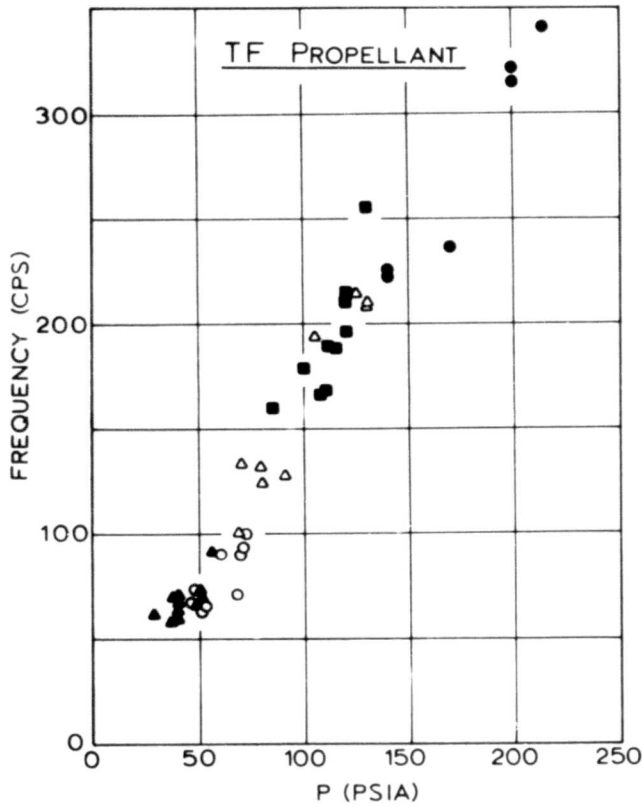
Figure 14. Preferred-frequency pressure plot of data.

from the two propellants are in excellent agreement even though
aluminum content is probably higher for Eisel's propellant than
XF propellant. It appears that this method of correlating instability
.a has merit.

It has been noted previously that the frequency of the oscillations
ried during a firing as L* varied, and the values of L* and the fre-
iencies have been determined for these conditions. Data of this
ature appeared to correlate well when plotted as frequency versus the
reciprocal of L*, and those data obtained for TF propellant have
therefore been presented as Figure 15. The various nozzle sizes,
corresponding to different symbols on the curve, represent different
pressures, and a pressure effect is apparent. This effect was elimi-
nated by using the dimensionless variables as suggested by the form of
Equation (2.19). This equation can be written as

$$\gamma = \frac{1}{\xi} \left[\frac{F \tan \zeta - 1}{F (1-\eta\tan\zeta) + \eta + \tan \zeta} \right] \qquad (2.19)$$

The form of this equation suggests that γ be plotted versus $1/\xi$. Figures
16, 17, and 18 contain the data of TF, F, and XF propellants, respectively,
plotted in this manner. The same symbols have been used for the nozzle
sizes that were used in Figure 15 and these will be used consistently
throughout the remainder of the text. The data of Figure 16 are the
same data that are plotted in Figure 15. A comparison of the two figures
indicates the advantage of using the dimensionless coordinates to elimi-
nate the pressure effect. The data of Figures 16, 17, and 18 extend
over a limited range of frequencies and L*, and, therefore, it is
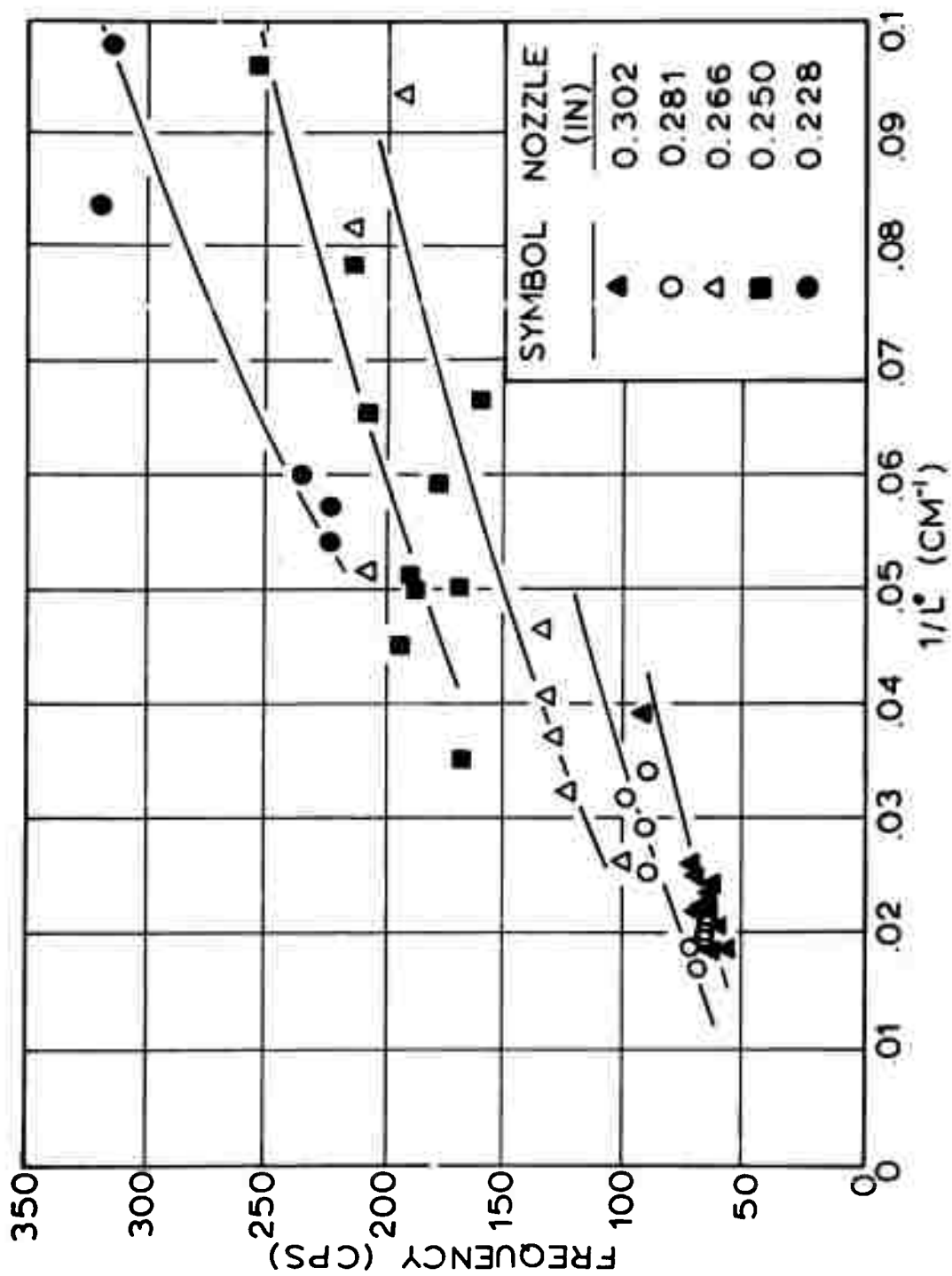
Figure 15. Frequency versus 1/L* for TF propellant. Lines have been drawn through data taken at approximately constant pressure.
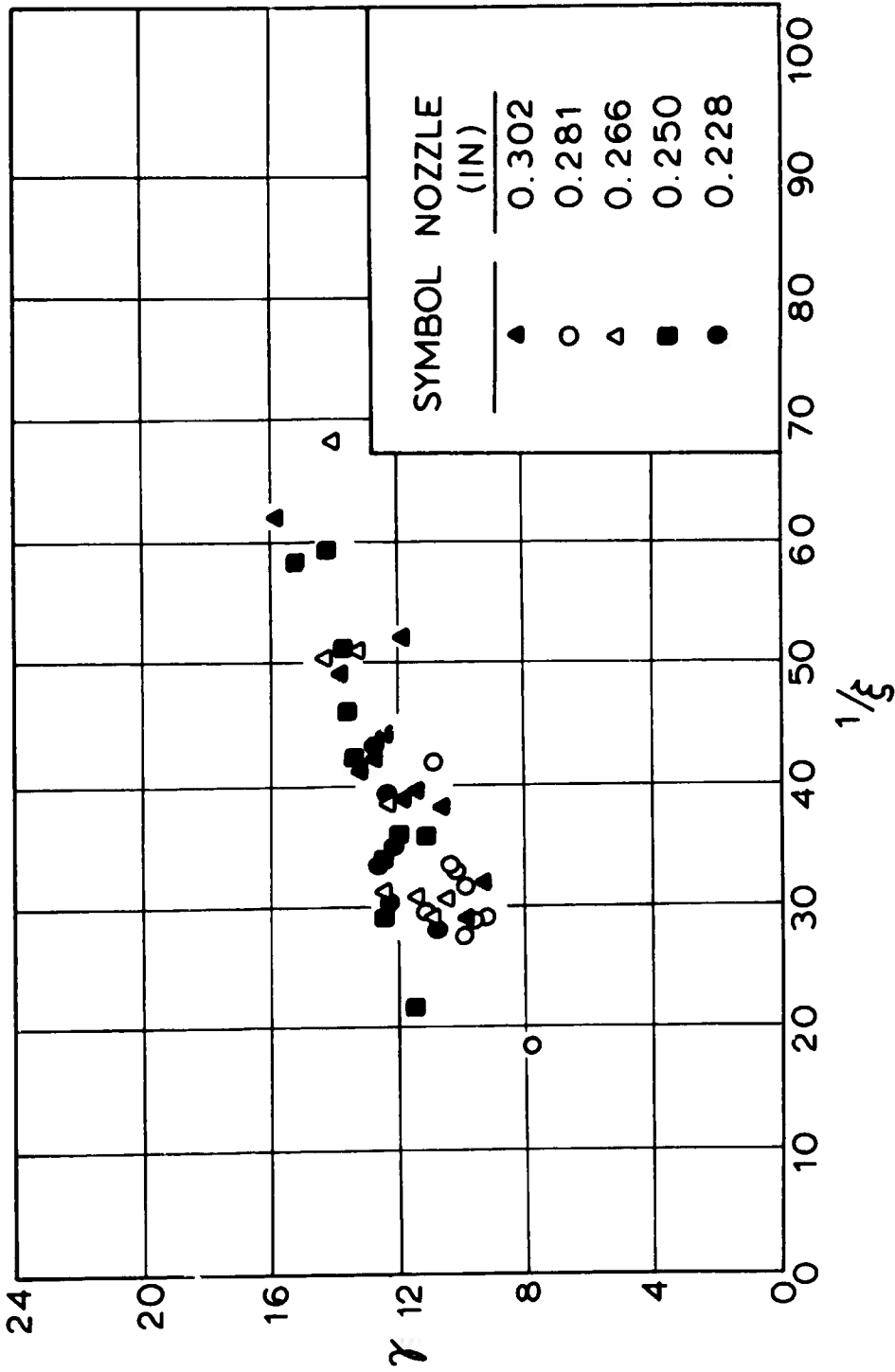
Figure 16. γ versus $1/\xi$ for TF propellant.

SYMBOL	NOZZLE (IN)
◄	0.302
○	0.281
△	0.266
■	0.250
●	0.228
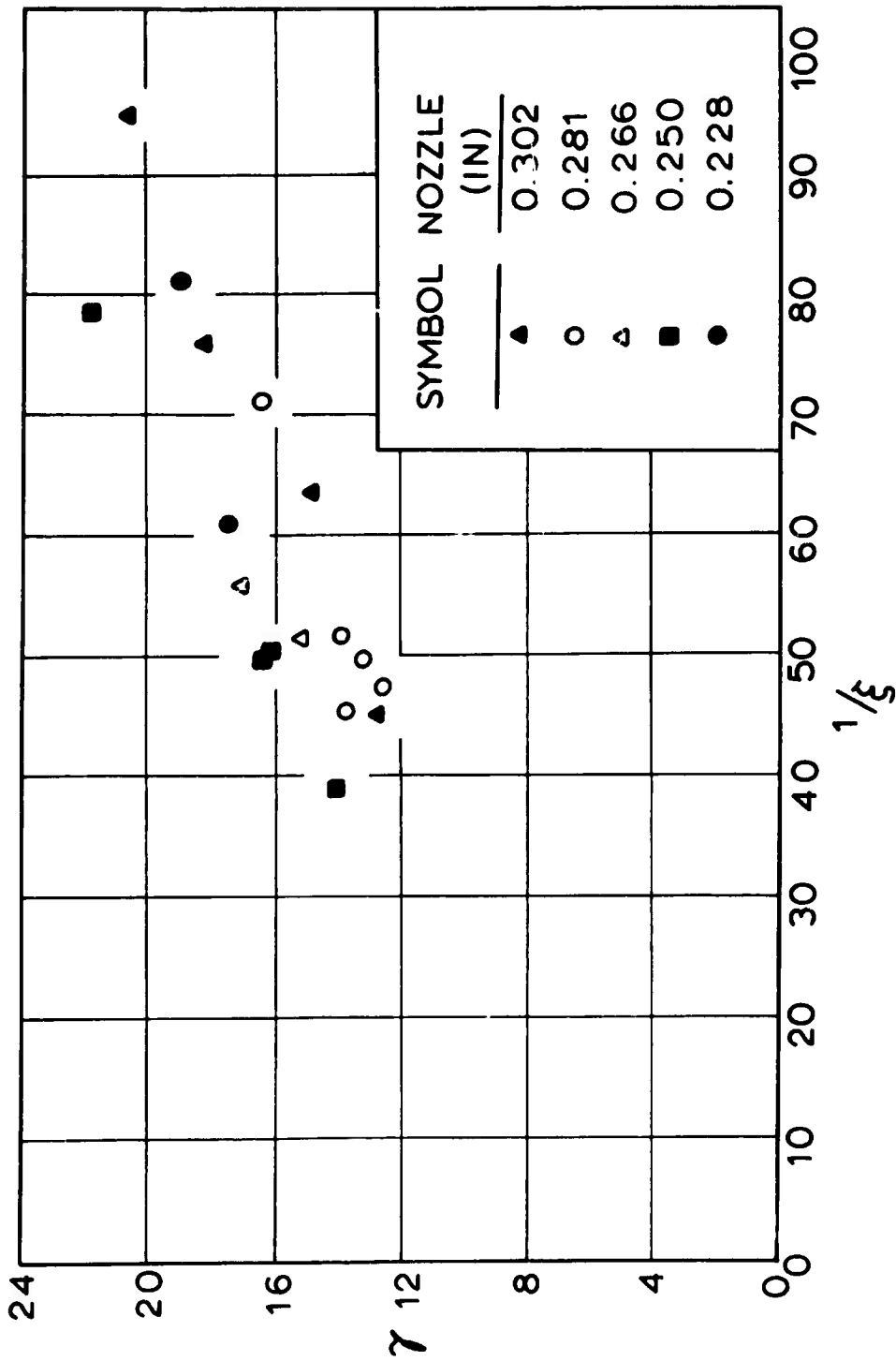
Figure 17. γ versus $1/\xi$ for F propellant.

SYMBOL	NOZZLE (IN)
◀	0.302
○	0.281
△	0.266
■	0.250
●	0.228
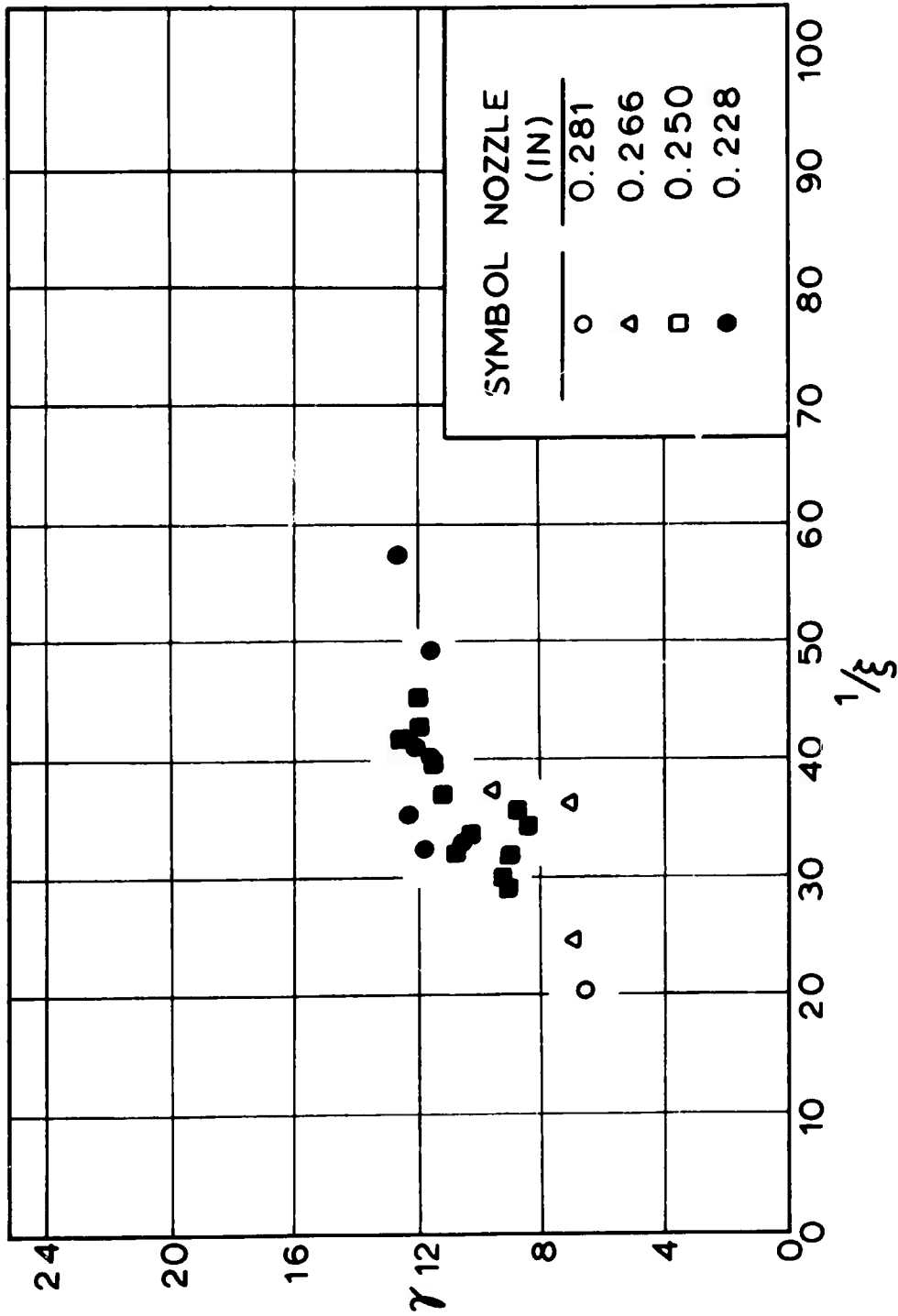
Figure 18. γ versus $1/\xi$ for XF propellant.

difficult to determine the exact shape of the curve. However, in the following chapter the general nature of the curve will be postulated.

It should be noted that small values of $1/\xi$ actually represent large values of L* and are therefore indicative of a more stable regime. Because of this, there are very few data points for $1/\xi$ values of about 30 or less. As the value of $1/\xi$ becomes larger, the value of L* becomes smaller approaching the limiting conditions of the low-L* burner. In terms of experimental results, this corresponds to a region of erratic chuffing where it was difficult if not impossible to obtain firings containing oscillations that were consistent enough to analyze in terms of the frequency and L*.

Figure 19 is a plot of G propellant data on γ - $1/\xi$ coordinates. It is readily observed from this figure that there is a pressure effect of some nature. However, the higher frequency data represent three different nozzles and a pressure range of between approximately 20 to 40 psia, whereas the lower curve (excluding the data of GB propellant) is data representing one nozzle size only, corresponding to a pressure of 20 psia. A precise explanation as to the radical change in frequency with the change in pressure is not readily available at this time. However, as was discussed briefly in Section C of this chapter, data obtained using GB propellant indicate that the transmission of radiant energy through G propellant probably is an important factor. Two of the data points obtained with GB propellant represent firings made at 45 to 50 psia, and even at these comparatively high pressures the frequencies for the run were in the lower range, thus implying that radiation does cause the large increase in the frequency.
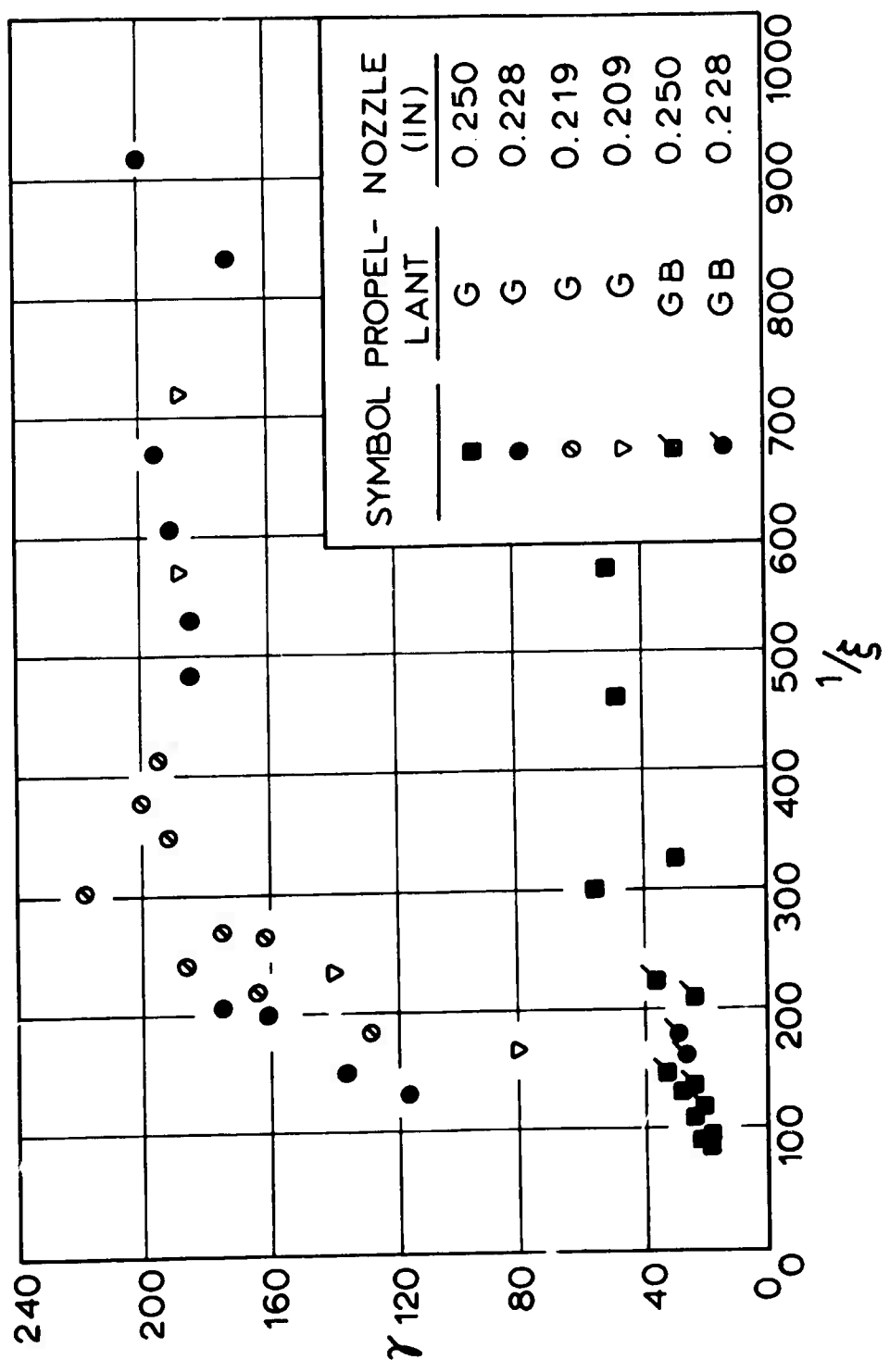
Figure 19. γ versus $1/\xi$ for G and GB propellant.

In order to show the relative location of the different data from the various propellants, the data of TF, F, XF, and GB propellants have been plotted together on semi-logarithmic coordinates in Figure 20 (1/£ being the logarithmic scale in order to better include the data of GB propellant). The data of the three catalyzed propellants seem to fall on essentially the same curve with the GB propellant data at the extreme of the curve. The data of the least stable of the propellants, XF, are found at the left of the plot with the GB propellant data representing the most stable propellant on the right of the plot.

It is impossible to compare the results of the frequency-L* plots with results of other investigators because data of this type have not been reported before. Although other investigators have reported a qualitative influence of L* in studies of NAI, prior to the present investigation a quantitative dependence of non-acoustic frequencies on L* has not been reported. The following chapter contains a comparison of the results of the theoretical analysis made in Chapter II with the experimental results that have been presented in this chapter.
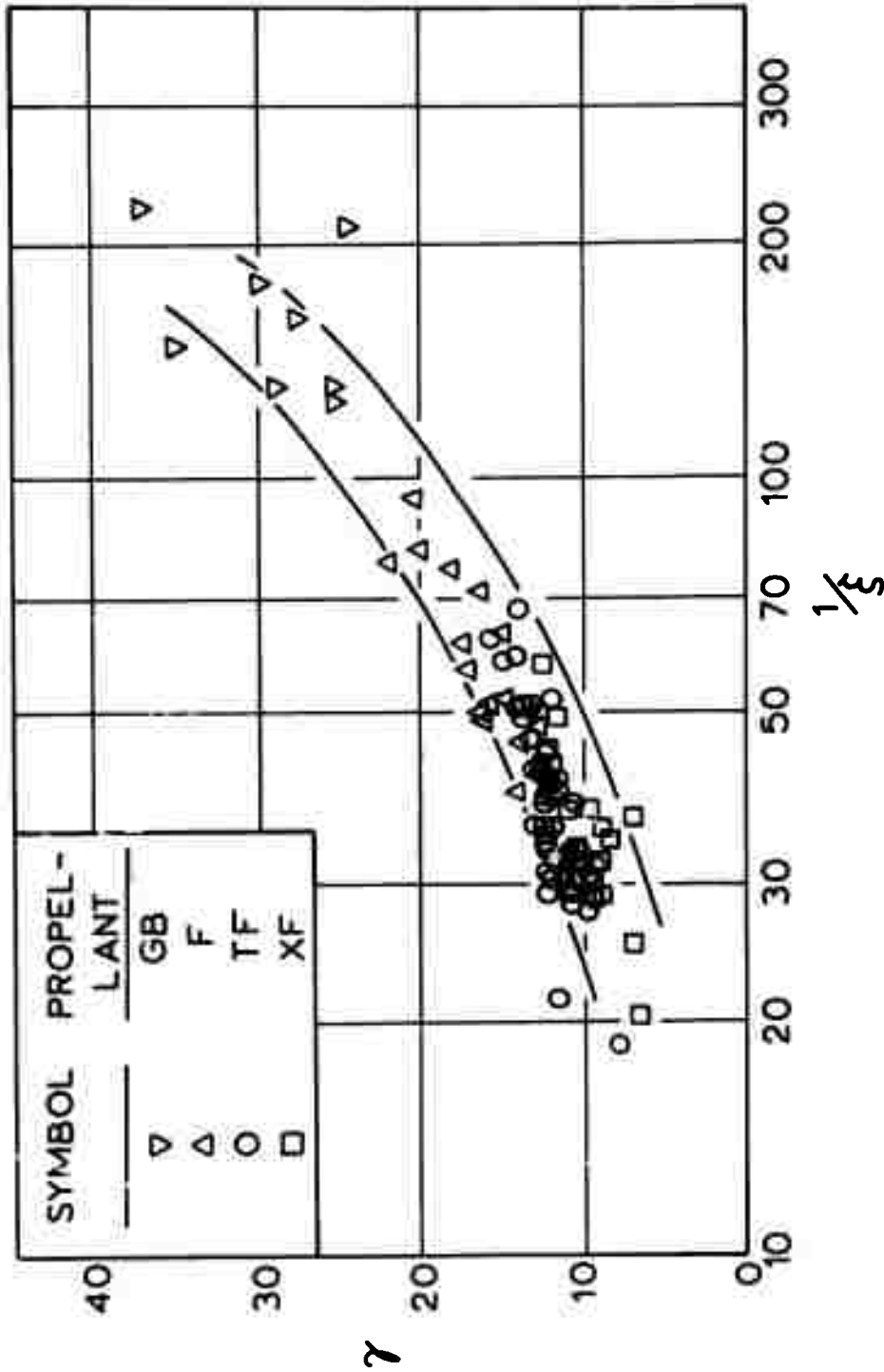
Figure 20. Semi-logarithmic plot of four PBAA propellants. Bounding lines for the data have been included.

CHAPTER V

A COMPARISON OF THEORETICAL AND EXPERIMENTAL RESULTS

FOR TF PROPELLANT

This chapter is devoted to a discussion of the results obtained
from a parametric study of Equations (2.19) and (2.27), and also an
interpretation of the observations. The data obtained from TF pro-
pellant, the most thoroughly studied of the five investigated, have
been used as a reference by which the results of the computations
are judged.

It will be recalled from Chapter II that Equations (2.19) and
(2.27) are analogous equations representing, respectively, the cases
for which kinetic factors and thermodynamic factors regulate the sur-
face reactions. Both equations are of the form

$$1/\xi = \gamma f \ (\gamma, \ \eta, \ \text{parameters}) \hspace{3cm} (5.1)$$

where $f \ (\gamma, \ \eta, \ \text{parameters})$ represents two different functions as
defined by Equations (2.19) and (2.27). These equations formed the
basis of the parametric study and were programed to be run on the IBM
7040 digital computer of the University of Utah Computer Center.
The fortran statements for the two programs have been recorded as
Appendix H in the present work.

A.   A Discussion of the Parameters

The parameters that were varied in this study were the activation energy (E), the mean surface temperature ($\bar{T}_s$), and the heat of gasification (q). It has been noted previously that activation energies have been reported everywhere from 16 to 50 Kcal/mole, with Nachbar and Williams [22] calculating a value of approximately 30 Kcal/mole from a mathematical model for a hot plate experiment taking into account a possible discrepancy in the surface temperature of the plate.

Powling and Smith [23,24] have studied the surface temperature of burning strands of ammonium perchlorate as well as composite propellants. Their studies indicate that the surface temperature of the burning propellant should be between 775 and 900°K for pressures ranging from 20 to 200 psia.

The heat of gasification at the burning surface is not as well defined as the other terms and is therefore much more difficult to measure or evaluate. However, a qualitative range of bounding values can be approximated. The heat of sublimation of ammonium perchlorate is 56 Kcal/mole or approximately 480 cal/gm and can be considered as an upper limit for the heat of gasification. The reactions occurring at the surface involve both the ammonium perchlorate and the fuel binder reacting together as well as the thermal decomposition of the ammonium perchlorate. Heterogeneous reactions between the oxidizer and fuel would tend to be exothermic, thus causing the overall heat of gasification to be considerably smaller (more exothermic) than the heat of sublimation.

These three parameters are implicitly related to and connected with the surface of the burning propellant. Therefore, it might be worthwhile to interject considerations of the real character of the propellant surface. While it is difficult to determine the exact nature of the surface during burning, it is possible to interrupt the burning and observe the quenched surface.

Figure 21 is a photomicrograph of the surface of a sample of propellant that was extinguished during chuffing. The large solid crystals of the perchlorate can be seen protruding well above the fuel binder and rest of the propellant, demonstrating the lack of homogeneity and uniformity at the surface.

In the propellants used in this study, fifty per cent by weight of the ammonium perchlorate in the propellant was coarse material, crystals ranging between 150 to 300 microns in size. Even for the slowest burning propellant, the heated zone adjacent to the burning surface extends only about 200 microns into the solid. Crystals, such as seen in Figure 21, are probably at the initial temperature at one extreme and protruding well into the flame zone at the other. To discuss a value for a surface temperature in the light of such knowledge might appear, and indeed is, naive. However, the tractability of the problem depends upon the assumption that to talk about a surface temperature is meaningful. Some comfort can be taken from the fact that the concept of an ignition temperature, to which the same objections can be raised, has proved to be highly successful in describing the ignition process [for example see reference 32].
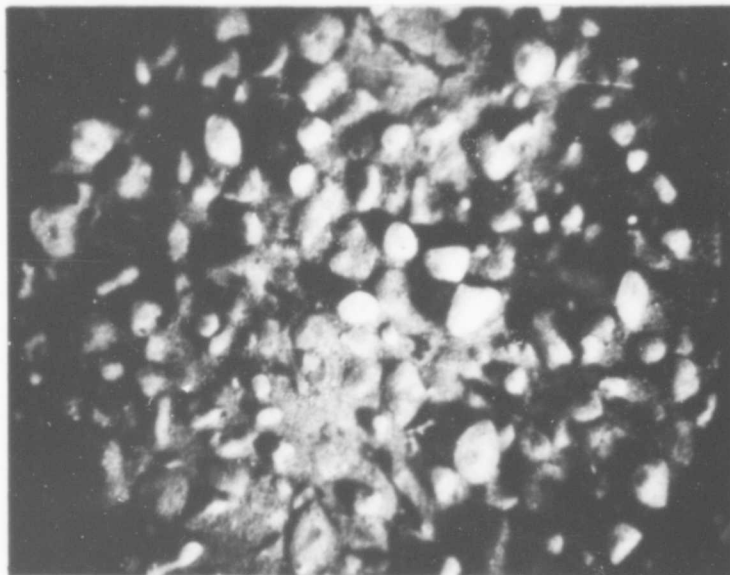
Scale ⊢   ⊢ 1 mm.

Figure 21. The nature of the burning surface. A photomicrograph of the surface of a sample of F propellant which extinguished after burning unstably.

The difficulty in evaluating the heat of gasification can now be better understood. The heat of gasification is the sum of heats of reaction and sublimation for all reactions in which a solid phase participates, including pyrolysis of the binder, the sublimation or thermal decomposition of the perchlorate crystals themselves, and whatever heterogeneous reactions occur.

In the following sections of this chapter, variation of these parameters to produce agreement between Equations (2.19) and (2.27) and the data will be discussed.

B. Theoretical Results for the Kinetic Limited Case

It has been noted several times that Equation (2.19) (or (5.1)) describes $1/\xi$ as a function of γ, η, and the parameters. The assumption that the surface temperature is determined by kinetic factors introduces an activation energy into the theory (see Equation (2.21)), and this activation energy will therefore be included in the discussion of the parameters. Because the stability limit is of primary concern, η has been taken as equal to zero in the discussion that follows except where otherwise noted. The phase shift between the pressure and the energy flux that appears as tangent ζ in the equations has also been taken as zero except where noted.

After varying the value of the heat of gasification over a range of values between -100 to 400 cal/gm, it was determined that values of q near zero gave the best fit of the computer solution with the experimental results. Figure 22 demonstrates the dependency of
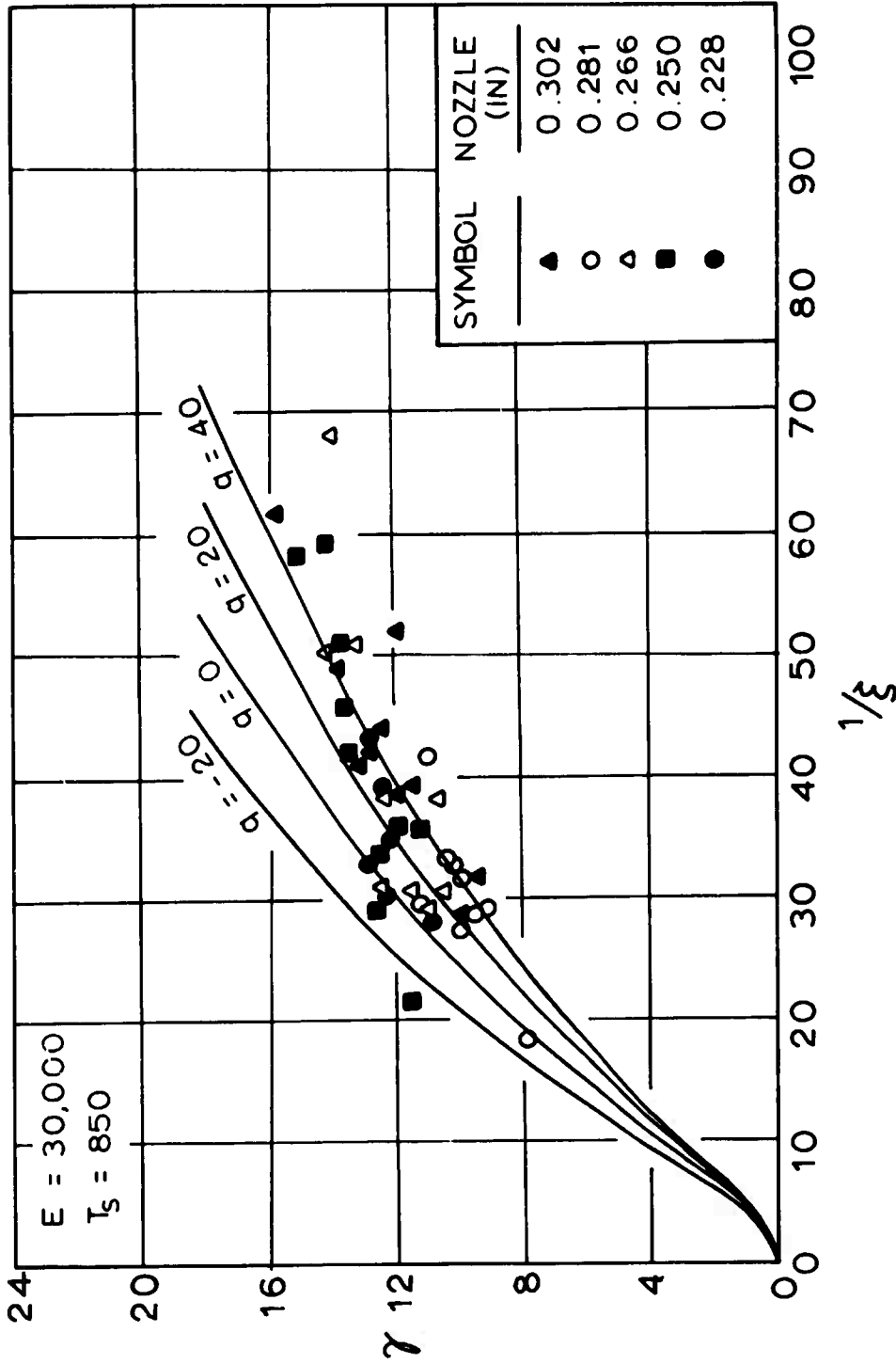
Figure 22. Effect of varying the value of q on the theoretical results ($\eta=0$).

the theoretical curve on the value of q when other parameters are held
constant.

One should keep in mind that the stable regime for combustion
lies to the left of the paper, corresponding to large values of L^*,
and with the growth factor taken as zero, the curves in Figure 22
correspond to stability boundaries. The point where the actual stability
boundary passes through the data points can be determined from the
experimental results. Two of the triangular points in Figure 22
corresponding to the approximate coordinates of γ equal 11 and $1/\xi$ equal
30 were actually located in the stable regime and have negative growth
factors. The remainder of the points on the plot correspond to data
obtained in the unstable regime with a few neutral points. Considering
this and utilizing the results of Figure 13 (the correlation of growth
factor data), the stability limit can be approximately located at the
coordinates mentioned above (i.e., $\gamma = 11$, $1/\xi = 30$).

With this information and referring again to Figure 22 it
appears that the value of q which agrees best with the experimental
results is between 0 and 20 cal/gm. (depending of course on the values
of E and $\bar{T}_s$). The value for the activation energy was varied between
20,000 and 40,000 kcal/mole with the results represented in Figure 23.
The best fit with the experimental results yields a number between
30,000 and 40,000 Kcal/mole. The former may be a more reasonable value
to select considering that it coincides with that reported by Nachbar
and Williams [22].

Figure 24 demonstrates the effect of varying the mean surface
temperature between 750 and 950 K. From the results of this figure
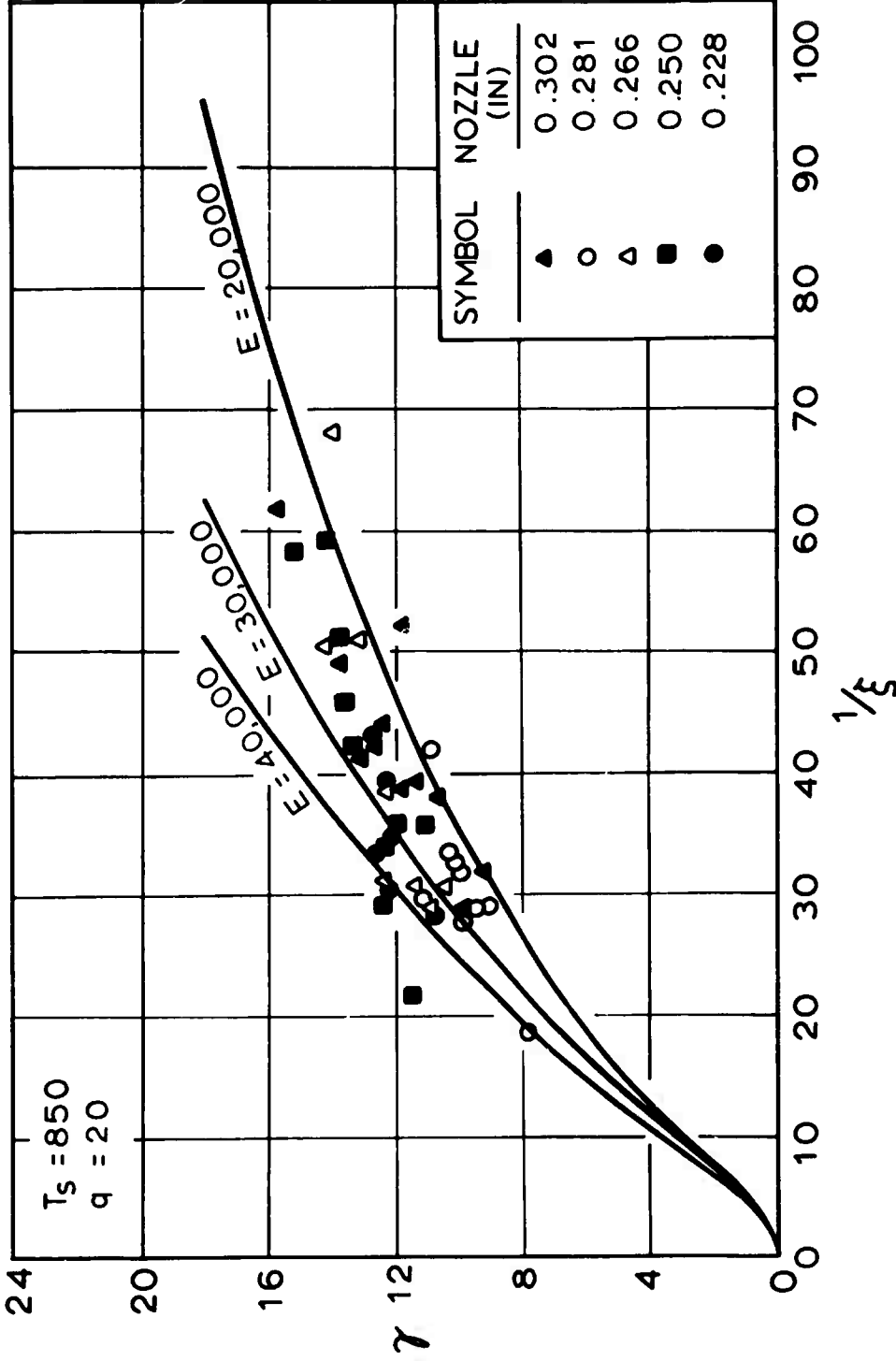
Figure 23. Effect of activation energy on theoretical results ($\eta=0$).
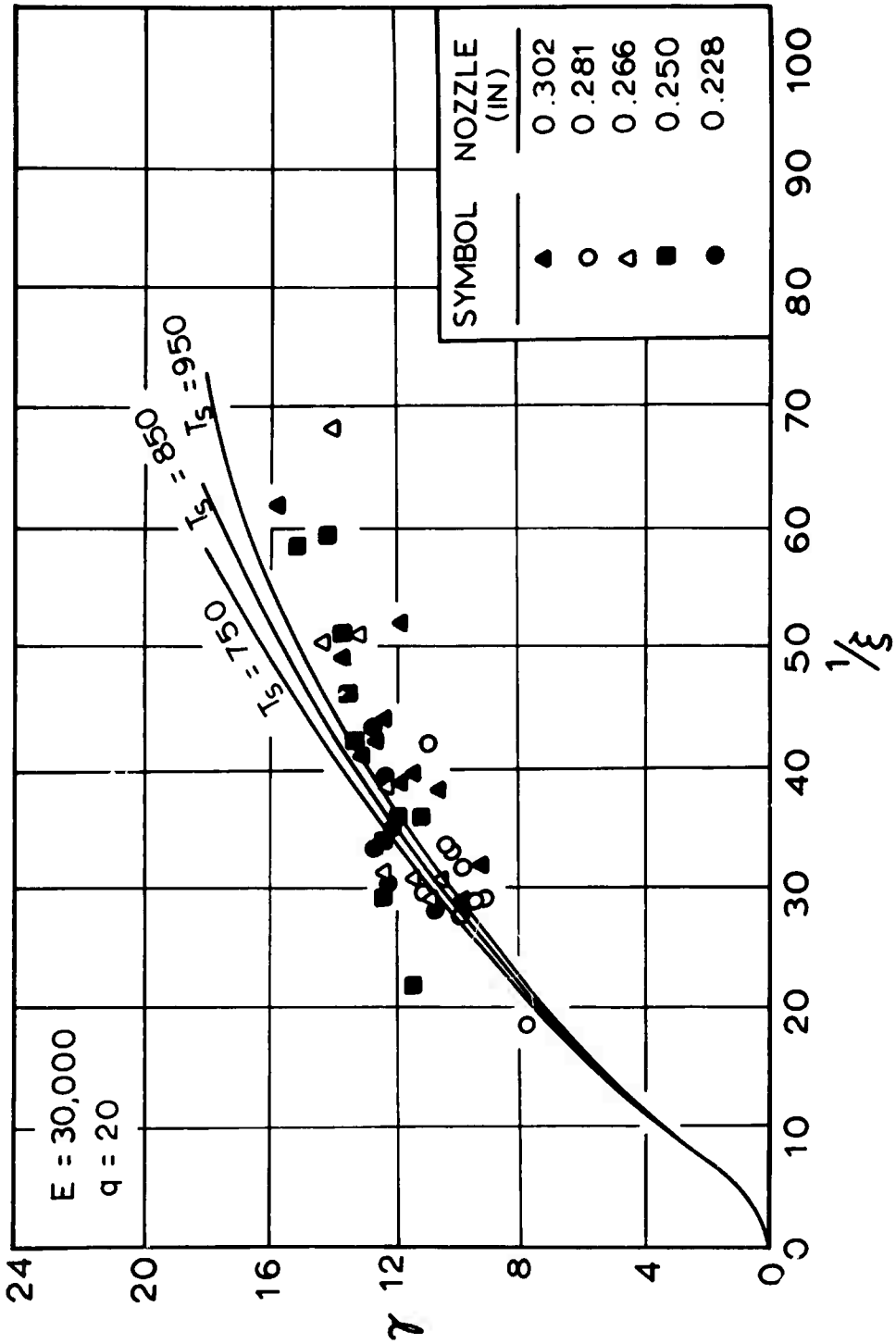
Figure 24. Effect of surface temperature on theoretical results ($\eta=0$).

it can be concluded that the solution of Equation (2.19) is only slightly sensitive to variations in the surface temperature. An average value of 850 K was therefore used in the remainder of the calculations without taking into account the small variation in temperature that occurs with change in pressure level.

The computer curves of Figures 22, 23, and 24 correspond to solutions with the growth factor taken as zero. In the previous discussion it was pointed out that the growth term is zero only at one point of the dimensionless L*-frequency domain, the stability limit. In order to determine the effect of η on the theoretical results, an empirical relationship between η, γ and ξ was obtained by means of Figure 13 in the preceding chapter. If the straight line relationship that was discussed is considered, then Equation (5.2) follows as the mathematical expression corresponding to Figure 13

$$1/\xi = \frac{\gamma^2}{4} \tag{5.2}$$

This equation has been plotted in Figure 25 along with the computer solution to Equation (2.19) using what appears to be the best values of the parameters. The intersection of these two curves should define the stability limit. If the value of q is taken as zero, the intersection of the computer solution with Equation (5.2) occurs at approximately $\gamma = 10$ and $1/\xi = 25$ instead of the location observed in Figure 25. From the above discussion of the location of the stability limit, it can be seen that the value of q should be between 0 and 20 cal/gm. (assuming that the other parameters are correct). The exact location
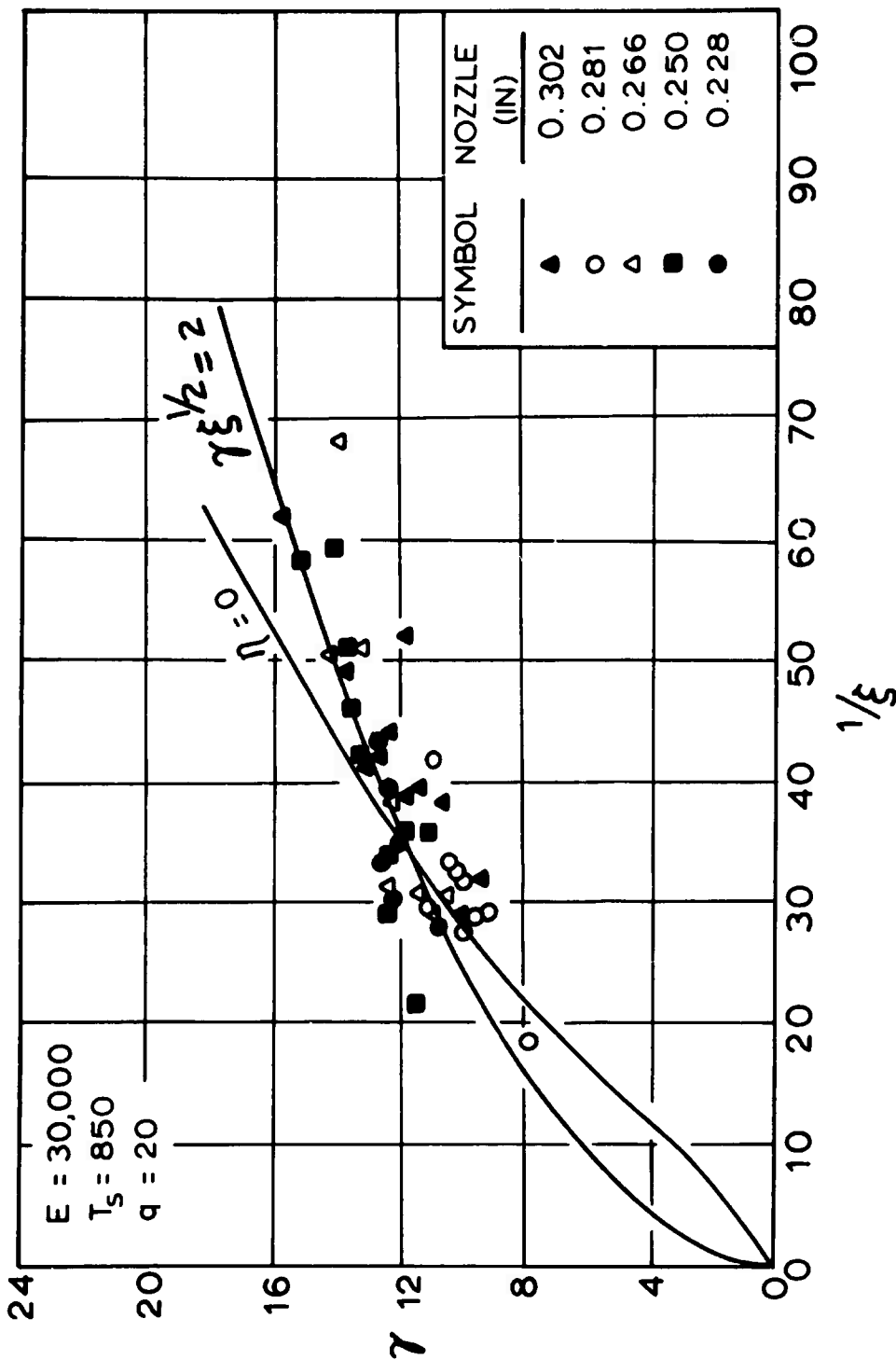
Figure 25. Comparison of theoretical results ($\eta=0$) with the empirical results obtained from growth factor data (the parabolic curve).

of this intersection is determined by Equation (5.2), an empirical
relationship, because a theoretical basis for locating it has not yet
been achieved.

It will be recalled that Equation (2.19) includes a phase shift
between the pressure and the energy flux which was taken as zero in
Figures 22-25. The results of taking the tangent of the phase angle
as 0.3, and the assumed best values of the activation energy and the
surface temperature from the parametric study, have been plotted as
Figure 26. The shape of the curves for various values of q are similar
to those where the phase shift is taken as zero, but larger values of
q are now needed to fit the experimental results better. A small
negative phase shift was also considered, but there were no solutions
to the equation for these conditions. These results indicate that in
order to obtain meaningful results from Equation (2.19), either the
energy flux must lead the pressure by a small positive phase angle
or the two are in phase. This is in agreement with the discussion in
Chapter II, where the relationship between the flux and the pressure
was considered in some detail. It was concluded there that a phase
shift should be small or zero.

C. Theoretical Results for the Equilibrium Vaporization Case

The assumption that the surface temperature is determined by
equilibrium vaporization and subject to evaluation by the Clausius-
Clapeyron equation, introduces a heat of sublimation into the analysis
(see Equations (2.24) and (2.27)). The value of the heat of sublimation
for ammonium perchlorate has been reported in the literature as being
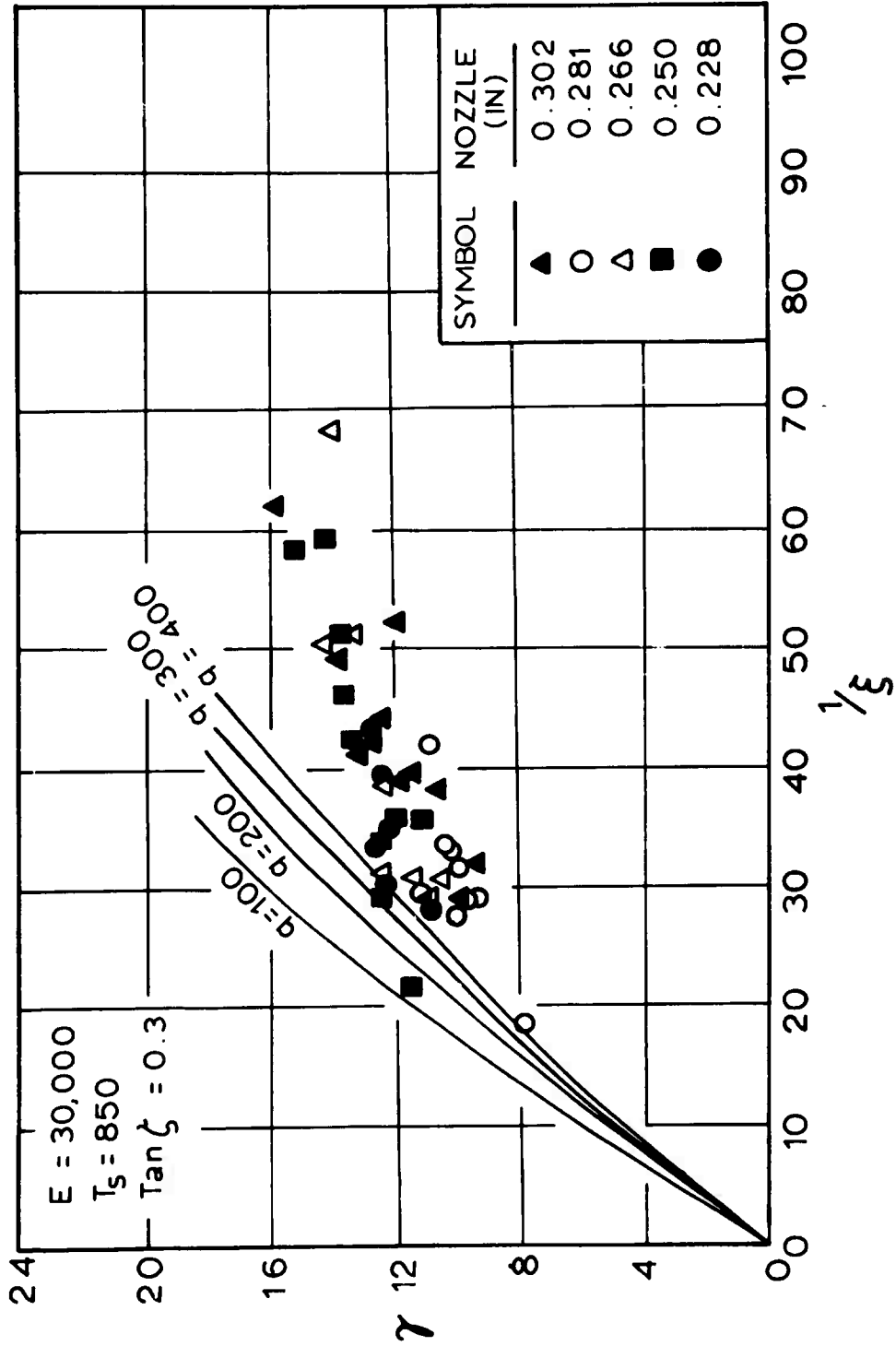
Figure 26. Effect of including a phase shift on theoretical results ($\eta=0$).

56 Kcal/mole [22,23,24], and will not be subjected to the parametric study but will be considered as a known constant. Powling and Smith, who are among those that propose the thermodynamic mechanism, report surface temperatures as a function of pressure [24]. They report values between 775 and 900 K for pressures up to 200 psia, and the appropriate values were used in this particular study, thus excluding another parameter, and leaving only the heat of gasification to be varied.

Figure 27 contains the results of the analysis carried out varying q in Equation (2.27). The curves for q equal to 80 and 100 cal/gm. appear to pass nearest the location of the stability point. Utilization of Equation (5.2) with the results of Figure 27 indicates that the assumption of equilibrium vaporization appears to be valid, at least for TF propellant.

The results of this chapter have been for TF propellant only. The extension and applicability of these results to the other propellants used in this study and other classes of propellants in general will be considered in the next chapter.
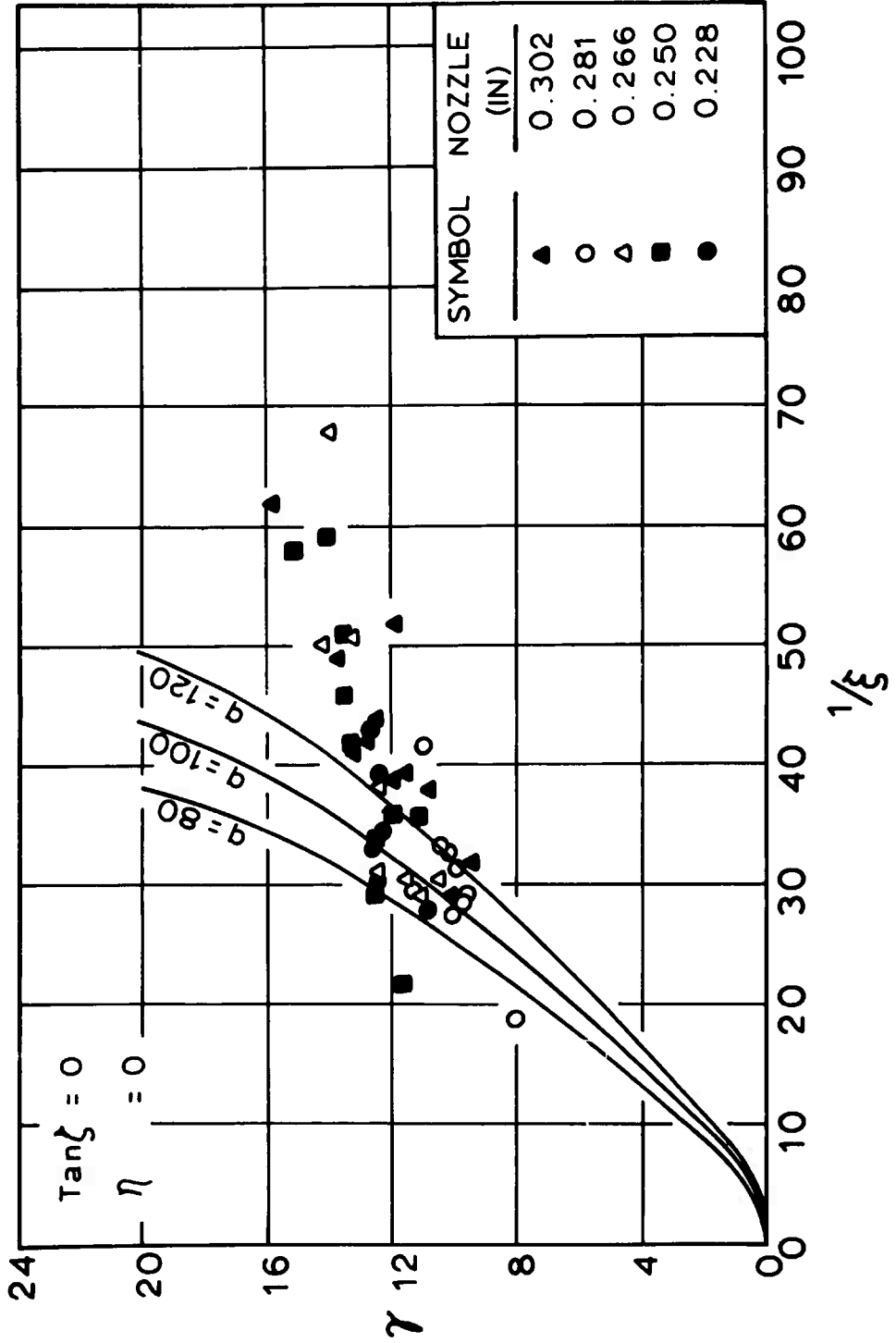
Figure 27. Computer solution for the equilibrium vaporization case, varying q (η=0).

CHAPTER VI

THE OVERALL SCOPE OF THE THEORETICAL RESULTS

The parameters of the theoretical equations have been adjusted to fit the data for TF propellant. We inquire now as to the applicability of these parameter values to the other propellants of this study or to other classes of propellants. An examination of Equations (5.1), (2.19), and (2.18) reveals that the parameters involved are the activation energy, the mean surface temperature, the initial temperature of the propellant, the heat of gasification, and the heat capacity of the solid. The initial temperature is arbitrary and can be considered as a constant for present purposes. The heat capacity varies slightly among propellants and actually enters into the calculations in a rather minor way, so that variations in this quantity can be ignored. This leaves the three parameters that have already been discussed in some detail. It can therefore be concluded that the curves in Figures 22 through 27 apply to any propellant whose parameters have the values specified for the individual cases. The questions now arise as to whether these parameter values vary from propellant to propellant, and if so, to what extent.

A. The PBAA Propellants Used in this Study

For convenience, the definition of the dimensionless L* and frequency are repeated here as Equation (6.1)

$$\pi = \frac{4\alpha\omega}{\bar{r}^2}$$

$$\xi = \frac{C*\bar{r}^2 L*}{4\alpha R T_f}$$

(6.1)

From these definitions it can be seen that other properties of the propellant, particularly the burning rate, enter into the calculations of the dimensionless variables and therefore contribute to the location of the points along the curve.

If it is assumed that propellants F, XF, and GB have the same activation energy, surface temperature, and heat of gasification as propellant TF the remarks of the previous chapter apply to these propellants also. From Figure 28 it can be seen that the results for various propellants follow the same trend, the difference in propellants being mainly in the general location of data points along a common correlating line. The aluminized propellants fall further to the left on the dimensionless plot, while the non-aluminized propellants are shifted to the right. It will be recalled that the termination of these points determines the stability limit, which is of prime interest and will now be considered further.

In Figure 28 the upper curve (marked q=20) is the computer solution of Equation (2.19) with an activation energy of 30,000 Kcal/mole, a surface temperature of 850 K, a heat of gasification of 20 cal/gm., and the growth factor taken as zero. We assume for the moment that the same parameter values apply to F, XF, and GB propellants as well as TF propellant. The second curve is the empirically determined relationship for TF propellant that was obtained from the growth factor data for
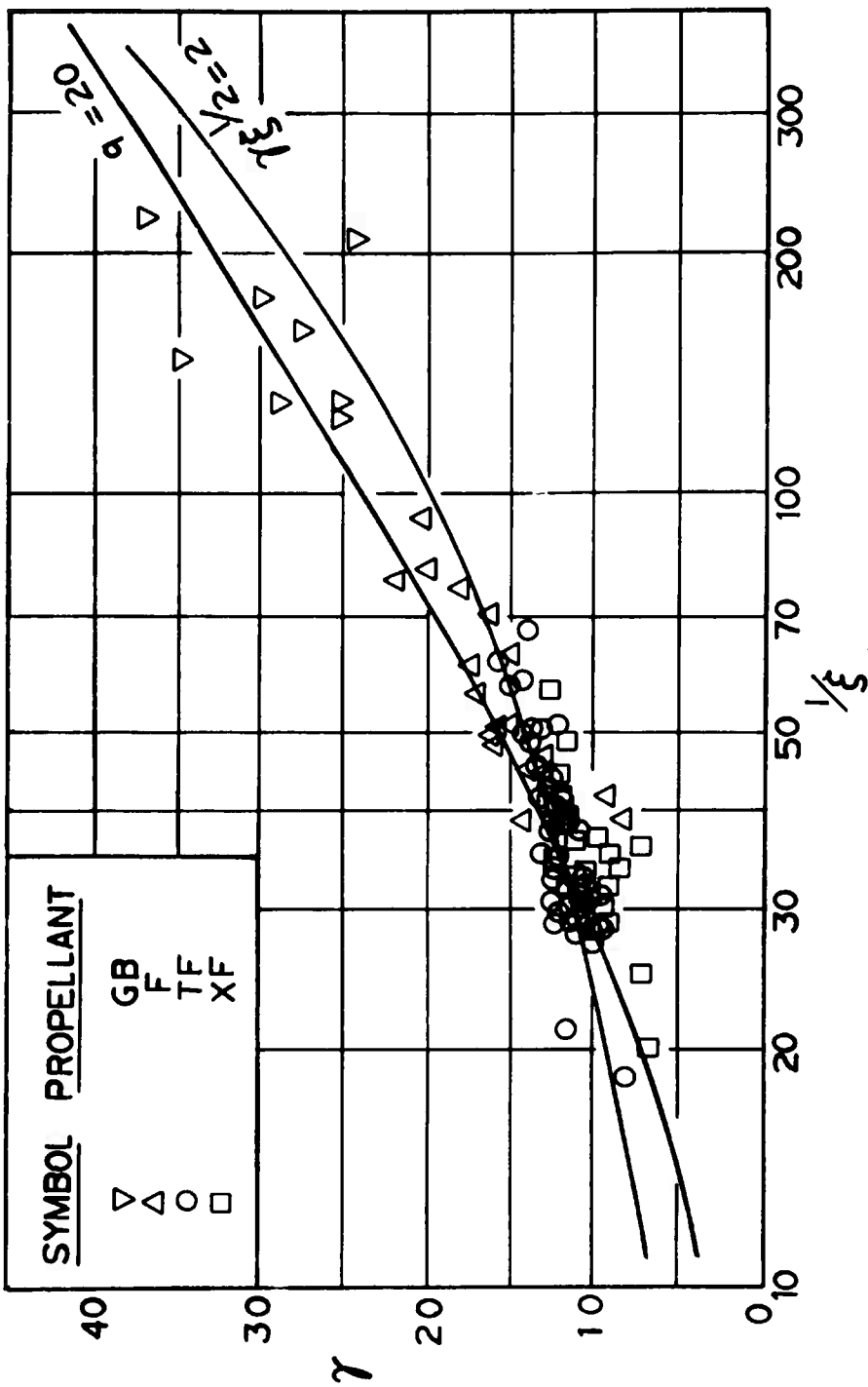
Figure 28. A comparison of the data from the four PBAA propellants with the computer solution for E = 30,000, $\bar{T}_s$ = 850, q = 20, and η = 0. The empirical relationship of Figure 13 has also been included.

that propellant, Equation (5.2). The intersection of these two curves should be the stability limit for TF propellant. The empirical relationship appears to follow the trend of all the data quite well, so that if it were assumed that the same relationship held for all four propellants, then there would be a unique stability limit for the four propellants. The experimentally determined fact that the stability limit varies from propellant to propellant indicates that one of two possibilities exists: either (1) the empirical relationship does not hold for all of the propellants, or (2) the values of the parameters change from one propellant to the next. Actually a third possibility exists in that both of the preceding two could be true.

Recalling the nature of the heat of gasification term, it could well be suspected of being different for various propellants. The activation energy is probably different also, particularly between catalyzed and uncatalyzed propellants.

The data at hand do not allow obtaining growth factor values for propellants other than TF. The fact that Equation (5.2) fits the γ vs. $1/\xi$ data for the other propellants quite well could imply that an expression of this type might be general for a class of propellants.

Further investigation is necessary to determine the effect of propellant composition upon the above-mentioned parameters, and the nature of the relationship between γ, ξ, and the growth factor.

B. Extension of the Theory to Other Propellants

In the preceding chapter it was shown that variations in the surface temperature and the activation energy have a very slight effect

on the theoretical results. Also, it is probably true that the values
of these parameters depend to a large extent on the nature of the oxidizer
and are fairly independent of the binder in the propellant (for example,
see [4] and [22]). This would tend to indicate that the values used
for these parameters would be approximately the same for ammonium per-
chlorate propellants using a binder other than PBAA. Therefore, the
location of the theoretical curve appears to be dependent on the value
of the heat of gasification more than any other parameter. This con-
clusion does not seem unreasonable when one considers the nature of
the term. It must be dependent upon the binder of the propellant
and the manner in which it reacts with the oxidizer, and is probably
influenced by metal additives in the propellant also.

The present study has been involved with composite propellants,
but it is reasonable to assume that the analysis could be applied to
double-base propellants without difficulty. The values of the surface
temperatures, activation energies, and heats of gasification for these
propellants are considerably different from those for composite pro-
pellants, but so are the stability limits (L^* as high as 5000 cm. [20]).
The use of the correct values for these parameters with Equation (2.19)
(evaluating θ_0/β properly) should give reasonable results.

CHAPTER VII

SUMMARY AND CONCLUSIONS

The objectives of the present study were twofold: to investigate non-acoustic instability experimentally, determining stability limits for the reference propellants, and to attempt a mathematical explanation of the experimental observations. The present chapter will include a discussion of these two objectives plus a comparison of the theoretical implications of the study with the experimental observations of other investigators.

A. Experimental Observations

The experimentally determined stability limits have been presented as Figure 10. The results of this figure indicate that the more highly aluminized propellants are more unstable and the uncatalyzed G and GB propellants appear to be the most stable of the propellants in terms of the pressure-L* domain.

It was observed that non-acoustic frequencies are dependent on the value of L* and can be correlated by plotting frequency versus the reciprocal of L* (see Figure 15). Using the dimensionless coordinates of γ and $1/\xi$, the pressure effect of the frequency-L* dependency was eliminated. Figure 20 shows the data obtained using TF, F, XF, and GB propellants plotted on the dimensionless coordinates. The data from the four propellants fall within approximately the same bounds, being grouped

according to the respective propellants. The general trend is for frequency to increase as L* decreases.

One of the propellants tested, G, behaved quite differently from the others and the data obtained for this propellant did not correlate with those obtained for the others. The results for G propellant are graphically displayed in Figure 19. It is thought that this discrepancy is probably due to the effects of radiation (G propellant is slightly translucent); therefore, its composition was modified slightly to include carbon black in an attempt to eliminate these effects. The data of GB propellant, that containing the carbon black, do correlate with the data of the other propellants, and therefore it is felt that the discrepancies observed in the data of G propellant were in fact due to radiation.

Assuming that the growth of the pressure oscillations was exponential, growth factors were calculated from the pressure time traces. A correlation between these and the dimensionless frequency and L* indicated a relationship almost independent of the growth factor (see Equation (5.2) and Figure 13). This correlation was used to locate the stability limit for TF propellant with respect to the dimensionless coordinates.

B. Theoretical Results

The theoretical analysis that was developed in Chapter II is based on an energy balance for the solid propellant considering energy accumulation in the solid and a mass balance on the rocket chamber considering mass accumulation in the gas phase. The analysis is based on the

assumption that oscillations grow from small perturbations. Two other assumptions which are very important in the analysis are: (1) the burning surface is homogeneous and uniform, and (2) the phase lag between the pressure and the energy flux is small or zero.

The analysis thus developed, reduces to an expression of the form

$$1/\xi = \gamma \; f \; (\gamma, \; \eta, \; \text{parameters}) \tag{5.1}$$

The principle parameters involved are the activation energy, the mean surface temperature, and the heat of gasification. The parametric study discussed in Chapter V indicates that an activation energy of 30,000 Kcal/mole, a surface temperature of 850 K, and a heat of gasification of between 0 and 20 cal/gm. result in the best fit of the experimental results, although other combinations of the parameter values fit quite well also. The values of the first two of these parameters are comparable to those reported in the literature. The value for the heat of gasification appears to be the right order of magnitude even though this quantity has not been measured experimentally.

The fact that the theoretical analysis results in an expression that agrees quantitatively with the experimental results tends to vindicate the analysis and its attendent assumptions.

The analysis was developed considering composite propellants but should be applicable to double-base propellants as well.

C. A Comparison with the Results of Other Investigators

The theoretical results of this study with the best-fit parameters are concisely presented in Figures 25 and 28, and can be used

to describe the results reported by others in a qualitative manner.

Considering first the theory developed by Akiba and Tanno and extended by Sehgal and Strand, it is observed that with the aid of the empirical relationship relating the growth factor to the frequency and L*, Figure 13, a stability limit can be determined. The value of L* at that limit is

$$L^*_{cr} = \frac{4\alpha RT_f}{C^* \bar{r}^2} \; \xi_{cr} \qquad (7.1)$$

This is essentially the same equation that is developed by the above authors with ξ_{cr} replaced by a theoretically determined τ_{cr}. Thus the present analysis appears to be compatible with the results of the Akiba-Tanno theory.

Yount and Angelus [40] have observed little or no dependency of frequency upon L*. It would appear to the author that they are probably operating at small ξ values where it appears (see Figure 25) that the frequency exhibits very litttle dependency on L*.

Price et al. report data from their low-L* burner in terms of the preferred frequency concept that has been discussed to some extent already (see Figure 14). This also is in qualitative agreement with the results of the present investigation. Figure 15 is a plot of frequency versus the reciprocal of L* and the lines through the data represent constant pressure lines for an idealized system (as predicted by the theory). If one follows along a constant pressure curve beginning at the stability limit (which corresponds to a particular frequency), the frequency increases as L* decreases until what has an appearance of

being an asymptotic limit is reached for a very small L^*. One obtains
a band of frequencies having values between those corresponding to the
stability limit and the "asymptotic" limit. An increase in the pres-
sure would result in another band of frequencies at a higher level,
the result being the preferred frequency concept.

In conclusion it can be noted that although the observation and
prediction of a frequency-L^* dependency reported in the present investi-
gation may appear somewhat radical (in that it has not been reported
before), it is not contradictory with the results of previously reported
work. In fact it is complementary to the results of other investigators
and tends to correlate somewhat the apparently unrelated results that
have been reported up to the present time.

LIST OF REFERENCES

(1) Akiba, R., and Tanno, M., "Low frequency instability in solid
      propellant rocket motors," Proceedings of the First Symposium
      (International) on Rockets and Astronautics (Tokyo, 1959),
      pp. 74-82.

(2) Anderson, F. A., Strehlow, R. A., and Strand, L. D., "An experi-
      mental investigation of the low pressure combustion limits
      of some solid propellants," T. M. No. 33-134, Jet Propulsion
      Lab., Pasadena, California (1963).

(3) Angelus, T. A., "Panel discussion on solid propellant combustion
      instability," Eighth Symposium (International) on Combustion
      (Williams and Wilkins Co., Baltimore, Md., 1962), pp.921-924.

(4) Arden, E. A., Powling, J., and Smith, W. A. W., "Observations on
      the burning of ammonium perchlorate," Combustion and Flame 6,
      21-33 (1962).

(5) Bartley, C. E. and Mills, M. M., Solid Propellant Rockets, in
      section H, volume II of High Speed Aerodynamics and Jet
      Propulsion, ed. C. duP. Donaldson (Princeton University Press,
      Princeton, N. J., 1950), pp. 87-91.

(6) Blair, D. W., Bastress, E. K., Hermance, C. E., Hall, K. P., and
      Summerfield, M., "Some research problems in steady-state burning
      of composite solid propellants," Progress in Astronautics and
      Rocketry, Vol. 1: Solid Propellant Rocket Research, ed. M.
      Summerfield (Academic Press, New York, 1960), pp. 183-206.

(7) Cantrell, R. H., McClure, F. T., and Hart, R. W., "Effects of
      thermal radiation on the acoustic response of solid propellants,"
      Rept. No. TG-335-18, Applied Physics Lab., Silver Springs,
      Md. (1964).

(8) Coates, R. L., "A quantitative experimental study of the oscillatory
      combustion of solid rocket propellants," unpublished Ph.D.
      thesis, University of Utah, Dept. of Chemical Engineering
      (Salt Lake City, Aug. 1962).

(9) Coates, R. L., personal communication, Lockheed Propulsion Co.,
      Redlands, Calif. (Oct. 1964).

(10) Clemmow, D. M., and Huffington, J. D., "An extension of the theory of thermal explosion and its application to the oscillatory burning of explosives," Trans. of the Faraday Soc., 52, 385-394 (1956).

(11) Ecker, E. R. G., and Drake, R. M., Heat and Mass Transfer (McGraw-Hill Book Co., Inc., New York 1959), p. 383.

(12) Eisel, J. L., Horton, M. D., Price, E. W., and Rice, D. W., "Preferred frequency oscillatory combusion of solid propellants," AIAA J. 2, 1319-1323 (1964).

(13) Frank-Kamenetskii, D. A., Diffusion and Heat Exchange in Chemical Kinetics (Princeton University Press, Princeton, N. J., 1955) Chaps. 6 and 7.

(14) Gorring, R. L., and Churchill, S. W., "Thermal conductivities of heterogeneous materials," Chem. Eng. Prog. 57, 53-59 (1961).

(15) Green, Leon, Jr., "Some properties of a simplified model of solid propellant burning," Jet Propulsion 28, 386-392 (1958).

(16) Hart, R. W., and Cantrell, R. H., "Amplification and attenuation of sound by burning propellants," AIAA J. 1, 398-404 (1963).

(17) Hart, R. W. and McClure, F. T., "Combustion instability: acoustic interaction with a burning propellant surface," J. Chem. Phys. 30, 1501-1514 (1959).

(18) Hart, R. W., and McClure, F. T., "Theory of acoustic instability in solid propellant rocket combustion," Tenth Symposium (International) on Combustion (to be published).

(19) Horton, M. D., Eisel, J. L., and Price, E. W., "Low frequency acoustic oscillatory combustion," AIAA J. 1, 398-404 (1963).

(20) Horton, M. D., Eisel, J. L., and Price, E. W., "Low frequency combustion instability of solid rocket propellants," Tech. Prog. Rept. 318, U. S. Naval Ordnance Test Station, China Lake, Calif. (May 1963).

(21) Huffington, J. D., "The unsteady burning of cordite," Trans. of the Faraday Soc. 50, 942-952 (1954).

(22) Nachbar, W., and Williams, F. A., "On the analysis of linear pyrolysis experiments," Ninth Symposium (International) on Combustion, pp. 345-357.

(23) Powling, J., and Smith, W. A. W., "The surface temperature of burning ammonium perchlorate," Combustion and Flame 7, 269-275 (1963).

(24) Powling, J., and Smith, W. A. W., "The surface temperature of ammonium perchlorate burning at elevated pressures," Tenth Symposium (International) on Combustion (to be published).

(25) Price, E. W., "Combustion instability in solid propellant rockets," ARS preprint No. 1492-60 (Dec. 1960).

(26) Price, E. W., "Low frequency combustion instability of solid rocket propellants," Tech. Prog. Rept. 301, U. S. Naval Ordnance Test Station, China Lake, Calif. (Dec. 1962).

(27) Price, E. W., personal communication, U. S. Naval Ordnance Test Station, China Lake, Calif. (July 1963).

(28) Price, E. W., Rice, D. W., and Crump, J. E., "Low frequency combustion instability of solid rocket propellants," Tech. Prog. Rept. 360, U. S. Naval Ordnance Test Station, China Lake, Calif. (July 1964).

(29) Price, E. W., "Review of the combustion instability characteristics of solid propellants," Prepared for presentation at the 25th meeting of the AGARD Combustion and Propulsion Panel, San Diego, Calif., April 22-24, 1965.

(30) Price, E. W., "Experimental solid rocket combustion instability," Tenth Symposium (International) on Combustion (to be published).

(31) Rice, D. W., personal communication, U. S. Naval Ordnance Test Station, China Lake, Calif. (Aug. 1963).

(32) Ryan, N. W., Baer, A. K., Keller, J. A., and Mitchell, R. C., "Ignition and combustion of solid propellants," Technical Report Air Force Grant 62-99, AFOSR 62-99, University of Utah (Salt Lake City, Utah, Sept. 1962).

(33) Ryan, N. W., "Combustion irregularities of solid propellants," Prog. Rept. Grant AF AFSOR 446-63, University of Utah, Salt Lake City, Utah (Aug. 1964).

(34) Ryan, N. W., "Contribution to discussion of combustion instability," Tenth Symposium (International) on Combustion (to be published)

(35) Sehgal, R., and Strand, L., "A theory of low-frequency combustion instability in solid rocket motors," AIAA J. 2, 696-702 (1964).

(36) Shinnar, R., and Dishon, M., "Heat transfer stability analysis of solid propellant rocket motors," Progress in Astronautics and Rocketry, Volume 1: Solid Propellant Rocket Research, ed. by M. Summerfield (Academic Press Inc., New York, 1960), pp. 359-374.

(37) Summerfield, M., Sutherland, G. S., Webb, M. J., Taback, N. J., and Hall, K. B., "Burning mechanism of ammonium perchlorate propellants," Progress in Astronautics and Rocketry, Volume 1: Solid Propellant Rocket Research, ed. by M. Summerfield (Academic Press Inc., New York, 1960), pp. 141-182.

(38) Wylie, C. R., Jr., Advanced Engineering Mathematics (McGraw-Hill Book Co., Inc., New York, 1960), 2nd ed.

(39) Yoshiyama, I., Tanno, M., and Fukida, T., "Studies of the stable burning of composite propellants at low pressures," International Symposium on Space Technology and Science 4th Proceedings, Tokyo (Aug. 1962), pp. 333-344.

(40) Yount, R. A., and Angelus, T. A., "Chuffing and non-acoustic instability phenomena in solid propellant rockets," AIAA J. 2, 1307-1313 (1964).

APPENDICES

APPENDIX A

NOMENCLATURE

Dimensions: L = length, M = mass, Θ = time, and T = temperature

Roman Letters

A_b	area of burning surface	L^2
A_t	nozzle throat area	L^2
A	Arrhenius frequency factor	L/Θ
C^*	characteristic velocity	L/Θ
C_D	nozzle coefficient	$1/\Theta$
c_p	specific heat at constant pressure	$L^2/T^1\Theta^2$
E	activation energy	L^2/Θ^2
f	incident energy flux	M/Θ^3
F	$\dfrac{Re(\phi/\beta)}{Im(\phi/\beta)}$	dimensionless
G	$\dfrac{c_p\bar{T}_s\Theta_0}{H\beta}$	dimensionless
G_1	$\dfrac{\gamma c_p\bar{T}_s\Theta_0}{2HS\beta}$	dimensionless
H_s	temperature gradient at the surface	T/L
H_s+	temperature gradient on the gas phase side of the surface	T/L
H	$q + c_p(\bar{T}_s - T_0)$	L^2/Θ^2
i	$(-1)^{1/2}$	dimensionless
$Im(\ )$	imaginary part of a complex expression	

Roman Letters (cont'd)

K_N	ratio of the burning surface area to the nozzle throat area	dimensionless
k	thermal conductivity	$ML/T\theta^3$
K_g	time constant	$1/\theta$
L*	ratio of motor free volume to nozzle throat area	L
M	molecular weight	dimensionless
n	burning rate exponent	dimensionless
P	pressure	$M/L\theta^2$
P_o	ambient pressure into which the rocket exhausts	$M/L\theta^2$
Q	heat of phase change	L^2/θ^2
q	heat of gasification	L^2/θ^2
r	burning rate	L/θ
R	gas constant	$L^2/\theta^2 T$
Re( )	Real part of a complex expression	
S	$(\sigma + 1)^2 + \tau^2$	dimensionless
T	temperature	T
T_f	adiabatic flame temperature	T
T_o	temperature at $x = \infty$	T
t	time	θ
V	volume	L^3
W	$\dfrac{4(\bar{T}_s - T_o)}{\gamma(1 + \eta)\bar{T}_s}$	dimensionless
x	distance into the propellant	L
Y	$\dfrac{2c_p(\bar{T}_s - T_o)}{HS}$	dimensionless

- 103 -

Roman Letters (cont'd)

Y_1 $\quad \dfrac{\gamma c_p R \bar{T}_s^2}{2HS\Delta H_s}$ $\qquad$ dimensionless

Y_2 $\quad \dfrac{c_p R \bar{T}_s^2}{H\Delta H_s}$ $\qquad$ dimensionless

Greek Letters

α	thermal diffusivity	L^2/θ
α_g	growth factor	$1/\theta$
β	burning rate perturbation	dimensionless
γ	$\dfrac{4\alpha\omega}{\bar{r}^2}$	dimensionless
Γ	ratio of specific heats	dimensionless
ΔH_s	heat of sublimation	L^2/θ^2
ϵ	volume fraction	dimensionless
ζ	phase shift between flux and pressure	radians
η	growth factor (α_g/ω)	dimensionless
Θ	temperature perturbation	dimensionless
Θ_0	surface temperature perturbation	dimensionless
λ	$\dfrac{\bar{r}}{2\alpha}$	$1/L$
υ	ratio of thermal conductivities	dimensionless
ξ	L*, nondimensionalized by $\dfrac{C^*\bar{r}^2}{4\alpha RT_f}$	dimensionless
π	pressure perturbation	dimensionless
ρ	density	M/L^3
σ	dummy variable defined by Equation (2.11c)	dimensionless
τ	dummy variable defined by Equation (2.11d)	dimensionless

Greek Letters (cont'd)

ϕ	energy flux perturbation	dimensionless
ω	angular frequency	$1/\theta$

Subscripts

cr	refers to the stability limit
ch, g	refers to a condition or property in the gas chamber
p	refers to a property of the propellant
s	refers to the gas-solid interface
t	refers to conditions at the nozzle throat

Superscripts

Bar over a symbol (e.g. $\bar{r}$)   refers to the time-averaged value

Note: Additional nomenclature specific to Appendix G has been listed

in that Appendix.

APPENDIX B

PROPELLANT PROPERTIES AND COMPOSITIONS

Propellant Compositions

PBAA (polybutadiene-acrylic acid polymer) and ammonium perchlorate
are the basic constituents of the propellants considered in the present
investigation. The propellants each contain 82 per cent (by weight)dispersed
solids and 18 per cent polymeric binder; however, several variations
were obtained through the use of various additives. The exact compo-
sition, as well as corresponding designation of each propellant, is recorded
in Table 1. The procedure and conditions for compounding the propel-
lant are as follows: the propellant was mixed at 65°C at an absolute
pressure of 7 to 8 mm. Hg for 60 minutes, cast   at a pressure of
7 to 8 mm. Hg and cured at 80° for 7 days.

The composition of the polyurethane propellant that was used was
obtained from the Naval Ordnance Test Station [31] and is recorded in
Table 2. The composition was modified from that obtained from NOTS to
the extent that the ratio of coarse to fine ammonium perchlorate was
changed from 50:50 to 70:30 in order to reduce the viscosity of the
uncured propellant during the mixing and casting process. The mixing
procedure that was used is as follows: the estane, 1,4-BD, TEA, and
coarse NH_4ClO_4 were blended together in a pre-mix for 15 minutes; the
fine NH_4ClO_4 was then added and mixed for 10 minutes; finally the TMP
was added and mixing continued for 45 minutes. The mixing temperature

TABLE 1

COMPOSITION OF PBAA PROPELLANTS[a]

Propel-lant Code	Solid Ingredients (weight per cent)		Copper Chromite Catalyst[d]	Carbon Black[e]	Aluminum[f]
	NH_4ClO_4				
	Coarse[b]	15 micron[c]			
G	41	41	C	0	0
GB	40	40	0	2	0
F	40	40	2	0	0
TF	37.5	37.5	2	0	5
XF	35	35	2	0	10

(a) All of the propellants in this table had a PBAA (Thiokol, poly-butadiene-acrylic acid copolymer) binder composed of 85 per cent (by weight) PBAA and 15 per cent epoxy resin (Shell Chemical Co., Epon 828).

(b) American Potash and Chemical Corp., designated as -48 +100.

(c) American Potash and Chemical Corp., designated as 50% less than 15 micron.

(d) Harshaw Chemical Co., Cu-0202 P.

(e) Cabot Corp., Sterling VR carbon black

(f) Reynolds Aluminum, No. 1-511 atomized powder (50 per cent less than 25 micron).

TABLE 2

COMPOSITION OF POLYURETHANE PROPELLANT

Weight per cent	Ingredient
56	-48 +100 ammonium perchlorate[a]
24	10 micron ammonium perchlorate[b]
19.32	Estane[c]
0.46	TMP (Trimethylol propane)[c]
0.14	1,4-BD (Butanediol)[c]
0.08	TEA (Triethanolamine)[c]

(a) See table 1, footnote (b).

(b) American Potash and Chemical Co., designated as 10 micron
(50 weight per cent less than 10 micron)

(c) All of the ingredients for the binder were received from the
Naval Ordnance Test Station at China Lake, California.

was 75°C and both the mixing and casting pressure were 8 mm. Hg.
The propellant was cured for two days at 80°C.

Many thermal, chemical, and physical properties of the propellants were needed in the various calculations throughout the course of the study. The methods of measuring, calculating, or approximating these properties will be discussed in the following paragraphs.

Density

The density of the propellants was determined by measuring a cylindrical piece of propellant approximately 1.5 inches long by 1.5 inches in diameter with a micrometer and then weighing the sample on an analytical balance. The densities of the cured binders were measured by water displacement, and the density of ammonium perchlorate was obtained from the International Critical Tables.

Heat Capacity

The heat capacity of the cured binders and of F and G propellant was determined with a Dewar-flask-calorimeter as per Ryan, et al. [32]. Those of TF and XF propellants were calculated from the known heat capacities and compositions of their constituents.

Thermal Diffusivity

The thermal diffusivity of F and G propellant, the cured binders, and ammonium perchlorate was the same as that determined by Ryan et al. [32], and were determined by a transient technique dependent upon the temperature-time relationship at the center of a sample. The

thermal diffusivity of XF and TF propellant was calculated from the
equation

$$\alpha = \frac{k}{\rho c}$$

Thermal Conductivity

The thermal conductivity of TF and XF propellant was calculated
from the Maxwell equation for the electrical resistivity of heterogeneous
materials as modified for thermal conductivities and reported by Gorring
and Churchill (14). This equation is

$$\frac{k}{k_1} = \frac{2 + \upsilon - 2\epsilon\ (1-\upsilon)}{2 + \upsilon + \epsilon(1-\upsilon)} \qquad \text{(B-1)}$$

where υ is the ratio of the thermal conductivities of the discontinuous
phase (the aluminum) to that of the continuous phase (F propellant),
ϵ is the volume fraction of the discontinuous phase, and k_1 is the
thermal conductivity of the continuous phase. The thermal conductivity
of an aluminized propellant whose thermal diffusivity had been measured
by the method outlined above was checked by use of Equation (B-1)
and found to be within 4 per cent of the measured value, indicating
that the equation is probably an excellent approximation.

The measurements of the density, the heat capacity, and the thermal
diffusivity are probably all within 2 per cent. The error in the
approximation for the thermal conductivity from Equation (B-1) should
be less than 10 per cent.

Properties of the Combustion Products

The adiabatic flame temperature, the characteristic velocity, and the ratio of the specific heats for the combustion products of F, G, and TF propellant were calculated considering thermodynamic equilibrium of these products. The results of these calculations were obtained for the University of Utah by Dr. Ralph Coates [9] of the Lockheed Propulsion Co. The average molecular weight of the combustion products was then calculated from the definition of the characteristic velocity

$$C*^2 = \frac{RT_f}{M\Gamma \left(\frac{2}{\Gamma+1}\right)^{\frac{\Gamma+1}{\Gamma-1}}} \qquad \text{(B-2)}$$

The values of the above properties have been tabulated and appear in Table 3. It was assumed that the properties of GB propellant were essentially the same as for G propellant, and those of XF propellant were estimated from those of TF propellant.

Linear Burning Rate

The steady-state burning rate of the propellant enters into the equations of Chapter II in several places, and is therefore a very important property. Data on the steady burning rate for the various propellants was obtained from a constant pressure strand bomb. Propellant strands 1/4 x 1/4 inch and approximately 3 inches long were burned in an atmosphere of nitrogen to provide these data. The results are plotted in Figure 29 showing the relationship between the steady burning rate and pressure for G, F, TF, and XF propellants. Several

- 111 -

TABLE 3

PROPERTIES OF THE PROPELLANTS

Propellant or Ingredients	Specific Gravity	Specific Heat cal/(gm°C)	Thermal Diffusivity (in²/sec)	Combustion Products			
				Characteristic Velocity (ft/sec)	Adiabatic Flame Temp (°K)	Ratio of Specific Heats	Molecular Weight
Ingredients							
Ammonium perchlorate	1.95	0.256	3.45 x 10⁻⁴				
F-propellant binder	1.11	.424	1.64				
G-propellant binder	0.956	.465	1.52				
Propellants							
F	1.63	.316	2.63	4790	2600	1.24	23.5
TF	1.69	.302(a)	3.04(b)	4920	2860	1.22	25.1
XF	1.71	.299(a)	3.25(b)	5050(c)	3000(c)	1.20(c)	...
G	1.60	.311	2.65	4810	2630	1.24	23.5
GB(d)	1.60	.311	2.65	4810	2630	1.24	...

(a) Calculated from the specific heats of the ingredients.
(b) Calculated from Equations (B-2) and (B-1).
(c) Approximated
(d) The properties of GB propellant were assumed to be the same as those for G.
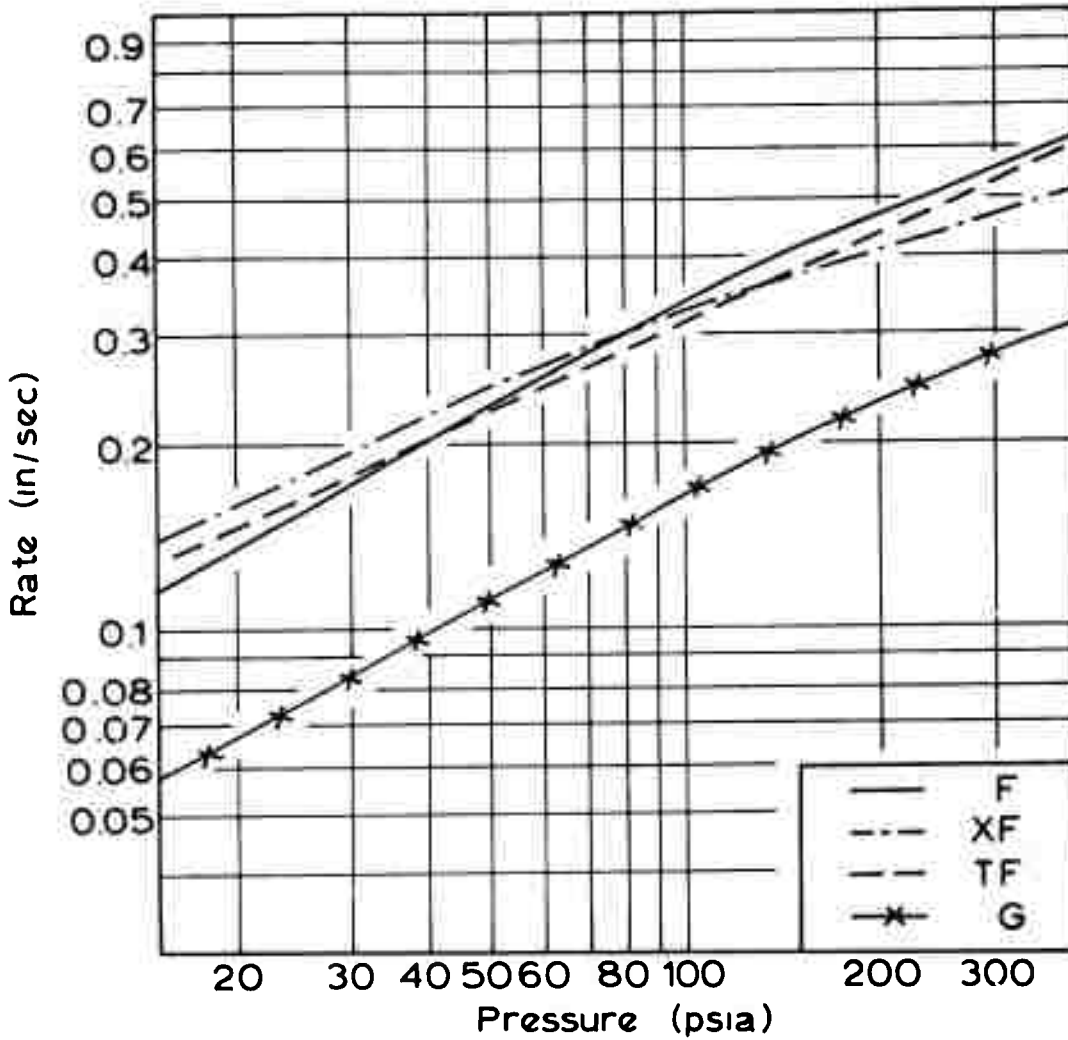
Figure 29. Burning rate versus pressure for F, TF, XF, and G propellants. Data of GB propellant fall on the same line as for G propellant.

data points were obtained for GB propellant and fall essentially on the line determined for G propellant. It was therefore assumed that their burning rates are the same. Raw data have been included in Table 19, Appendix I.

APPENDIX C

EVALUATION OF THE INTEGRAL $\int \Theta/\beta \, dx$

In perturbing the energy balance, the integral of Θ/β as a function of x evolved in the form

$$\frac{\phi}{\beta} = 1 + \frac{c_p \, \omega \, \bar{T}_s}{H\bar{r}} \, (1 + \eta) \int_0^\infty \Theta/\beta \, dx + \frac{c_p \, \bar{T}_s}{H} \, \frac{\Theta_0}{\beta} \qquad (2.6)$$

The perturbed, unsteady heat conduction equation provided an expression for Θ/β as

$$\frac{\Theta(x)}{\beta} = \left[\frac{\Theta_0}{\beta} + \frac{4(\bar{T}_s - T_0)}{\gamma(1+\eta) \, \bar{T}_s} \right] e^{-\lambda(1+\sigma+1\tau)x} - \frac{4(\bar{T}_s - T_0)}{\gamma(1+\eta) \, \bar{T}_s} e^{-2\lambda x}$$

$$(2.1)$$

The task at hand then, is to evaluate the integral

$$\int_0^\infty \frac{\Theta(x)}{\beta} \, dx = \int_0^\infty \left\{ \left[\frac{\Theta_0}{\beta} + \frac{4(\bar{T}_s - T_0)}{\gamma(1+\eta) \, \bar{T}_s} \right] e^{-\lambda(1+\sigma+1\tau)x} - \frac{4(\bar{T}_s - T_0)}{\gamma(1+\eta)\bar{T}_s} e^{-2\lambda x} \right\} dx$$

$$(C-1)$$

For the sake of convenience, let $W = \dfrac{4(\bar{T}_s - T_0)}{\gamma(1+\eta) \, \bar{T}_s}$. Equation (C-1) reduces to

$$\int_0^\infty \frac{\Theta(x)}{\beta} \, dx = \left(\frac{\Theta_0}{\beta} + W \right) \int_0^\infty e^{-\lambda(\sigma+1+1\tau)x} \, dx - W \int_0^\infty e^{-2\lambda x} \, dx$$
$$(C-1a)$$

Carrying out the integration leaves

$$= \left(\frac{\theta_0}{\beta} + W\right) \left[\frac{e^{-\lambda(\sigma+1+i\tau)x}}{-\lambda(\sigma+1+i\tau)}\right]_0^\infty + \frac{W}{2\lambda} \ e^{-2\lambda x} \Big|_0^\infty \qquad \text{(C-2)}$$

$$= \frac{\frac{\theta_0}{\beta} + W}{\lambda(1+\sigma+i\tau)} - \frac{W}{2\lambda}$$

$$= \frac{\frac{\theta_0}{\beta} + W}{\lambda S} (1+\sigma-i\tau) - \frac{W}{2\lambda} \qquad \text{(C-3)}$$

where $S \equiv (1+\sigma)^2 + \tau^2$

Substitution of (C-3) into (2.6) gives

$$\frac{\phi}{\beta} = 1 + \frac{c_p \omega \bar{T}_s}{H \bar{r} \lambda} (1+\eta)\left[\left(\frac{\theta_0}{\beta S} + \frac{W}{S}\right)(1+\sigma-i\tau) - \frac{W}{2}\right] + \frac{c_p \bar{T}_s}{H} \frac{\theta_0}{\beta} \qquad \text{(C-4)}$$

This can be reduced as follows

$$\frac{\phi}{\beta} = 1 + \frac{c_p \omega \bar{T}_s}{H \bar{r} \lambda S} \frac{\theta_0}{\beta} (1+\eta)(\sigma+1-i\tau) + \frac{\bar{T}_s c_p \omega W}{H \bar{r} \lambda S} (1+\eta)(\sigma+1-i\tau)$$

$$+ \frac{c_p \bar{T}_s}{H} \frac{\theta_0}{\beta} - \frac{\bar{T}_s c_p \omega W}{2 H \bar{r} \lambda} (1+\eta) \qquad \text{(C-5)}$$

Substituting the definition of W into (C-5), and recognizing that $\frac{\omega}{\bar{r}\lambda} = \frac{\gamma}{2}$, and simplifying yields

$$\frac{\phi}{\beta} = 1 + \frac{c_p \bar{T}_s \gamma}{2H \ S} \frac{\theta_0}{\beta} \ [\eta(\sigma+1) + \tau + i \ (\sigma+1-\eta\tau)] + \frac{c_p \bar{T}_s}{H} \frac{\theta_0}{\beta}$$

$$+ \frac{\bar{T}_s c_p \gamma}{H} \frac{(\bar{T}_s - T_0)}{\gamma(1+\eta) \ \bar{T}_s} (1+\eta) \left[\frac{\sigma+1-i\tau}{S} - \frac{1}{2}\right] \qquad \text{(C-6)}$$

$$= 1 + G_1 \ [\eta(\sigma+1) + \tau] + Y \ (\sigma+1 - \frac{S}{2}) + G$$

$$+ i \ [G_1 \ (\sigma+1-\eta\tau) - Y\tau] \qquad \text{(C-7)}$$

where $G_1 \equiv \dfrac{c_p \gamma \bar{T}_s}{2\ H\ S} \quad \dfrac{\theta_0}{\beta}$

$$Y \equiv \dfrac{2\ c_p\ (\bar{T}_s - T_0)}{H\ S}$$

and

$$G \equiv \dfrac{c_p \bar{T}_s}{H} \quad \dfrac{\theta_0}{\beta}$$

APPENDIX D

APPROXIMATION FOR θ_0 - THE THERMODYNAMIC LIMITED CASE

The Clausius-Clapeyron equation is

$$\frac{dP}{dT_s} = \frac{P \triangle H_s}{RT_s^2} \tag{2.23}$$

The perturbed pressure and surface temperature are

$$T_s = \bar{T}_s [1 + \theta_0 \; e^{(1+\eta)\omega t}] \tag{2.4a}$$

$$P = \bar{P} [1 + \pi \; e^{(1+\eta)\omega t}] \tag{2.4d}$$

Substituting (2.4) into (2.23) yields

$$\frac{P_0 \pi \omega \; (1+\eta) \; e^{(1+\eta)\omega t}}{\bar{T}_s \theta_0 \omega (1+\eta) \; e^{(1+\eta)\omega t}} = \frac{\triangle H_s \; \bar{P} \; [1 + \pi \; e^{(1+\eta)\omega t}]}{R\bar{T}_s^2 \; [1 + \theta_0 \; e^{(1+\eta)\omega t}]^2} \tag{D-1}$$

If unity is much greater than the perturbations, then (D-1) reduces to

$$\frac{\bar{P} \; \pi}{\bar{T}_s \theta_0} = \frac{\triangle H_s \; \bar{P}}{R\bar{T}_s^2}$$

and

$$\frac{\theta_0}{\pi} = \frac{R\bar{T}_s}{\triangle H_s} \tag{D-2}$$

APPENDIX E

RAW DATA

TABLE 4

POLYURETHANE PROPELLANT DATA FROM LOW-L* BURNER

Run Number	Propellant Code	Nozzle Dia. (in)	L_p (in)	L_{ch} (in)	P_o(a) (psia)	Pressure Range (psia)	Results(b)	Comments
39-141	UG-1	0.250	0.50	0.75	atm.	--(d)	C-E	Chuffed several times(e)
39-143	UG-1	.228	.50	0.75	atm.	--(d)	C-E	Chuffed several times(e)
39-161	UG-1	.228	.38(f)	0.75	atm.	--(d)	C-E	Chuffed several times(e)
39-162	UG-1	.228	.25(f)	0.75	atm.	--(d)	C-E	Chuffed several times(e)
310-114	UG-3(g)	.228	.50	1.13	atm.	--(d)	C	Chuffed several times(e)
310-115	UG-3	.228	.50	1.88	atm.	--(d)	C	Chuffed several times(e)
310-287	UG-3	.228	.50	1.88	atm.	--(d)	C	Chuffed several times(e)
310-141	UG-3	.228	.50	2.75	atm.	12.5	S	Burned at atmospheric pressure(e)
310-144	UG-3	.201	.25	0.75	atm.	45-55	C-S	Chuffed once
310-041	UG-3	.201	.47	1.34	atm.	--(d)	C-E	Chuffed several times(e)
310-291	UG-3	.201	.50	1.88	atm.	--(d)	C	Chuffed several times(e)
310-042	UG-3	.201	.38	1.88	atm.	--(h)	C-E	Chuffed twice(e)
310-071	UG-3	.201	.38	1.88	atm.	13-15	C-E	Chuffed 3 times(e)
310-072	UG-3	.201	.25(f)	1.88	atm.	13-15	C-S	Chuffed 3 times(e)
310-301	UG-3	.201	.25	1.88	atm.	13-15	C-S	Chuffed twice(e)
310-142	UG-3	.201	.50	2.75	atm.	14-16	C-E	Burned stably and then chuffed(e)
310-143	UG-3	.201	.40(f)	2.75	atm.	14-16	C-E	Burned stably and then chuffed(e)
311-159	UG-4(g)	.189	.50	0.75	atm.	25-40	C-S-U	Chuffed twice
311-1510	UG-4	.189	.50	1.06	atm.	25-35	C-S-U	Chuffed once
310-112	UG-3	.180	.38	0.75	atm.	50	C-E	Chuffed 3 times
310-286	UG-3	.180	.38	0.75	atm.	30	C-E	Chuffed twice
310-113	UG-3	.180	.20(f)	0.75	atm.	45-55	C-S	Chuffed twice
310-284	UG-3	.180	.25	0.75	atm.	25-30	C-S	Chuffed twice
310-285	UG-3	.180	.56	1.06	atm.	29-34	S	Chuffed once

TABLE 4 (Continued)

Run Number	Propellant Code	Nozzle Dia. (in)	L_p (in)	L_{ch} (in)	P_o(a) (psia)	Pressure Range (psia)	Results(b)	Comments
310-283	UG-3	.169	.38	0.50	atm.	45-50	C-S	Chuffed once
310-292	UG-3	.169	.38	0.50	atm.	--(d)	C-E	Chuffed once
310-281	UG-3	.169	.50	0.75	atm.	26	C-E	Chuffed once
310-282	UG-3	.169	.45(f)	0.75	atm.	45	S	
310-111	UG-3	.159	.38	0.50	atm.	85	S	
310-258	UG-3	.159	.38	0.50	atm.	75-90	S-U	
310-075	UG-3	.159	.50	0.75	atm.	56	S	
310-074	UG-3	.159	.38	1.03	atm.	52	S	
310-073	UG-3	.159	.38	1.50	atm.	--(h)	S	

(a) In this column, the abbreviation "atm" has been used to indicate that the burner exhausted to the atmosphere.

(b) In this column, "C" represents chuffing; "O" represents oscillatory burning; "S" represents stable burning; "E" represents that the sample extinguished; and "U" represents uneven or irregular burning.

(c) No. L*-frequency data were obtained from the runs with polyurethane propellant.

(d) The pressure was so irregular or low that an approximation of a mean pressure range would be meaningless.

(e) The chamber pressure was so low that critical flow was not maintained in the nozzle.

(f) The exact length of this sample is uncertain because the extinguished propellant from a previous run was used.

(g) UG-3 and UG-4 differ from UG-1 in that they contain a 70:30 ratio of coarse ammonium perchlorate to fine AP whereas UG-1 contains a 50:50 ratio.

(h) A photographic record of the oscilloscope trace was not obtained.

TABLE 5

F PROPELLANT DATA FROM LOW-L* BURNER

Run Number	Propellant Code	Nozzle Dia. (in)	L_p (in)	L_{ch} (in)	P_o(a) (psia)	Pressure Range (psia)	Results(b)	Comments
49-171	F-59	0.328	0.34	0.50	4.9	--(c)	C-E	Chuffed many times
310-253	F-22	.328	.50	0.75	atm.	--(c)	C	Chuffed many times
310-234	F-21	.328	.50	0.75	atm.	--(c)	C	Chuffed many times
310-255	F-22	.328	.75	1.06	atm.	--(c)	C	Chuffed many times
310-233	F-21	.328	.50	1.06	atm.	--(c)	C	Chuffed many times
49-181	F-59	.328	.34	1.06	4.9	35-40	C	Chuffed several times
49-281	F-59	.328	.25	1.06	4.9	30-38	C-U	Chuffed several times
49-295	F-59	.328	.25	1.06	4.9	--(c)	C	Water cooled adaptor used
411-064	F-57	.328	.25	1.25	3.9	--(c)	C-U	
49-282	F-59	.328	.28	1.81	4.9	23	C-S	Water cooled adaptor used
410-081	F-59	.328	.25	1.84	4.9	27	C-0	Chuffed several times
410-162	F-62	.328	.25	2.00	7.4	--(c)	C	Chuffed many times
410-281	F-62	.328	.25	2.00	3.9	12	C-0	Results inconclusive(e)
410-171	F-62	.328	.25	2.00	7.4	10	C-0	Results inconclusive(e)
410-273	F-62	.328	.25	2.00	7.4	10-15	C-0	Results inconclusive(e)
42-063(d)	F-22	.302	.25	0.50	atm.	35-45	C-0	
47-291(d)	F-59	.302	.38	0.75	atm.	35-40	C-0-S	
42-064	F-22	.302	.38	0.75	atm.	--(c)	C-0-U	Chuffed once
410-082	F-59	.302	.31	0.75	9.8	40-60	C-0-U	Chuffed once
410-143	F-62	.302	.31	0.75	9.8	40-80	C-U	Chuffed once
42-062	F-22	.302	.25	0.75	atm.	30	C-S	Chuffed once
49-291	F-59	.302	.25	0.75	4.9	--(c)	C-E	Water cooled adaptor used
49-292	F-59	.302	.25	0.75	4.9	--(c)	C-E	Water cooled adaptor used
49-293	F-59	.302	.25	0.75	4.9	45	C-S	Water cooled adaptor used
410-061	F-59	.302	.25	0.75	9.8	40-60	U	

TABLE 5 (Continued)

Run Number	Propellant Code	Nozzle Dia. (in)	L_p (in)	L_{ch} (in)	P_o(a) (psia)	Pressure Range (psia)	Results(b)	Comments
410-144	F-59	.302	.25	0.75	9.8	40-55	C-U	Chuffed once
410-161(d)	F-62	.302	.25	0.75	atm.	40	C-0-S	
410-172	F-62	.302	.25	0.75	7.4	25	C-S	Chuffed once
410-285	F-62	.302	.22	0.75	7.4	25-35	C-S	Chuffed once
311-131(d)	F-22	.281	.38	0.50	atm.	30-50	C-0-S	Chuffed several times
310-232	F-21	.281	.38	0.50	atm.	50-60	C-0-S	Chuffed several times(f)
47-251	F-59	.281	.38	0.50	atm.	50-60	C-0-S	Chuffed several times(f)
410-082	F-59	.281	.31	0.50	atm.	--(c)	C-U	Large pressure increase(f)
310-254	F-22	.281	.50	0.75	atm.	35	C-0-U	Chuffed several times
47-241	F-59	.281	.25	0.50	atm.	47-53	C-S	Chuffed once (f)
47-252	F-59	.281	.25	0.50	atm.	40-55	C-0-S	Chuffed twice(f)
310-231	F-21	.281	.50	0.75	atm.	35-40	C-0-S	Chuffed 3 times(f)
410-146(d)	F-62	.281	.23	0.50	19.7	50-60	C-0-S	Chuffed 3 times
411-071(d)	F-57	.281	.34	0.75	atm.	50	C-S-U	Large pressure rise at end.
410-062	F-59	.281	.38	0.75	9.8	--(c)	U	
42-065	F-22	.281	.38	0.75	atm.	--(c)	U	
410-173(d)	F-62	.281	.38	0.75	9.8	28-35	C-S	Chuffed once
310-237	F-21	.281	.38	0.75	atm.	30-35	C-S	Chuffed once(f)
49-294	F-59	.281	.38	0.75	4.9	35	S	Water cooled adaptor used
410-164	F-62	.281	.38	0.75	19.7	30	S	
410-202	F-62	.281	.38	0.75	atm.	30	S	
42-052(d)	F-22	.266	.38	0.50	atm.	50-80	C-S	Chuffed once
410-166(d)	F-62	.266	.38	0.50	19.7	80-90	0-S	
410-165	F-62	.266	.34	0.50	19.7	80	S	
410-145	F-62	.266	.31	0.50	19.7	80	S	

TABLE 5 (continued)

Run Number	Propellant Code	Nozzle Dia. (in)	L_p (in)	L_{ch} (in)	P_o(a) (psia)	Pressure Range (psia)	Results(b)	Comments
42-041	F-22	.266	.25	0.50	atm.	90	S	
42-062	F-22	.266	.50	0.75	atm.	80	S	
311-134	F-22	.250	.44	0.50	atm.	50-55	C-E	Low mean pressure
410-163(d)	F-62	.250	.41	0.50	19.7	70-80	C-0-S	Chuffed twice
410-201	F-62	.250	.41	0.50	19.7	60	C-0-S	Chuffed once(f)
310-238	F-21	.250	.38	0.50	atm.	80	C-S	Large pressure rise at end(f)
310-241	F-21	.250	.38	0.50	atm.	--(c)	C-E	Chuffed twice(f)
311-133	F-22	.250	.38	0.50	atm.	98	C-S	Chuffed once
311-135(d)	F-22	.250	.38	0.50	atm.	70-75	C-S	Chuffed once
410-174	F-62	.250	.38	0.50	19.7	--(c)	U	
410-147(d)	F-62	.250	.36	0.50	29.5	98.5	0-S	
410-085	F-59	.250	.34	0.50	atm.	100	S	
310-242	F-21	.250	.31	0.50	atm.	70	S	
311-132	F-22	.250	.50	0.75	atm.	50-90	S	Uneven pressure
311-137	F-22	.250	.50	0.75	atm.	70-95	S	Uneven pressure
311-138	F-22	.250	.50	1.06	atm.	80-90	S	
410-211(d)	F-62	.238	.44	0.50	19.7	80	C-E	Chuffed once
410-212(d)	F-62	.238	.41	0.50	19.7	75	C-E	Chuffed once
410-213	F-62	.238	.38	0.50	19.7	110-125	0-U	
311-136	F-22	.228	.44	0.50	atm.	110-125	S	
310-306	F-22	.228	.38	0.50	atm.	100-120	S	
310-305	F-22	.228	.50	0.75	atm.	110	S	
310-304	F-22	.228	.50	1.06	atm.	85	S	

TABLE 5 (Continued)

(a) In this column, the abbreviation "atm" has been used to indicate that the burner exhausted to the atmosphere.

(b) In this column, "C" represents chuffing; "O" represents oscillatory burning; "S" represents stable burning; "E" represents that the sample extinguished; and "U" represents uneven or irregular burning.

(c) The pressure was so irregular that an approximation of a mean pressure range would be meaningless.

(d) L*-frequency data were obtained from this run.

(e) The chamber pressure was sufficiently low that it is doubtful that critical flow was maintained in the nozzle.

(f) A record of this run was not obtained with the tape recorder.

TABLE 6

TF PROPELLANT DATA FROM LOW-L* BURNER

Run Number	Propellant Code	Nozzle Dia. (in)	L_p (in)	L_{ch} (in)	P_o(a) (psia)	Pressure Range (psia)	Results(b)	Comments
48-254	TF-3	0.328	0.25	1.06	atm.	--(c)	C	Chuffed many times
47-285	TF-2	.302	.25	0.50	atm.	--(c)	C	Chuffed many times
51-041	TF-2	.302	.38	0.75	19.7	--(c)	C	Chuffed many times
47-286(d)	TF-2	.302	.38	0.75	atm.	40	C-0	Chuffed many times
47-287(d)	TF-2	.302	.25	0.75	atm.	38-48	C-0	Chuffed several times
48-261(d)	TF-2	.302	.44	1.03	atm.	35-40	C-0	Chuffed 5 times
48-019(d)	TF-2	.302	.44	1.06	atm.	45-60	C-0-S	Chuffed twice
48-262	TF-2	.302	.31	1.06	atm.	40	S	
47-281	TF-2	.281	.25	0.50	atm.	--(c)	C	Chuffed many times
47-225	TF-2	.281	.25	0.50	atm.	--(c)	C	Chuffed many times(e)
51-051	TF-3	.281	.19	0.50	atm.	50-65	C-0	Uneven pressure
47-282(d)	TF-2	.281	.38	0.75	atm.	60-70	C-0-S	Chuffed 4 times
47-253	TF-2	.281	.38	0.75	atm.	50-55	C-0	Chuffed many times(e)
47-254	TF-2	.281	.25	0.75	atm.	52-56	C-0	Chuffed 3 times(e)
47-284(d)	TF-2	.281	.44	1.06	atm.	45-52	C-0-S	Chuffed 3 times
51-042(d)	TF-3	.281	.38	1.06	atm.	52	0-S	
48-256(d)	TF-3	.281	.31	1.06	atm.	60-70	0-S	Small amplitude oscillations
51-044(d)	TF-3	.266	.38	0.50	atm.	100-150	C-0-S	Chuffed twice
48-011(d)	TF-2	.266	.25	0.50	atm.	68-80	C-0-S	Chuffed twice
51-043(d)	TF-3	.266	.44	0.75	atm.	90-95	0-S	
48-014	TF-2	.266	.39	0.75	atm.	75-90	S	

PAGE 126 OMITTED

TABLE 6 (Continued)

Run Number	Propellant Code	Nozzle Dia. (in)	L_p (in)	L_{ch} (in)	P_o(a) (psia)	Pressure Range (psia)	Results(b)	Comments
48-255	TF-3	.266	.38	0.75	atm.	75-95	S	
48-012	TF-2	.266	.38	0.75	atm.	75-110	C-U	Chuffed once(e)
48-013	TF-2	.266	.44	1.06	atm.	85-95	S	
48-015(d)	TF-2	.250	.44	0.50	atm.	105-125	C-O-S	Chuffed several times
48-016	TF-2	.250	.38	0.50	atm.	90-100	C-O-S	Chuffed 4 times(e)
51-045(d)	TF-3	.250	.34	0.50	atm.	100-110	C-O-S	Chuffed 3 times
48-017(d)	TF-2	.250	.31	0.50	atm.	110	C-S	Chuffed once
47-221	TF-2	.250	.31	0.50	atm.	120	C-O-S	Chuffed once(e)
47-224	TF-2	.250	.25	0.50	atm.	105	S	(e)
48-018	TF-2	.250	.25	0.50	atm.	105	S-U	
48-264(d)	TF-3	.228	.44	0.50	atm.	160-200	C-O-S	Chuffed 4 times
48-263(d)	TF-3	.228	.38	0.50	atm.	140-160	C-O-S	Chuffed twice
47-222	TF-2	.228	.56	0.75	atm.	150-200	C-S	Chuffed once(e)

(a) In this column, the abbreviation "atm" has been used to indicate that the burner exhausted to the atmosphere.

(b) In this column, "C" represents chuffing; "O" represents oscillatory burning; "S" represents stable burning; "E" represents that the sample extinguished; and "U" represents uneven or irregular burning.

(c) The pressure was so irregular that an approximation of a mean pressure range would be meaningless.

(d) L*-frequency data were obtained from this run.

(e) A record of this run was not obtained with the tape recorder.

TABLE 7

XF PROPELLANT DATA FROM LOW-L* BURNER

Run No.	Propellant Code	Nozzle Dia. (in)	L_p (in)	L_{ch} (in)	P_o(a) (psia)	Pressure Range (psia)	Results(b)	Comments
48-265	XF-1	0.281	0.25	0.75	atm.	--(c)	C	Chuffed many times
48-267	XF-1	.281	.44	1.06	atm.	--(c)	C-O	Chuffed many times
48-266(d)	XF-1	.281	.31	1.03	atm.	50-55	O-S	
49-027(d)	XF-1	.266	.25	0.50	atm.	75-80	O-S	
49-026(d)	XF-1	.266	.39	0.75	atm.	80-85	O-S	Large pressure rise at end
48-268	XF-1	.266	.38	0.75	atm.	75-100	S-U	Burned past the O-ring seal
49-025(d)	XF-1	.266	.31	0.75	atm.	70-80	C-S	Chuffed once
48-269(d)	XF-1	.250	.38	0.50	atm.	90-120	C-O-S	Chuffed several times
49-021(d)	XF-1	.250	.31	0.50	atm.	100-125	C-O-S	Chuffed twice
49-022(d)	XF-1	.250	.25	0.50	atm.	70-85	C-O-S	Low mean pressure
49-023(d)	XF-1	.228	.44	0.50	atm.	150-180	C-O-S	Chuffed several times
49-024(d)	XF-1	.228	.38	0.50	atm.	130-140	C-O-S	Chuffed twice

(a) In this column, the abbreviation "atm" has been used to indicate that the burner exhausted to the atmosphere.

(b) In this column, "C" represents chuffing; "O" represents oscillatory burning; "S" represents stable burning; "E" represents that the sample extinguished; and "U" represents uneven or irregular burning.

(c) The pressure was so irregular that an approximation of a mean pressure range would be meaningless.

(d) L*-frequency data were obtained from this run.

TABLE 8

G PROPELLANT DATA FROM LOW-L* BURNER

Run Number	Propellant Code	Nozzle Dia. (in)	L_p (in)	L_{ch} (in)	P_o(a) (psia)	Pressure Range (psia)	Results(b)	Comments
310-145	G-9	0.250	0.38	0.50	atm.	17	C-0	Chuffed several times(c)(d)
49-231(e)	G-14	.250	.31	0.50	4.9	24	C-E	Chuffed once
310-146	G-9	.250	.50	0.75	atm.	16	0	(c)(d)
310-212	G-9	.250	.50	0.75	atm.	15	0	(c)
49-241(c)	G-14	.250	.22	0.50	4.9	25	C-E	Chuffed twice
310-162	G-9	.250	.75	1.06	atm.	20	0	(c)(d)
310-211	G-9	.250	.75	1.06	atm.	16	0	(c)
49-242(e)	G-14	.250	.25	0.75	4.9	20	C-E	Chuffed once
310-147	G-9	.250	.50	1.06	atm.	17	0	(c)(d)
410-193	G-17	.250	.38	1.06	4.9	--(f)	C-E	(c)(d)
410-194(e)	G-17	.250	.31	1.06	4.9	16	C-E	Chuffed once, uneven pressure
410-195	G-17	.250	.25	1.06	4.9	--(f)	C-U	Chuffed several times
310-161	G-9	.250	.86	1.86	atm.	21	0	(c)(d)
49-251	G-14	.250	.25	1.31	4.9	21	C-U	Chuffed several times
49-308(e)	G-14	.250	.25	1.31	7.4	29	C-0	Chuffed 3 times
49-252	G-14	.250	.34	1.63	4.9	27	C-0-E	(d)
49-309(e)	G-14	.250	.31	1.63	7.4	18	C-0	Chuffed 3 times
410-052	G-14	.250	.23	1.63	4.9	20	C-0-E	Chuffed once
49-246	G-14	.250	.22	1.63	4.9	--(f)	C	Chuffed several times
410-056	G-14	.250	.21	1.78	4.9	--(f)	C-U	Chuffed several times
410-051	G-14	.250	.25	1.78	2.5	--(f)	C-U	Chuffed several times
49-253	G-14	.250	.22	1.78	4.9	--(f)	C-U	Chuffed several times
410-064(e)	G-14	.250	.25	1.84	4.9	22	C-0-E	Chuffed 4 times
49-254	G-14	.250	.22	1.84	4.9	--(f)	U	(c)

TABLE 8 (Continued)

Run Number	Propellant Code	Nozzle Dia. (in)	L_p (in)	L_{ch} (in)	P_o(a) (psia)	Pressure Range (psia)	Results(b)	Comments
410-073(e)	G-14	.250	.25	2.00	4.9	20	C-0	Chuffed 3 times
410-074	G-14	.250	.25	2.25	4.9	--(f)	C-U	
410-168	G-14	.250	.25	2.25	4.9	--(f)	C-0-U	(c)(g)
410-141	G-14	.250	.22	2.25	4.9	--(f)	U	
410-282	G-14	.250	.25	2.50	4.9	--(f)	U	(g)
410-272	G-14	.250	.25	2.50	4.9	--(f)	C-0-U	
411-072	G-17	.250	.25	2.50	4.9	17-26	U	(h)
410-215	G-17	.238	.38	0.75	4.9	15	0-S	
410-192	G-17	.238	.25	0.75	4.9	19	S	
410-175	G-17	.238	.25	1.06	4.9	19	S	
410-167	G-17	.238	.25	1.19	4.9	23	S	
410-274	G-17	.238	.25	1.63	4.9	22	C-E	Chuffed several times
311-153(e)	G-9	.228	.44	0.50	atm.	26	C-0-E	(i) Chuffed 4 times
310-163(e)	G-9	.228	.66	0.75	atm.	30	0-S	(i)
39-233	G-8	.228	.63	0.75	atm.	26	C-0-S	(i)(d)
311-154(e)	G-9	.228	.34	0.50	atm.	27	C-0-E	(i) Chuffed once
311-155(e)	G-9	.228	.31	0.50	atm.	26	0	(i)
39-231	G-8	.228	.25	0.75	atm.	30	0-S	(d)
49-306(e)	G-14	.228	.31	0.75	9.8	40	0-S	
49-307	G-14	.228	.31	0.75	9.8	16	S	Water cooled adaptor used
410-026	G-14	.228	.28	0.75	9.8	35-40	S	
410-027	G-14	.228	.28	0.75	9.8	40-42	S	
410-053	G-17	.228	.28	0.75	9.8	25-30	0-S	
410-071(e)	G-17	.228	.28	0.75	9.8	30	0-S	(d)
410-054	G-17	.228	.23	0.75	9.8	30	S	

TABLE 8 (Continued)

Run Number	Propellant Code	Nozzle Dia. (in)	L_p (in)	L_{ch} (in)	P_o(a) (psia)	Pressure Range (psia)	Results(b)	Comments
410-214(e)	G-17	.219	.31	0.50	atm.	25-30	0-S	Pressure rising during oscillations
410-176(e)	G-17	.219	.25	0.50	9.8	25-34	0-S	Pressure rising during oscillations
411-061(e)	G-17	.219	.22	0.50	7.4	30-50	0-S-U	Pressure rising during oscillations
411-062(e)	G-17	.219	.19	0.50	9.8	30-50	0-S-U	Pressure rising during oscillations
410-284	G-17	.219	.19	0.50	7.4	36	S	
410-191(e)	G-17	.219	.16	0.50	9.8	28-34	0-S	Pressure rising during oscillations
311-075(e)	G-9	.209	.44	0.50	atm.	20-30	C-0-S	(c)
311-074(e)	G-9	.209	.38	0.50	atm.	30-36	0-S	
49-305(e)	G-14	.209	.38	0.50	9.8	50-70	0-S	
410-022	G-14	.209	.38	0.50	9.8	53	0-S	(d)
410-023	G-14	.209	.38	0.50	9.8	40-100	C-S	One small chuff
410-055	G-17	.209	.38	0.50	9.8	50-55	0-S	Dropping pressure
410-021	G-14	.209	.34	0.50	9.8	45-100	0-S	Dropping pressure
410-024	G-14	.209	.34	0.50	9.8	45-100	S	
49-302	G-14	.209	.31	0.50	9.8	38	S	Water cooled adaptor used
49-304	G-14	.209	.31	0.50	9.8	45-60	S	
49-303	G-14	.209	.28	0.50	9.8	45-60	S	
49-301	G-14	.209	.25	0.50	9.8	30	S	Water cooled adaptor used
410-025	G-14	.209	.25	0.75	9.8	50-90	S	
410-065	G-17	.201	.44	0.50	atm.	-(f)	C-E	Chuffed twice
311-139	G-9	.201	.44	0.50	atm.	20-40	S	
410-072	G-17	.201	.41	0.50	atm.	60	S	

TABLE 8 (Continued)

(a) In this column, the abbreviation "atm" has been used to indicate that the burner exhausted to the atmosphere.

(b) In this column, "C" represents chuffing; "O" represents oscillatory burning; "S" represents stable burning; "E" represents that the sample extinguished; and "U" represents uneven or irregular burning.

(c) The chamber pressure was so low that critical flow was not maintained in the nozzle.

(d) A record of this run was not obtained with the tape recorder.

(e) L*-frequency data were obtained from this run.

(f) The pressure was so irregular that an approximation of a mean pressure range would be meaningless.

(g) A thin slab of F propellant approximately 1/16 inch thick was bonded to the sample in an effort to obtain uniform ignition.

(h) A thin slab of F propellant with a hole in the center was bonded to the wall of the burner approximately 1/2 inch from the sample for ignition purposes.

(i) The minimum pressure of the pressure oscillations was probably below the critical pressure needed to maintain critical flow in the nozzle.

TABLE 9

GB PROPELLANT DATA FROM LOW-L* BURNER

Run No.	Propellant Code	Nozzle Dia. (in)	L_p (in)	L_{ch} (in)	P_o(a) (psia)	Pressure Range (psia)	Results(b)	Comments
53-066(c)	GB-1	0.250	0.28	0.750	7.4	28	C-O-E	Chuffed twice
53-067(c)	GB-1	.250	.28	1.06	7.4	18-25	C-O-U	Chuffed twice
53-068(c)	GB-1	.250	.28	1.25	7.4	24	C-E	Chuffed twice
53-069	GB-1	.250	.28	1.50	7.4	23	S	
53-063(c)	GB-1	.228	.25	0.50	7.4	50	C-E	Chuffed once
53-064(c)	GB-1	.228	.22	0.50	7.4	46	C-E	Chuffed once
53-065	GB-1	.228	.13	0.50	7.4	46	S	
53-062	GB-1	.228	.31	0.75	7.4	35-60	S	Uneven pressure
53-061	GB-1	.228	.25	0.75	9.8	30-50	U	

(a) In this column, the abbreviation "atm" has been used to indicate that the burner exhausted to the atmosphere.

(b) In this column, "C" represents chuffing; "O" represents oscillatory burning; "S" represents stable burning; "E" represents that the sample extinguished; and "U" represents uneven or irregular burning.

(c) L*-frequency data were obtained for this run.

APPENDIX F

ANALYZED DATA

TABLE 10

CRITICAL L* AS A FUNCTION OF PRESSURE - F PROPELLANT

Run Number	Pressure (psia)	Critical L* (in)
42-063	45	9.3
4/-291	34	10.1
410-161	38	15.0
311-131	48	7.3
47-251	53	7.4
47-241	53	7.9
47-252	45	9.5
310-231	39	9.0
410-146	57	10.0
410-071	50	10.0(a)
42-052	80(b)	4.4
410-166	88	5.0
410-163	80	5.8
410-201	56	5.4
311-133	95(b)	4.5(a)
311-135	85	5.4

(a) Approximated without the aid of the planimeter.

(b) The mean pressure at which the propellant burned stably after chuffing once.

TABLE 11

CRITICAL L* AS A FUNCTION OF PRESSURE - TF PROPELLANT

Run Number	Pressure (psia)	Critical L* (in)
48-261	35	20.9
48-019	48	21
47-282	69	15.4
47-254	53	18.8
47-284	50	19.9
51-042	48	20.8
48-256	68	23(a)
51-044	130	7.6
48-011	82	12.0
48-015	110	7.7
48-016	95	6.4
51-045	115	7.8
48-017	108	7.8
47-221	122	7.7
48-264	170	6.5
48-263	140	7.2

(a) Approximated without the aid of the planimeter.

TABLE 12

CRITICAL L* AS A FUNCTION OF PRESSURE - XF PROPELLANT

Run Number	Pressure (psia)	Critical L* (in)
48-266	67	21(a)
49-027	78	9.9
49-026	95	13(a)
49-025	75	14.5
48-269	90	10.5
49-021	120	9.2
49-022	80	12.6
49-023	170	6.6
49-024	122	8.4

(a) Approximated without the aid of the planimeter.

TABLE 13

CRITICAL L* AS A FUNCTION OF PRESSURE - G PROPELLANT

Run Number	Pressure (psia)	Critical L*(in)(a)
39-233	30	24(b)
310-163	30	22.7
49-306	35(c)	25
410-053	32	25
410-071	32	23
410-214	30(c)	12
410-176	34(d)	14
411-061	42(d)	15.3
411-062	34(d)	16
410-191	34(d)	17
311-075	30(e)	7.1
311-074	36	13.1
410-022	53	8.4
410-065	60(f)	3.5

(a) Determined at the point where oscillations cease.

(b) Approximated without the planimeter.

(c) Pressure uncertain due to drift in transducer output.

(d) The mean pressure at which the propellant burned stably after oscillating.

TABLE 14

L*-FREQUENCY DATA - F PROPELLANT

Run No.	L*(in)	Frequency (cps)	Pressure (psia)	1/ξ	γ
49-181	17 (a)	50 (b)	36	42	9.1
	19 (a)	43 (b)	35	40	8.2
42-063	7.2(a)	121	38	95	20.7
	9.0	103	44	64	14.9
47-291	10.1	94 (b)	34	76	18.2
410-161	15.0	75	38	45	12.8
311-131	7.3	125	48	71	16.4
410-146	8.1	131	57	52	13.9
	9.1	115	56	48	12.6
	10.0	120	53	46	13.8
411-071	10.0(a)	105 (b)	50	50	13.2
42-052	4.7(a)	255	85	56	17.1
410-166	5.0	236	88	51	15.3
410-163	4.2	260	70	79	21.8
	5.8	226	80	49	16.3
311-135	5.4	241	85	49	16.2
410-147	5.7	250	98	39	14.2
410-211	3.5(c)	274	80	81	19.8
410-212	5.0(c)	225	75	61	17.5

(a) Approximate.

(b) Measured from less than four complete pressure oscillations.

(c) Calculated from the dimensions of the remaining propellant after extinguishment.

TABLE 15

L*-FREQUENCY DATA FOR TF PROPELLANT

Run No.	L*(in)	Frequency (cps)	Pressure (psia)	1/ξ	γ	η (a)
47-286	10 (b)	91	56	52	12.0	...
	16 (b)	63	28 (c)	62	15.8	...
47-287	15 (b)	74	50	38	10.7	0.041
48-261	15.7	71	37	49	13.8	.062
	16.6	67	39	44	12.4	.046
	17.4	69	39	42	12.8	.050
	17.8	71 (d)	39	41	13.2	...
	18.6	62	39	40	11.5	.038
	20.9	58	35	39	11.9	.000
48-019	17.6	66	51	32	9.4	.040
	21	65	48	29	9.9	.028
47-282	11.4	91	62	42	10.9	.052
	12.3	100	73	33	10.3	.073
	13.4	93	70	31	9.9	.072
	15.4	91	69	27	9.8	.035
47-284	18.7	66	47	33	10.3	.078
	19.3	67	52	29	9.4	.088
	19.9	67	50	29	9.7	.036
51-042	20.8	74	48	29	11.3	...
48-256	23 (b)	72	68	19	7.9	.000
51-044	4.2	194	105	68	14.0	...
	4.8	214	125	51	13.2	...
	7.6	209	130	31	12.4	...
48-011	8.4	134	70	50	14.3	.135
	9.6	133	80	38	12.3	.080
	12.0	124	80	31	11.5	-.028
	14.8	101	58	29	11.0	-.063
51-043	10.6	128	92	31	10.5	...
48-015	4.1	256	130	58	15.2	.106
	5.0	214	120	51	13.7	.125
	6.0	209	120	42	13.4	.082
	7.7	190	110	36	13.1	.000
51-045	5.9	161	85	59	14.2	...
	6.6	178	100	46	13.5	...
	7.8	189	115	34	12.5	...
	8.7	196	120	29	12.5	...
	11.2	168	110	22	11.6	...

TABLE 15 (Continued)

Run No.	L*(in)	Frequency (cps)	Pressure (psia)	$1/\xi$	γ	η (a)
48-017	7.8	169	108	36	11.9	.111
48-264	3.4	342	215	43	12.7	.145
	4.0	316	200	39	12.4	.140
	4.7	322	200	33	12.6	.135
	6.5	237	170	28	10.9	.084
48-263	6.3	224	140	35	12.3	.156
	7.2	225	140	30	12.4	.138

(a) It was not possible to obtain approximations for the growth term on all of the runs.

(b) Approximate.

(c) The minimum pressure of the pressure oscillations was probably below the critical pressure needed to maintain sonic conditions in the nozzle.

(d) Measured from less than four complete pressure oscillations.

TABLE 16

L*-FREQUENCY DATA FOR XF PROPELLANT

Run No.	L*(in)	Frequency (cps)	Pressure (psia)	1/ξ	γ
48-266	21 (a)	65	67	20	6.6
49-027	9.9	109	78	38	9.6
49-026	13 (a)	89	95	25	6.9
49-025	14.5	77	75	37	7.0
48-269	6.3	178 (b)	115	45	12.1
	6.8	173	112	43	12.0
	7.3	173	105	42	12.6
	7.9	151	100	40	11.5
	8.8	143	95	37	11.1
	9.8	130	92	34	10.3
	10.5	134	90	32	10.7
49-021	7.7	133	130	34	8.4
	9.2	141	120	30	9.3
49-022	9.7	107	85	36	8.8
	10.8	109	85	32	9.0
	12.6	105	80	29	9.1
49-023	3.6	260 (b)	195	58	12.6
	4.2	236 (b)	190	50	11.6
	5.2	237	180	41	12.1
	6.6	200	170	33	10.5
49-024	6.2	197	140	40	11.7
	7.7	190	125	35	12.3
	8.4	181	122	33	11.8

(a) Calculated from the initial L*.

(b) Measured from less than four complete pressure oscillations.

TABLE 17

L*-FREQUENCY DATA FOR G PROPELLANT

Run No.	L* (in)	Frequency (cps)	Pressure (psia)	$1/\xi$	γ
49-231	8.5(a)	42 (b)	24	570	51
49-241	10.5(a)	40 (b)	24	461	49
49-242	18 (a)	20 (b)	20	328	30
410-194	29 (a)	25 (b)	14 (a)	302	55
49-308	42 (a)	18 (b)	28	96	18
49-308	52 (a)	15	17	137	27
410-052	54 (a)	17	20	110	25
410-064	64 (a)	15	21	87	21
410-073	70 (a)	13.5	19	90	21
311-153	4.0(d)	177	20 (e)	1480	264
	5.0	174	24 (e)	920	201
	6.5	177	26 (e)	670	195
310-163	4.5	180	30 (e)	835	171
	18.9	170	30	200	161
311-154	7 (d)	177	27 (e)	608	190
	8 (a)	172	27 (e)	532	184
311-155	9 (d)	167	26 (e)	485	184
	21 (d)	159	26 (e)	208	175
49-306	22	158	38	131	115
410-071	23.3	153	32	151	135
410-214	10.5(d)	176	26 (e)	415	194
	11.5	189	29	349	192
410-176	12 (d)	174	25	379	201
	13.2	183	32	265	162
411-061	14 (d)	187	30	269	177
	14.7	188	40	185	128
411-062	15 (d)	189	25	306	219
	16.0	184	32	219	163
410-191	16.7	182	28	242	186
311-075	5.6	183	28 (e)	723	187
	7.1	183	28 (e)	570	187
311-074	13.0	179	36	236	139
49-305	8.0	233	75	169	80

TABLE 17 (Continued)

(a) Calculated from the dimensions of the remaining propellant after extinguishment.

(b) Measured from less than four complete pressure oscillations.

(c) Uneven pressure.

(d) Approximated from the pressure trace.

(e) The minimum of the pressure oscillations was probably below the pressure needed to maintain sonic conditions in the nozzle.

TABLE 18

L*-FREQUENCY DATA - GB PROPELLANT

Run No.	L* (in)		Frequency (cps)	Pressure (psia)	$1/\xi$	γ
53-066	20	(a)	23	27	210	24.4
53-067	30	(b)	22	18	223	37.1
	31	(b)	30	25	148	34.7
	36	(b)	25	25	131	28.9
53-068	38	(a)	20	23	132	25.4
	40	(a)	20 (c)	23	126	25.4
53-063	12	(a)	55	49	179	29.8
53-064	14	(a)	48	46	162	27.5

(a) Calculated from the dimensions of the remaining propellant after extinguishment.

(b) Approximate.

(c) Calculated from less than four complete pressure oscillations.

APPENDIX G

THE EFFECTS OF THERMAL

RADIATION ON THE ANALYSIS OF CHAPTER II

The experimental results discussed in Chapter IV indicate the
possibility of a different mechanism causing NAI in G propellant than
in the other propellants. It was pointed out that the addition of
2 per cent carbon black to the composition of G propellant (to make
GB propellant) seemed to remedy the discrepancy (i.e., data from GB
propellant firings seemed to follow the same trend as data from the
other propellants). It was concluded that at least part of the reason
for the discrepancy was due to penetration of thermal radiation into
G propellant. Consequently, an attempt was made to include these
effects in the mathematical analysis.

Cantrell, Mc_ure, and Hart [7] have studied the effects of
thermal radiation on the acoustic response of solid propellants.
Although they were interested mainly in an acoustic phenomenon, the
qualitative results of their analysis can be applied to the problem
at hand. Their analysis indicated that radiation should be responsible
for a considerable increase in the propellant response for the low
frequency regime when the mean burning rate of the propellant is rela-
tively low. They also concluded that for a rather typical propellant,
their analysis would be valid for burning rates down to approximately
0.13 inches/second. For slower burning rates the effects of thermal

radiation would exceed the limits of their assumptions. The burning
rate of G propellant in the range of interest is less than 0.10 inches/
second. Therefore, it might well be expected that radiation should
have a strong effect on the unstable behavior of the propellant.

In order to include the effects of thermal radiation it was
assumed that radiation penetrating the solid phase would obey Beer's
law as adapted to thermal radiation [11, p. 383]. This can be written
as

$$f_r = f_{rs} \ e^{-\delta x} \qquad\qquad (G-1)$$

where f_r is the radiant flux at any point in the solid, f_{rs} is the
radiant flux at the surface, and δ is the absorption coefficient.
Nomenclature specific to this Appendix only, has been included at the
end of the Appendix. The unsteady heat conduction equation, derived
with the inclusion of this term to account for radiation effects, is

$$\rho_p c_\rho \frac{\partial T}{\partial t} = k \frac{\partial^2 T}{\partial x^2} + \rho_p r c_p \frac{\partial T}{\partial x} + \delta f_{rs} \ e^{-\delta x} \qquad (G-2)$$

Solving the steady-state form of this equation yields

$$\bar{T} = T_0 + \left(\bar{T}_s - T_0 + \frac{\bar{T}_s f_1}{\delta_1 - 1} \right) e^{-2\lambda x} - \frac{f_1 \bar{T}_s}{\delta_1 - 1} e^{-\delta x} \qquad (G-3)$$

where $f_1 \equiv \dfrac{\bar{f}_{rs}}{\bar{T}_s \bar{r} \rho c}$, and $\delta_1 \equiv \dfrac{\alpha \delta}{\bar{r}}$

Differentiating (G-3) gives the thermal gradient in the solid including
the effect of radiation as

$$\frac{d\bar{T}}{dx} = -2\lambda \left(T_s - T_0 \cdot \frac{f_1 T_s}{\delta_1 - 1} \right) e^{-2\lambda x} + \frac{\delta f_1 T_s}{\delta_1 - 1} e^{-\delta x} \quad (G-4)$$

The perturbation of the incident radiative flux at the surface of the propellant is defined as the other perturbed quantities have been defined

$$f_{rs} = \bar{f}_{rs} [1 + \Phi e^{(1+\eta)\omega t}] \quad (G-5)$$

where it is recognized that the radiative flux, f_r is a fraction of the total incident flux at the surface, f. Substituting the perturbed radiant flux, burning rate, and temperature (see Equations (G-5), (2.4a), and (2.4b)) into Equation (G-2), subtracting the steady-state terms, and neglecting second order perturbations, yields the following second order differential equation in terms of the perturbed quantities

$$\frac{d^2\theta}{dx^2} + 2\lambda \frac{d\theta}{dx} - (\eta+1) \frac{\omega}{\alpha} \theta = \frac{-2\lambda\beta}{\bar{T}_s} \frac{d\bar{T}}{dx} - \frac{\delta \bar{f}_{rs}}{\alpha\rho c_p \bar{T}_s} \Phi e^{-\delta x} \quad (G-6)$$

Substituting Equation (G-4) into (G-6) results in

$$\frac{d^2\theta}{dx^2} + 2\lambda \frac{d\theta}{dx} - (\eta+1)\frac{\omega}{\alpha} \theta = 4\lambda^2\beta \left(\frac{\bar{T}_s - T_0}{\bar{T}_s} + \frac{f_1}{\delta_1 - 1} \right) e^{-2\lambda x}$$

$$- \frac{\delta \bar{r} f_1}{\alpha} [\frac{\beta}{\delta_1 - 1} + \Phi] e^{-\delta x} \quad (G-7)$$

Applying the boundary conditions that

$$\text{at } x = 0 \qquad \theta(0) = \theta_0$$

$$\text{and at } x = \infty \qquad \theta(\infty) = 0$$

to Equation (G-7) and solving as in Chapter II, where radiation effects were not included, gives the solution

$$\frac{\theta(x)}{\beta} = (\frac{\theta_0}{\beta} - C_1 - C_2)\, e^{-\lambda(\sigma+1+1\tau)x} + C_1 e^{-2\lambda x} + C_2\, e^{-\delta x}$$

$$\text{(G-8)}$$

where $C_1 = \dfrac{-4\left(\dfrac{\bar{T}_s - T_0}{\bar{T}_s} + \dfrac{f_1}{\delta_1 - 1}\right)}{\gamma(\eta+1)}$

$$C_2 = \frac{-f_1\left(\dfrac{1}{\delta_1 - 1} + \dfrac{\Phi}{\beta}\right)}{\delta_1 - 1 - \dfrac{\gamma}{4\delta_1}(\eta + 1)}$$

Equation (G-8) is analogous to Equation (2.11) of the main text.

The incentive for deriving an equation such as (G-8) was to permit the integration of the integral in Equation (2.6). Recalling that the radiant flux is a fraction of the total energy flux, f, it can then be seen that Equation (2.6) will be the same even when the effects of radiation are considered. For convenience this equation has been repeated

$$\frac{\phi}{\beta} = 1 + \frac{c_p \bar{T}_s}{H}\,\frac{\theta_0}{\beta} + \frac{c_p\, \omega\, \bar{T}_s}{\bar{r}\, H}\,(\eta+1)\int_0^\infty \frac{\theta(x)}{\beta}\, dx \qquad (2.6)$$

Utilizing the results of Equation (G-8) the indicated integration can be carried out as in Appendix C. The results, after algebraic manipulation, are

$$\frac{\phi}{\beta} = 1 + G + G_1\,[\eta(\sigma+1) + \tau + 1(\sigma+1-\eta\tau)] - Y_3[S - 2(\sigma+1-1\tau)] \quad \text{(G-9)}$$

$$- Y_4\,\frac{f_1\,\Phi_1}{(\gamma_2-\eta)^2 + 1}\left[\gamma_2\left(\frac{S\eta}{2\delta_1} - \tau\right) + \sigma + 1 - \frac{S}{2\delta_1}(\eta^2+1)\right.$$

$$\left. + 1\left[\gamma_2\left(\frac{S}{2\delta_1} + \eta\tau\right) - \tau(\eta^2+1) - \eta(\sigma+1)\right]\right]$$

where $Y_3 \equiv \dfrac{2c_p \bar{T}_s}{HS} \left[\dfrac{\bar{T}_s - T_0}{\bar{T}_s} + \dfrac{f_1}{\delta_1 - 1} \right]$

$Y_4 \equiv \dfrac{\gamma c_p \bar{T}_s}{2HS}$

$\Phi_1 \equiv \dfrac{1}{\delta_1 - 1} + \dfrac{\phi}{\beta}$

$\gamma_2 \equiv \dfrac{4\delta_1 (\delta_1 - 1)}{\gamma}$

Separating Equation (G-9) into its real and imaginary parts yields

$$\frac{\dot{\phi}}{\beta} = \mathrm{Re}\left(\frac{\dot{\phi}}{\beta}\right) + i \, \mathrm{Im}\left(\frac{\dot{\phi}}{\beta}\right) \qquad\qquad\text{(G-10)}$$

where $\mathrm{Re}\left(\dfrac{\dot{\phi}}{\beta}\right) \equiv 1 + G + G_1 \left[\eta(\sigma+1) + \tau \right] - Y_3 \left[S - 2(\sigma+1) \right]$

$\qquad\qquad - Y_4 \, \Phi_2 \left[\gamma_2 \left(\dfrac{S\eta}{2\delta_1} - \tau \right) + \sigma + 1 - \dfrac{S}{2\delta_1} (\eta^2 + 1) \right]$

$\qquad \mathrm{Im}\left(\dfrac{\dot{\phi}}{\beta}\right) \equiv G_1 (\sigma + 1 - \eta\tau) - 2 Y_3 \tau - Y_4 \, \Phi_2 \left[\gamma_2 \left(\dfrac{S}{2\delta_1} + \eta\tau \right) - \tau(\eta^2 + 1) - \eta(\sigma+1) \right]$

and $\Phi_2 \equiv \dfrac{f_1 \, \Phi_1}{(\gamma_2 - \eta)^2 + 1}$

This equation is analogous to Equation (2.12) and can now be combined with the results of the perturbed mass balance (Equation (2.17)) obtaining an equation analogous to Equation (2.19).

This was done and the results were programmed and run on the IBM 7040 computer. However, positive results, agreeing with the

experimental data, were not obtained in the initial effort. Therefore,
the project was not pursued.

NOMENCLATURE FOR APPENDIX G

__ROMAN LETTERS__

c_1
$$\dfrac{-4\left[\dfrac{(T_s - T_0)}{\bar{T}_s} + \dfrac{f_1}{\delta_1 - 1}\right]}{\gamma\,(\eta + 1)}$$
dimensionless

c_2
$$\dfrac{-f_1\left[\dfrac{1}{\delta_1 - 1} + \dfrac{\Phi}{\beta}\right]}{\delta_1 - 1 - \dfrac{\gamma}{4\delta_1}(\eta + 1)}$$
dimensionless

f_r radiant flux m/θ^3

f_1
$$\dfrac{\bar{f}_{rs}}{\bar{T}_s\,\rho\,\bar{r}\,c_p}$$
dimensionless

Y_3
$$\dfrac{2c_p\bar{T}_s}{HS}\left[\dfrac{\bar{T}_s - T_0}{\bar{T}_s} + \dfrac{f_1}{\delta_1 - 1}\right]$$
dimensionless

Y_4
$$\dfrac{\gamma c_p\bar{T}_s}{2HS}$$
dimensionless

__GREEK LETTERS__

γ_2
$$\dfrac{4\delta_1(\delta_1 - 1)}{\gamma}$$
dimensionless

δ adsorption coefficient $1/L$

δ_1
$$\dfrac{\alpha\delta}{\bar{r}}$$
dimensionless

Φ radiant flux perturbation at the surface   dimensionless

GREEK LETTERS
(Cont'd)

$$\phi_1 \qquad \frac{1}{\delta_1 - 1} + \frac{\phi}{\beta} \qquad\qquad \text{dimensionless}$$

$$\phi_2 \qquad \frac{f_1 \, \phi_1}{(\gamma_2 - \eta)^2 + 1} \qquad\qquad \text{dimensionless}$$

PAGES 154 THROUGH 158 OMITTED

APPENDIX I

STRAND BOMB DATA

TABLE 19

Run No.	Propellant Type	Strand Length (in.)	T_0 (°C)	P (psia)	Rate (in./sec.)
3	F-40	2.0	25	45	0.216
5	F-40	2.0	19	34	0.193
9	F-40	2.0	20	53	0.241
12	F-40	2.0	21	32	0.169
13	F-40	2.0	24	28	0.164
15	F-40	2.0	25	38	0.216
17	F-40	1.98	25	43	0.208
21	F-40	2.0	29	39	0.200
22	F-47	2.0	28	18	0.128
23	F-47	2.0	28	22	0.140
24	F-47	2.0	28	28	0.166
25	F-47	2.0	28	33	0.176
26	F-47	2.0	26	37	0.190
27	F-47	2.0	26	43	0.206
28	F-47	2.0	26	47	0.225
29	F-47	2.0	26	51	0.234
30	F-47	2.02	28	57	0.254
31	F-47	2.02	28	64	0.268
32	F-47	2.0	29	67	0.286
33	F-47	2.02	26	66	0.284
34	F-47	2.03	29	14	0.120
35	F-47	2.00	30	15	0.124
36	F-47	2.02	30	17	0.126
38	F-47	2.00	30	17	0.128
39	F-47	2.00	30	20	0.135
41	F-47	1.98	31	26	0.160
42	G-12	2.00	27	26	0.0798
43	G-12	2.02	27	17	0.0642
45	G-12	2.01	29	18	0.0640
46	G-12	2.02	30	21	0.0720
47	G-12	2.01	31	22	0.0720
48	G-12	2.00	32	23	0.0737
49	G-12	2.00	32	25	0.0793
50	G-12	1.99	30	26	0.0790
51	G-12	2.00	30	40	0.0943

TABLE 9 (continued)

Run No.	Propellant Type	Strand Length (in.)	T_0 (°C)	P (psia)	Rate (in./sec.)
52	G-12	2.00	29	28	0.0839
53	G-12	2.00	30	30	0.0841
54	G-12	2.00	31	32	0.0913
55	G-12	2.00	31	34	0.0876
56	G-12	2.00	28	14	0.0545
57	G-12	1.99	28	15	0.0592
58	G-12	2.00	29	16	0.0593
59	G-12	2.02	29	17	0.0615
60	G-12	2.00	31	19	0.0674
61	G-12	2.00	31	36	0.0887
62	G-12	2.01	32	37	0.0900
63	G-12	2.01	32	41	0.0949
64	G-12	2.01	33	48	0.1091
65	G-12	2.00	30	51	0.1083
66	G-12	2.00	31	66	0.119
67	G-12	2.00	31	56	0.105
68	G-12	2.00	31	62	0.112
69	G-12	2.00	31	66	0.116
71	G-12	2.00	32	73	0.129
72	F-69	2.00	32	16	0.127
73	F-69	2.00	29	74	0.302
74	F-69	2.01	29	83	0.335
76	F-69	2.00	30	103	0.373
77	F-69	2.01	31	115	0.375
78	F-69	1.99	31	125	0.396
79	F-69	2.01	31	142	0.411
80	F-69	2.00	30	167	0.481
81	F-69	2.01	30	188	0.501
82	F-69	2.01	30	201	0.506
83	F-69	2.00	30	214	0.563
84	TF-1	2.00	32	29	0.175
85	TF-1	2.01	32	48	0.217
86	TF-1	1.99	32	72	0.286
87	TF-1	2.01	32	97	0.344
88	F-69	1.98	29	75	0.292

TABLE 9 (continued)

Run No.	Propellant Type	Strand Length (in.)	T_0 (°C)	P (psia)	Rate (in./sec.)
89	F-69	1.98	30	91	0.338
90	F-69	1.98	30	105	0.343
91	F-69	1.97	30	129	0.386
92	F-69	2.00	31	162	0.454
93	F-69	2.00	31	186	0.476
94	F-69	2.00	32	229	0.499
95	F-69	2.01	32	254	0.523
96	TF-1	2.00	33	15.3	0.151
97	TF-1	2.00	34	21	0.148
98	TF-1	2.00	34	39	0.200
99	TF-1	2.00	34	60.5	0.247
100	TF-1	2.00	34	88	0.304
101	TF-1	2.00	35	121	0.348
102	TF-1	2.00	35	145	0.385
103	TF-1	2.01	35	207	0.439
104	F-69	1.97	28	14	0.1145
105	F-69	1.97	29	15	0.124
106	F-69	1.98	29	16	0.126
107	F-69	1.98	30	17	0.134
108	TF-1	2.00	34	16	0.139
109	TF-1	1.99	34	21	0.163
110	TF-1	1.99	34	23	0.176
112	G-12	2.00	32	94	0.166
113	G-12	2.01	32	114	0.186
114	G-12	2.01	32	136	0.210
115	G-12	2.00	32	152	0.208
116	G-12	2.01	31	69	0.141
117	G-12	2.01	31	55	0.128
118	G-12	2.00	32	40.5	0.114
119	G-12	2.00	33	28.5	0.0911
120	G-12	2.01	30	14	0.0602
121	G-12	2.00	30	17	0.0725
1'	F-69	2.00	33	19	0.167
2'	F-69	2.01	33	15	0.139
3'	F-69	2.01	34	44	0.245

TABLE 9 (continued)

Run No.	Propellant Type	Strand Length (in.)	T_O (°C)	P (psia)	Rate (in./sec.)
4'	F-69	2.01	34	80	0.362
6'	F-69	2.01	35	28	0.195
7'	F-69	2.00	35	94	0.420
8'	F-69	2.01	35	126	0.455
9'	F-69	2.00	34	69	0.339
10'	F-69	2.01	34	59	0.302
122	G-12	2.00	30	22	0.0817
123	G-12	2.01	30	20	0.0753
124	G-13	2.01	34	20.5	0.0788
125	G-13	2.01	34	14	0.0612
126	G-13	2.01	34	18	0.0815
127	G-13	2.00	34	43	0.117
128	G-13	1.99	32	27	0.100
129	G-13	2.00	33	63	0.164
130	G-13	2.00	34	83	0.181
131	G-13	2.00	33	102	0.192
132	G-13	2.00	33	129	0.216
133	G-13	2.00	33	165	0.242
144	G-13	2.01	29	195	0.251
145	G-13	2.01	30	226	0.260
146	G-13	2.00	30	268	0.266
147	G-13	2.00	32	299	0.273
148	G-13	2.02	31	362	0.296
149	G-13	2.02	32	410	0.427
150	G-13	2.00	28	73	0.151
152	G-13	2.02	29	145	0.205
153	G-13	2.02	29	192	0.267
154	G-13	2.01	30	225	0.258
155	G-13	2.01	30	310	0.295
156	G-13	2.00	31	412	0.325
158	F-69	2.02	27	314	0.587
159	F-69	2.00	27	416	0.638
160	F-69	2.00	28	497	0.669
161	TF-1	2.01	31	309	0.535
162	TF-1	2.02	32	414	0.601

TABLE 9 (continued)

Run No.	Propellant Type	Strand Length (in.)	T_0 (°C)	P (psia)	Rate (in./sec.)
164	XF-2	2.01	27	13.5	0.142
165	XF-2	2.00	28	18	2.153
166	XF-2	2.01	28	29	0.193
168	XF-2	1.98	26	39.5	0.224
169	XF-2	1.98	28	54	0.255
170	XF-2	2.01	24	69.5	0.279
171	XF-2	1.97	24	90	0.296
172	XF-2	2.01	24	114.5	0.358
173	XF-2	1.97	20	143	0.371
174	XF-2	2.00	20	170	0.385
175	XF-2	2.00	19	15	0.134
176	XF-2	2.00	20	23	0.146
177	XF-2	2.01	20	221	0.431
179	XF-2	2.01	23	33	0.199
180	XF-2	2.01	24	49.5	0.239
182	XF-2	1.99	24	290	0.453
183	XF-2	2.01	25	383	0.508
184	XF-2	1.99	25	310	0.561
185	XF-2	1.99	24	13	0.130
186	XF-2	2.01	25	19	0.161
187	XF-2	2.00	25	27	0.182
190	U-1	2.01	25	13	0.148
194	U-1	2.51	26	19	0.158
195	U-1	2.50	26	23	0.185
197	U-1	2.49	24	38	0.227
198	U-1	2.52	24	53	0.274
199	U-1	2.51	25	74	0.341
200	U-1	2.51	25	104	0.418
201	U-1	2.51	25	156	0.506
202	U-1	2.50	21	13	0.127
204	U-1	2.52	22	13	0.127
206	U-1	2.53	23	15	0.140
207	U-1	2.51	23	232	0.612

DOCUMENT CONTROL DATA - R&D

(Security classification of title, body of abstract and indexing annotation must be entered when the overall report is classified)

1 ORIGINATING ACTIVITY (Corporate author)	2a. REPORT SECURITY CLASSIFICATION
University of Utah Chemical Engineering Department Salt Lake City, Utah 84112	Unclassified
	2b GROUP

3 REPORT TITLE

NON-ACOUSTIC COMBUSTION INSTABILITY OF SOLID PROPELLANTS

4 DESCRIPTIVE NOTES (Type of report and inclusive dates)

Scientific   Interim

5 AUTHOR(S) (Last name, first name, initial)

M. W. Beckstead

Norman W. Ryan

Alva D. Baer

6 REPORT DATE	7a. TOTAL NO. OF PAGES	7b. NO. OF REFS
August 1, 1966	173	40

8a CONTRACT OR GRANT NO.	9a. ORIGINATOR'S REPORT NUMBER(S)
AF AFOSR 446-63	
b PROJECT NO. 9713-01	
c. 61445014	9b. OTHER REPORT NO(S) (Any other numbers that may be assigned this report)
d 681308	AFOSR 66-1759

10 AVAILABILITY/LIMITATION NOTICES

1. Distribution of this document is unlimited

11 SUPPLEMENTARY NOTES	12. SPONSORING MILITARY ACTIVITY (SREP)
	Air Force Office of Scientific Research 1400 Wilson Boulevard Arlington, Virginia 22209

13 ABSTRACT

Non-acoustic combustion instability has been examined in an uncatalyzed, a catalyzed, and two aluminized composite propellants. These propellants were studied, burning cigarette fashion, in a burner capable of operating at values of L^* as small as 5 cm. It was observed that the frequency of the pressure oscillations varied with the value of L^*, frequency decreasing with increasing L^*. The data were correlated by plotting frequency versus the reciprocal of L^*, yielding a series of constant pressure curves. This pressure effect was eliminated by using dimensionless variables, allowing all of the data for a given propellant to be correlated along the same line.

A one-dimensional model is proposed that considers sinusoidal perturbations, allowing for growth of the disturbance. The pressure, the burning rate, the distributed temperature in the propellant, and the energy flux from the burning gases are the quantities perturbed.

KEY WORDS	LINK A		LINK B		LINK C	
	ROLE	WT	ROLE	WT	ROLE	WT
Combustion						
Combustion Instability						
Propellant						
Propellant Combustion						

INSTRUCTIONS

1. ORIGINATING ACTIVITY: Enter the name and address of the contractor, subcontractor, grantee, Department of Defense activity or other organization (*corporate author*) issuing the report.

2a. REPORT SECURITY CLASSIFICATION: Enter the overall security classification of the report. Indicate whether "Restricted Data" is included. Marking is to be in accordance with appropriate security regulations.

2b. GROUP: Automatic downgrading is specified in DoD Directive 5200.10 and Armed Forces Industrial Manual. Enter the group number. Also, when applicable, show that optional markings have been used for Group 3 and Group 4 as authorized.

3. REPORT TITLE: Enter the complete report title in all capital letters. Titles in all cases should be unclassified. If a meaningful title cannot be selected without classification, show title classification in all capitals in parenthesis immediately following the title.

4. DESCRIPTIVE NOTES: If appropriate, enter the type of report, e.g., interim, progress, summary, annual, or final. Give the inclusive dates when a specific reporting period is covered.

5. AUTHOR(S): Enter the name(s) of author(s) as shown on or in the report. Enter last name, first name, middle initial. If military, show rank and branch of service. The name of the principal author is an absolute minimum requirement.

6. REPORT DATE: Enter the date of the report as day, month, year; or month, year. If more than one date appears on the report, use date of publication.

7a. TOTAL NUMBER OF PAGES: The total page count should follow normal pagination procedures, i.e., enter the number of pages containing information.

7b. NUMBER OF REFERENCES: Enter the total number of references cited in the report.

8a. CONTRACT OR GRANT NUMBER: If appropriate, enter the applicable number of the contract or grant under which the report was written.

8b, 8c, & 8d. PROJECT NUMBER: Enter the appropriate military department identification, such as project number, subproject number, system numbers, task number, etc.

9a. ORIGINATOR'S REPORT NUMBER(S): Enter the official report number by which the document will be identified and controlled by the originating activity. This number must be unique to this report.

9b. OTHER REPORT NUMBER(S): If the report has been assigned any other report numbers (either by the originator or by the sponsor), also enter this number(s).

10. AVAILABILITY/LIMITATION NOTICES: Enter any limitations on further dissemination of the report, other than those imposed by security classification, using standard statements such as:

   (1) "Qualified requesters may obtain copies of this report from DDC."

   (2) "Foreign announcement and dissemination of this report by DDC is not authorized."

   (3) "U. S. Government agencies may obtain copies of this report directly from DDC. Other qualified DDC users shall request through

   _____ ."

   (4) "U. S. military agencies may obtain copies of this report directly from DDC. Other qualified users shall request through

   _____ ."

   (5) "All distribution of this report is controlled. Qualified DDC users shall request through

   _____ ."

If the report has been furnished to the Office of Technical Services, Department of Commerce, for sale to the public, indicate this fact and enter the price, if known.

11. SUPPLEMENTARY NOTES: Use for additional explanatory notes.

12. SPONSORING MILITARY ACTIVITY: Enter the name of the departmental project office or laboratory sponsoring (*paying for*) the research and development. Include address.

13. ABSTRACT: Enter an abstract giving a brief and factual summary of the document indicative of the report, even though it may also appear elsewhere in the body of the technical report. If additional space is required, a continuation sheet shall be attached.

It is highly desirable that the abstract of classified reports be unclassified. Each paragraph of the abstract shall end with an indication of the military security classification of the information in the paragraph, represented as (TS), (S), (C), or (U).

There is no limitation on the length of the abstract. However, the suggested length is from 150 to 225 words.

14. KEY WORDS: Key words are technically meaningful terms or short phrases that characterize a report and may be used as index entries for cataloging the report. Key words must be selected so that no security classification is required. Identifiers, such as equipment model designation, trade name, military project code name, geographic location, may be used as key words but will be followed by an indication of technical context. The assignment of links, rules, and weights is optional.